INFLUENCE OF ALIOVALENT DOPING AND MAGNETIC FIELD ASSISTED SHAPING ON STRUCTURAL, MAGNETIC AND MAGNETOELASTIC PROPERTIES OF COBALT FERRITE

A DISSERTATION SUBMITTED IN PARTIAL FULFILLMENT OF THE REQUIREMENTS FOR THE AWARD OF

DOCTOR OF PHILOSOPHY

In

MATERIALS ENGINEERING

By

VINITHA. M

School of Engineering Sciences and Technology

University of Hyderabad

Hyderabad 500046

India

To

My family

And

The Almighty

UNIVERSITY OF HYDERABAD
HYDERABAD-500046
INDIA

DECLARATION

I, **Vinitha. M,** hereby declare that the work embodied in this dissertation entitled **"Influence of Aliovalent Doping and Magnetic Field Assisted Shaping on Structural, Magnetic and Magnetoelastic Properties of Cobalt Ferrite"** submitted to the **School of Engineering Sciences and Technology**, University of Hyderabad, Hyderabad, for partial fulfillment of the degree of **Doctor of Philosophy in Materials Engineering** has been carried out by me under the supervision of **Dr. Dibakar Das**, is a bonafide work. I also declare that it has not been submitted previously in part or in full to this University or any other University or Institution for the award of any degree or diploma.

.

VINITHA.M

Reg.No: 10ETMM08

CERTIFICATE

This is certified that the thesis entitled **"Influence of aliovalent doping and magnetic field assisted shaping on structural, magnetic and magnetoelastic properties of cobalt ferrite"** Submitted by **M. Vinitha** bearing registration number **10ETMM08** in partial fulfilment of the requirements for award of **Doctor of Philosophy** in the **School of Engineering Sciences and Technology** is a bonafide work carried out by her under my supervision and guidance.

This thesis is free from plagiarism and has not been submitted previously in part or in full to this or any other University or Institution for award of any degree or diploma.
Parts of this thesis have been:

A: Published in the following publications:

1. **Vinitha Reddy Monaji**, Abdellah Lisfi, Sabin Pokharel and Dibakar Das, "Colossal Piezomagnetic Response in Magnetically Pressed Zr^{+4} Substituted Cobalt Ferrites", *Scientific reports,7:7935,* DOI: 10.1038/s41598-017-08160-1
2. **Vinitha Reddy Monaji**, Srinivas Indla, Sudhindra Rayaprol, Shara Sowmya, A. Srinivas, Dibakar Das, "Temperature dependent magnetic properties of $Co_{1+x}T_xFe_{2-2x}O_4$ (T = Zr, Ti), *Journal of Alloys and Compounds, 700, 92-97 (2017)*
3. **Vinitha Reddy Monaji** and D. Das, "Development of A Novel Magnetostrictive Material With Large Piezomagnetic Coefficient For Stress Sensor Applications", AIP proceedings, 1832, 140035 (2017)
4. **Vinitha Reddy Monaji**, Dibakar Das, "Influence of Zr doping on the structural, magnetic and magnetoelastic properties of cobalt-ferrites", *Journal of Alloys and Compounds 634, 99–103 (2015)*

B. Presented in the following conferences:

1) **Vinitha Reddy Monaji**, Paul Praveen J, Dibakar Das, "Effect of zinc doping on magnetic and magnetomechanical properties of cobalt ferrite", presented in AMPC conference-2013, Chennai
2) **Vinitha Reddy M**, Paul Praveen J and Dibakar Das, "Studies on magnetic and dielectric behavior of magnetoelectric $CoFe_2O_4$ – BCZT composites", presented in MAGMA 2013 in Guwahati.
3) Paul Praveen J ,**Vinitha Reddy M** and Dibakar Das, "Synthesis, characterization and dielectric properties of $(1-x)(Ba_{0.85}Ca_{0.15})(Zr_{0.1}Ti_{0.9})O_3–xCoFe_2O_4$ multiferroic composites", Presented in MAGMA 2013 in Guwahati.
4) **Vinitha Reddy M** ,Paul Praveen J , and Dibakar Das, "A study on ferroelectric and ferromagnetic properties of $(1-x)(Ba_{0.85}Ca_{0.15})$ $(Zr_{0.1}Ti_{0.9})O_3$ $–xCoFe_2O_4$ multiferroics composites", Poster presented at International Conference on Advanced Functional Materials (ICAFM-2014) in Thiruvananthapuram
5) **Vinitha Reddy Monaji**, Paul Praveen J, Manivel Raja, Dibakar Das, "Influence of cation distribution on the magnetic and dielectric properties of Zn doped CFO ceramics", presented in ICC conference-2015, Rajasthan

6) **Vinitha Reddy Monaji**, Dibakar Das, "Novel processing of substituted cobalt ferrites for stress sensing applications", presented in ICCGR-EI conference-2016, Hyderabad

7) **Vinitha Reddy Monaji**, Dibakar Das, "Development of A Magnetostrictive Material With Large Piezomagnetic Coefficient For Stress Sensor Applications", presented in DAE conference-2016, Bhubaneswar

Further the student has passed the following courses towards fulfillment of coursework requirements for Ph.D.

MT601	Research Methodology	4	Pass

and was exempted from doing coursework (recommended by Doctoral Committee) on the basis of the following courses passed during her M.Tech. Program (in Int. M.Tech. /Ph.D. Program) and the M.Tech. Degree was awarded:

Course Code	Name	Credits	Pass/Fail
MT401	Phase Transformation and Thermodynamics	4	Pass
MT402	Concepts of Materials Science	4	Pass
MT403	Metal forming: Science and Technology	4	Pass
MT404	Characterization of Materials	4	Pass
MT405	Seminar	2	Pass
MT406	Design and Selection of Engineering Materials	4	Pass
MT407	Materials processing and Characterization Laboratory	4	Pass
MT451	Materials & Technologies for Energy Systems	4	Pass
MT452	Diffusion and Kinetics	4	Pass
MT453	Modeling and Simulation	4	Pass
MT454	Powder Metallurgy and Ceramics	4	Pass
MT455	Surface Engineering and Advanced Nanofabrication Technologies	4	Pass
MT456	Polymer Science and Technology	2	Pass
MT457	Laboratory	4	Pass
MT458	Seminar	2	Pass
MT601	Research Methodology	4	Pass

Supervisor **Dean of School**

ACKNOWLEDGEMENTS

Completion of this dissertation was possible with the support of several people. I would like to express my sincere gratitude to all of them.

First and foremost I express my deep gratitude and respect to my guide **Dr. Dibakar Das**, for his valuable suggestions, strong motivation, constant encouragement and unconditional support throughout my research work. I thank him whole heartedly for introducing me to the area of ferrites.

I am also very thankful to Dean of SEST **Prof. M. Ghanshyam krishna**, Former deans, **Dr. Bhanushankar Rao, Prof. M. Sundarraman, Prof. R. Singh** and all other faculties in department for providing me the facilities and the guidance to carry out my research work. In particular I would like to record my gratitude to **Dr. S. Srinath (SOP), Dr. G. Venkatiah (SOP) and Valsa Kumar Sir** for their constant encouragement and support during the doctoral committee meetings.

I would like to thank **Prof. Abdellah Lisfi** (Morgan State University), **Dr. Sudhindra Rayaprol** (UGC-DAE-Consortium for Scientific Research), **Dr. Adiraj Srinivas** (DMRL) for their help in magnetic measurements.

I would like to acknowledge the (funding body) **DST-SERB** (sanction number SR/S3/ME/0012/2011) and **University of Hyderabad** for providing me with fellowship. The support received from **DST Purse and UPE grants** for consumable, contingencies and infrastructural supports are gratefully acknowledged. I would like to thank **Center for Nano Technology (CFN)**, University of Hyderabad, for allowing me to carryout magnetic measurements.

I wish my sincere thanks to all my lab mates **Paul Praveen, Swathi, Srinivas Indla, Chandrakala, Jaishree, Mohd Qasim, Kushi, Parthiban, Omkar, Harisha, Sateesh Prathapani, Suresh Beera, Ummen sabu, Urbashi, Madhu babu** and **all my classmates, department friends** for their support and encouragement while doing this work.

I would like to thank especially **Mr. Kamal Mankari, Mallesh anna and Venu**

anna for their constant support and also I would also like to thank the technicians and non-teaching staff of SEST.

I would like to register my gratitude to my friends in University of Hyderabad **Vinod Kumar Rao Patil, Shiva Ram, Suresh Pittala, Shara Sowmya, Nalla Somaiah, Ravider Reddy, Ashish Dhole** and to all other friends whom I have met in my Ph.D career.

Finally I would like to thank my parents **Lakshmi and Nagabhushanam, Manemma** (Grandmother), Suchitra (sister), Karunakar Reddy (brother) for their constant trust, support and encouragement.

VINITHA. M

CONTENTS

LIST OF FIGURES

Chapter I:

Chapter III:

Chapter IV:

Chapter V:

Chapter VI:

List of tables

Chapter V:

ABSTRACT

Cobalt-ferrite ($CoFe_2O_4$ (CFO)) has long been identified as a potential and reliable material for torque and various magnetoelastic stress sensing applications, owing to its superior strain sensitivity ($d\lambda/dH$), high magnetostriction (λ), high corrosion resistance and lower cost of production compared to rare-earth based magnetostrictive materials. Since, it is well known that the crystal field environment produced by the metal cations surrounding Co^{+2} ions in the octahedral site of CFO lattice plays a crucial role in determining the magnetic and magnetostrictive properties of cobalt ferrite, in this thesis work chemical substitution and magnetic compaction have been chosen to study their influence on the magnetic and magnetoelastic properties of cobalt ferrite. In this study magnetic and magnetoelastic properties of normally (NC) and magnetically (MC) compacted M-substituted cobalt ferrites, having nominal compositions $Co_{1+x}M_xFe_{2-2x}O_4$ (M = Zr^{+4}, Ti^{+4}; $0 \leq x \leq 0.4$) and $Co_{1+x}Ce_xFe_{2-2x}O_4$ ($0 \leq x \leq 0.04$) have been investigated. Dramatic increase in λ has been observed for $Co_{1.03}Ce_{0.03}Fe_{1.94}O_4$ - MC sample (~ -425 ppm) compared to the un-doped $CoFe_2O_4$ - NC samples (~ -181 ppm). A remarkable sevenfold increase in $d\lambda/dH$ of ~5.8 X 10^{-9} $A^{-1}m$ was observed for magnetically compacted (MC) Ti doped cobalt ferrite, $Co_{1.2}Ti_{0.2}Fe_{1.6}O_4$ compared to that obtained for normal compacted (NC) pure cobalt ferrite (~0.8 X 10^{-9} $A^{-1}m$). This investigation indicates that suitable chemical substitution together with magnetic field assisted processing could result CFO with tailored and enhanced magnetic and magnetoelastic properties suitable for various magnetic field sensing applications.

Chapter – 1

Introduction

In this chapter background of the present research work has been discussed. The basic introduction about different kinds of magnetism, classification of ferrites based on crystal structure, magnetism of spinel ferrites, magnetocrystalline anisotropy, induced anisotropy, anisotropy measurement techniques and origin of magnetostriction have been described. Methods to induce uniaxial anisotropy, such as, magnetic annealing and magnetic compaction have also been discussed.

1.1. Background

Magnetostriction is the property of a material, which causes them to change their shape/dimensions in the presence of an external applied magnetic field [1]. Magnetostrictive materials have high technological importance in many applications, such as magnetomechanical stress sensors, magnetostrictive transducers/actuators, vibration components in high frequency devices and in SONAR etc [2]. Cobalt ferrite is an ideal material over rare earth based magnetostrictive materials ($SmFe_2$, $TbFe_2$, $DyFe_2$, Terfenol-D) for the above mentioned applications, due to its high corrosion resistance, electrical resistivity, low magnetocrystalline anisotropy, large magnetostriction and strain sensitivity [3].

1.2. Fundamentals and types of magnetism

In a crystalline material the atoms are arranged in periodic array. Similar to crystal structure periodic arrangement of magnetic moments of atoms form a magnetic structure. Magnetic moments of an electron in an atom originate from two sources. These two magnetic moments are related to electron motion about its own axis and around the nucleus, which are named as spin (μ_{spin}) and orbital (μ_{orbit}) magnetic moments respectively [4].

$$\mu_{spin} = \mu_{orbit} = eh/4\pi mc = 9.27 \times 10^{-24}\ Am^2 \quad \text{.....(1)}$$

here ‘e’ and ‘m’ are charge (1.6×10^{-19} C) and mass (9.1×10^{-31} kg) of an electron respectively. ‘c’ velocity of light (3×10^8 m/s) and ‘h’ is Planck’s constant (6.6×10^{-34} Js). Spin and magnetic moment of an electron is represented by a special quantity ‘μ_B’, here μ_B is called as Bohr magneton, where $1\mu_B$ is equal to 9.27×10^{-24} Am^2. The net magnetic moment of an atom is considered as the vector sum of the orbital and spin magnetic moments of all the constituent electrons [5].

Magnetic moment is defined as the torque acting on the magnet of pole strength ‘p’, when it is placed in a magnet field of 1 Oe at right angles to the field direction.

$m = plH\sin\theta$ ………………… …..………………………… (2)

here 'l' is the distance between the poles. When H = 1 Oe and θ = 90˚

$m = pl$ ($A.m^2$) …………………………..……….……......(3)

Magnetic moment per unit volume can be defined as magnetization.

$M = m/v$ (A/m or emu/cm^3)………………………………….(4)

For smaller samples volume cannot be measured that accurately and also it varies with temperature depending on its coefficient of thermal expansion. Therefore it is more convenient to express the magnetization in terms of per unit mass rather than per unit volume, since mass is independent of temperature. Magnetic moment per unit mass is known as specific magnetization.

$\sigma = m/w$ (emu/g)…………………..……………..……….(5)

Based on the variation in magnetization of a material in response to the applied magnetic field, all substances can be classified into different categories. The ratio of magnetization to that of magnetic field is defined as susceptibility (χ)

$\chi = M/H$ ($emu/Oe.cm^3$)…………………………….………..(6)

here 'χ' value is different for different kind of magnetic materials.

(a) Diamagnetism:

Diamagnetism is a weak phenomenon, which occurs due to the change in orbital motion of an electron in the presence of an external magnetic field. Diamagnetic atoms do not show net magnetic moment, which occurs from filled shell electronic configuration. Even though all materials are inherently diamagnetic, the materials which exhibit no other magnetic behavior are specifically classified as diamagnetic substances. For example noble gases (He, Ne, etc), diatomic (H_2, N_2, etc) gases, ionic solids like NaCl, elements having covalent bonding (C, Si) and most of the organic compounds are diamagnetic, since they have no net magnetic moment. Diamagnetic substances show negative susceptibility, since these materials exhibit negative magnetization with increasing applied magnetic field [6].

(b) Paramagnetism:

Paramagnetism is a weak form of magnetism, which exists only in the presence of external applied magnetic field. The materials in which the constituent atoms have some net magnetic moment due to their incomplete cancellation of spin and orbital magnetic moments are said to be paramagnetic. Paramagnetic material possesses no net magnetization in the absence of an applied magnetic field, since the magnetic moments of atoms are randomly oriented. When the external magnetic field is applied atomic moments

tend to orient along the field direction but due to thermal agitation of atoms the net effect of applied magnetic field decreases, resulting in partial alignment of magnetic moments. The susceptibility of paramagnetic material is positive. Similar to diamagnetic materials paramagnetic materials are also considered as non-magnetic materials, since they exhibit magnetization in the presence of an external applied magnetic field [1].

(c) Ferromagnetism:

The materials, which possess permanent magnetic moment in the absence of external applied field by virtue of partial cancellation of spin and orbital magnetic moments of atoms, are classified as ferromagnetic materials. In a ferromagnetic material, alignment of magnetic moments of adjacent atoms takes place through exchange interaction energy and this alignment exists over large volume of crystal, called as domains. Ferromagnetic materials exhibit very large and positive susceptibility and at a particular temperature these materials transform to paramagnetic state, which is called the Curie temperature (T_C). According to Wiess theory, below T_C, due to the strong influence of molecular field, ferromagnetic materials can be easily magnetized to saturation even in the absence of an external applied magnetic field [1].

(d) Antiferromagnetism:

Antiferromagnetic materials also exhibit cooperative ordering behavior similar to ferromagnetic material, but they show zero net magnetic moment. Antiferromagnetic crystal lattice consists of two identical sub lattices, in each of which the ferromagnetic ordering exists but between them magnetic moments of equal magnitude are aligned anti parallel to each other, hence they exhibit no net magnetization. These materials show small and positive susceptibility and it increases to a maximum value up to a critical temperature called Neel temperature (T_N) and above this temperature it exhibits paramagnetic behavior. Antiferromagnetic materials obey Curie-Weiss law ($\chi = C/T-\theta$) similar to ferromagnetic materials ($\theta > 0$) with a negative 'θ' value. Examples of antiferromagnetic materials are MnO, NiO, Cr_2O_3, etc [1].

(e) Ferrimagnetism:

Similar to ferro- and antiferromagnetic materials, ferrimagnetic materials also show phenomenon of magnetic ordering. Crystal lattice of these materials also consists of two sublattices and their magnitudes of magnetic moments are different unlike antiferromagnetic materials, hence they show net magnetization but smaller in magnitude

compared to ferromagnets. Spontaneous magnetization of ferrimagnetic material vanishes at a transition temperature called Curie temperature (T_C) and they obey Curie-Weiss law. Ferrimagnetic materials possess large and positive susceptibility. Examples of these materials are magnetite (Fe_3O_4) and ferrites (cobalt ferrite, nickel ferrite, barium ferrite, strontium ferrite, etc) [6, 1]

(f) Magnetic anisotropy

Directional dependence of magnetic properties can be simply defined as magnetic anisotropy. In other way, preferential orientation of a magnetization vector along a particular direction in which it can be magnetized easily than in any other direction can be defined as magnetic anisotropy. Due to the effect of magnetic anisotropy it is difficult to orient the magnetization vector away from the easy direction of magnetization and it strongly influences the shape of the M-H (or B-H) hysteresis curve from which the ferro/ferri magnetic materials can be classified as soft (low coercivity and can be magnetized easily at lower field and possesses high saturation magnetization) or hard (high coercivity and larger fields are required to magnetize and possesses moderate saturation magnetization) magnets. Various kinds of magnetic anisotropies are exhibited by magnetic materials, such as magnetocrystalline anisotropy, shape anisotropy, stress anisotropy and the anisotropies induced by magnetic annealing, magnetic pressing, plastic deformation, irradiation and exchange anisotropy.

Magnetocrystalline anisotropy is an intrinsic property of a magnetic material, is also known as crystal anisotropy and it plays a key role in influencing the different magnetic properties, such as domain structure, magnetization processes, coercive force and permeability. Crystal anisotropy is a force, which holds the magnetization vector in a crystal along certain crystallographic directions. Therefore, due to the effect of crystal anisotropy the magnetization curves measured as a function of applied field will be different along different crystal directions. For example single crystal Fe and Ni disks having planes parallel to {110} consists of <100>, <110> and <111> directions as diameters. Since Fe and Ni have BCC and FCC crystal structures respectively, <111> and <110> directions of respective single crystals become magnetically hard due to the high atomic density along those directions. Magnetic measurements along <100> and <111> directions of Fe and Ni single crystals respectively requires lower fields to saturate the sample, hence these are called as easy directions [1].

In a magnetic crystalline material, interaction between two subsystems (crystal lattice and the magnetic system) takes place [7] and it can exist between the neighboring spins (spin-spin coupling), spin and orbit (spin-orbital coupling), spin and lattice (spin-lattice coupling), and orbit and lattice (orbital-lattice coupling). The spin-spin coupling is a strong interaction acts between the adjacent spins, it depends only on the angle between the spins and the exchange energy associated with it is isotropic, hence it will not contribute to the crystal anisotropy. In the lattice-orbit coupling strong interaction exists between orbit and lattice due to the crystal field created by the adjoining atoms and it results in partial or entire quenching of the orbital magnetic moment. There is also a coupling exists between spin and orbital magnetic moments but it is weak in nature compared to the lattice-orbit coupling. Since the interaction energy is strong between the orbit and lattice, it resists the rotation of an orbit when an external field is applied to orient the spin of an electron. The energy required to orient the spin away from the easy direction by overcoming the spin-orbit coupling is called the anisotropy energy. Hence, spin-orbit coupling, which couples the spin moments with lattice through electron orbit, is the main origin of magnetocrystalline anisotropy. The magnetocrystalline anisotropy energy (E) of a cubic crystal can be given by the following equation,

$$E = K_0 + K_1 (\alpha^2_1\alpha^2_2 + \alpha^2_2\alpha^2_3 + \alpha^2_1\alpha^2_3) + K_2 (\alpha^2_1\alpha^2_2\alpha^2_3) + \ldots..(7)$$

where K_0 is the isotropy energy contribution and K_1, K_2,… are so-called the anisotropy constants for a particular material. α_1, α_2, α_3 be the cosine of angle between the magnetization vector and crystallographic directions. Based on the sign of 'K_1' the direction of easy magnetization can be determined, provided 'K_2' is zero. If 'K_1' is positive anisotropy energy falls in the order $E_{100}<E_{110}<E_{111}$, hence <100> and <111> directions are easy and hard direction of magnetizations respectively. Similarly if 'K_1' is negative anisotropy energy is $E_{111}<E_{110}<E_{100}$, hence <111> and <100> directions are easy and hard direction of magnetizations respectively. If 'K_2' is not equal zero then the direction of magnetizations can be determined based on K_1 and K_2.

Several magnetic properties can be enhanced by inducing the magnetic anisotropy along a particular direction. Among the various techniques to induce magnetic anisotropy in a ferro/ferri magnetic material, magnetic annealing and magnetic compaction are the simplest methods compared to others. Heat treating and cooling a material in the presence of magnetic field is defined as magnetic annealing. This process develops a uniaxial anisotropy along the direction of the applied field and the material becomes magnetically

softer along that axis. Magnetic annealing should be performed at temperatures below the Curie temperature of the material and the applied magnetic field must be large enough to saturate the sample. Magnetic field assisted compaction is a well-known technique in producing anisotropic permanent magnets including hard ferrites. Magnetic field applied during compaction helps in inducing better degree of alignment of domains in powders. Compaction locks the particles in that state resulting in best magnetic homogeneity in the material. Magnetic compaction is a better technique to align the domains compared to magnetic annealing, since there is a possibility of degradation of magnetic properties of the magnetically annealed samples particularly when they are operated at high temperatures.

Anisotropy constants can be estimated from the torque curves and magnetization curves (using Law of approach to saturation).

(g) Magnetostriction

Ferro/ferri magnetic materials undergo dimensional changes, when they are subjected to magnetic field and conversely, magnetization of the material changes with the variation in mechanical state, this property is called magnetostriction. Similar to magnetic anisotropy spin-orbit coupling is the main origin of magnetostriction. When a ferro/ferri magnetic material is subjected to a magnetic field along with spin, orbital moment will try to orient in the direction of applied field if the spin-orbit coupling is strong. Since the orbit is strongly coupled to the lattice, rotation of orbit results in dimensional change in the material. Magnetostriction can be classified into two different kinds, spontaneous magnetostriction and field induced magnetostriction. The former mechanism arises due to the ordered magnetic structure, whereas the latter is accompanied by the reorientation of domains. Magnetostriction was first discovered by Joule, hence it is often called as Joule magnetostriction. Magnetostriction (λ) can be expressed as,

$$\lambda = \frac{\Delta l}{l} \qquad \ldots\ldots(8)$$

Here ‘l’ is the original length of the material and ‘Δl’ is the fractional change in length. Based on the response of the material to an applied magnetic field ‘λ’ can be either positive (expansion) or negative (contraction). The principal magnetostrictive effects observed are the Joule effect (change in length of a ferromagnetic rod, when it is placed in a longitudinal field), the Villari effect also called as magnetostrictive effect (change in magnetization, when ferromagnetic rod is subjected to longitudinal stress), the Matteucci effect (change in magnetization when a ferromagnetic material is subjected to torque), the Wiedemann effect

(change in torque when the material is subjected to a helical magnetic field). For isotropic materials or for randomly oriented polycrystals, if volume conservation is assumed, the magnetostriction can be expressed as a function of θ by,

$$\lambda = \frac{3}{2}\lambda s\left(\cos^2\theta - \frac{1}{3}\right) \quad \ldots\ldots(9)$$

where 'θ' is the angle between direction of magnetization and direction in which the magnetostriction is measured. θ = 0° and 90° denote the longitudinal (λ_l) and transverse magnetostriction (λ_t) respectively. If these two 'θ' values are substituted in the above equation it reduces to $\lambda_t = \lambda_l/2$. Decrease in length in the perpendicular direction will take place along with the increase in length in the direction of the field in ordered to conserve the volume.

1.3. Crystal structure of spinel cobalt ferrite

Ferrites are classified into three different groups based on their crystal structure, namely, spinel, garnet and magneto plumbite. Cobalt ferrite (CFO) has mixed spinel structure. Cubic spinel structure is formed by closely packed arrays of oxygen ions and it results in two different kinds of interstitial sites, tetrahedral (A-sites) and octahedral (B-sites) sites, as shown in Fig. 1. In one unit cell out of 64 A and 32 B-sites only 8 A and 16 B-sites are occupied, which indicates that one unit cell contains eight formula units. General chemical formula of cobalt ferrite can be represented as $(Co_{1-\delta}Fe_{\delta})_{tetra}[Co_{\delta}Fe_{2-\delta}]_{octa}O_4$, here 'δ' is defined as degree of inversion. The extent of inversion depends on sample synthesis method, chemical substitution and annealing processes. The factors that influence the cation distribution in tetra and octahedral sub lattices, when metal cations substituted into CFO lattice are ionic radii, cation valency and lattice energies. The large magnetocrystalline anisotropy of cobalt ferrite compared to other spinel ferrites is ascribed to the presence of Co^{2+} ions in the octahedral sites of spinel lattice. Single ion model explains that unquenched orbital moment of Co^{+2} ion contributes to the spin-orbit coupling, which is the main origin of magnetocrystalline anisotropy and magnetostriction. A typical example for normal spinel structure is zinc ferrite ($ZnFe_2O_4$) in which all the Zn^{+2} ions occupy tetrahedral sites and all the Fe^{+3} ions occupy the octahedral sites. An example of inverse structure is nickel ferrite ($NiFe_2O_4$), where all Ni^{+2} ions occupy the octahedral sites (B sites) and Fe^{+3} ions are evenly distributed in A and B sites. Cobalt ferrite ($CoFe_2O_4$) has partially inversed spinel structure, i.e., both Co^{+2} and Fe^{+3} ions are distributed in both A and B sites.

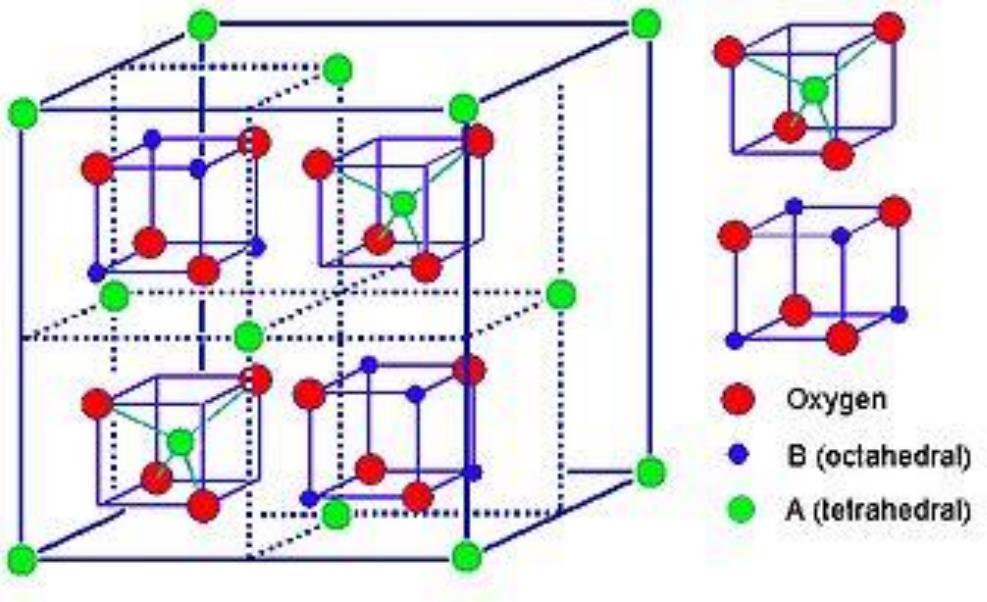

Figure1. The crystal structure of spinel ferrites. The unit cell consists of octants and the ions in tetrahedral site A (green circles) and octahedral site B (blue circles) as well as oxygen (red circles)

The inversion extent is dependent on the sample preparation processes and the heat treatment processes. Since Co^{+2} has a major contribution to the magnetocrystalline anisotropy of cobalt ferrite, the extent of inversion greatly affects the magnetic properties of the material, i.e. magnetic anisotropy, coercivity, saturation magnetization and magnetostriction. Three different kinds of interactions exist between the magnetic ions in A- (terta) and B- (octa) sublattices, they are A-O-B, A-O-A and B-O-B. Among these three exchange interactions A-O-B interaction is stronger compared to the other two interactions. According to the two-sublattice model proposed by Neel, the exchange energy between the ions in A- and B-site was negative, hence the net magnetization can be expressed as the difference between the magnetizations of each sublattice. The cubic ferrites containing cobalt have positive values of K_1, while K_1 is negative for all the cubic ferrites that contain no cobalt.

According to single-ion model, the cubic anisotropy constant of cobalt ferrite mainly depends on the concentration of Co^{+2} ions in B-site of spinel structure. Due to the cubic crystal field produced by the coulomb interaction between the oxygen ion and the electrons in the 3d orbitals, degenerate energy levels of Co^{+2} ion split into t_{2g} (d_{xy}, d_{yz}, d_{xz}) and e_g ($d_{x^2-y^2}$, d_{z^2}) levels. The orbitals, which are directed along the cubic axes (e_g levels), are raised in energy compared to others which are in between the axes (t_{2g} levels). For lower concentration of Co^{+2} ions in B site, neighboring iron ions produce trigonal field

around Co^{+2} ion and the axis of three fold symmetry lies along one of the body diagonals ([111], [1-11], [-1-11], [-111]) of cubic crystal. This trigonal crystal field splits the t_{2g} levels further into singlet and a doublet by distorting the cubic crystal field produced by the oxygen ions. Occupation of seventh electron of Co^{+2} ($3d^7$) in one of these doubly degenerate levels produces unquenched orbital momentum. Interaction of this orbital angular momentum with total spin momentum of Co^{+2} ion gives rise to magneto crystalline anisotropy through spin-orbit coupling [9, 10].

1.4. References

[1] Cullity, B.D., Graham, C.D., Introduction to Magnetic Materials (2nd ed., Wiley) (New Jersey, 2009)

[2] Bozorth, R. M. Ferromagnetism (D. Van Nostrand, New York, 1951)

[3] A.E.Clark, Ferromagnetic Materials, E.P. Wohlfarth(Ed.), Vol.1, North-Holland Publishing Co., Amsterdam, (1980)

[4] J. Smit, H.P.J. Wijn, Ferrites, Philips Research Laboratories, The Netherlands, (1959)

[5] W.D. Calister Jr, "Materials Science and Engineering", 3rd ed., Wiley, New York, 1985

[6] D.C. Jiles, Introduction to Magnetism and Magnetic Materials(Second Edition Chapman & Hall, New York 1998

[7] D.J. Craik and J. Derek, "Magnetic Oxides", Wiley, London, New York (1975), 327

[8] Alex Goldman, Modern Ferrite Technology, 2nd ed. Springer Science + Business Media, Inc., 2006

[9] J. Slonczewski, Origin of Magnetic Anisotropy in Cobalt-Substituted Magnetite, Physical Review, 110 (1958) 1341–1348

[10] M. Tachiki, Origin of the Magnetic Anisotropy Energy of Cobalt Ferrite, Progress of Theoretical Physics, 23 (1960) 1055–1072

Chapter – 2

Literature review

This chapter focuses on the literature review on various magnetostrictive materials and importance of cobalt ferrite material over rare earth based magnetostrictive materials. Also, the literature on magnetostriction of cobalt ferrite material influenced by synthesis method, processing conditions, substitution of different metal cations and magnetic anisotropy inducing methods have also been presented in this chapter. Based on the critical review of the existing literature on cobalt ferrite material objective of the current research work is framed, which is described at the end of this chapter.

2.1. Magnetostrictive materials

Rare earth elements (Tb and Dy) exhibit high magnetic anisotropy and magnetostriction (~10000 ppm) because of their unquenched orbital momentum. But, these elements are restricted to use in applications because of their low transition temperatures. In 1970's rare earth based intermetallic compounds ($DyFe_2$, $TbFe_2$) were developed for various sensor/actuator applications and because of the combination of rare earth and transition elements, transition temperature limitation can be compensated. $DyFe_2$ and $TbFe_2$ exhibit large magnetostrictions (650, 2630 ppm respectively) and high transition temperatures (>400˚C) compared to rare earth materials [1, 2].

The major issue of magnetocrystalline anisotropy with $DyFe_2$ and $TbFe_2$ was solved with the development of Terfenol-D ($Tb_{0.3}Dy_{0.7}Fe_2$) fabricated by unidirectional solidification, which is a fairly complex process. Here Tb and Dy have same sign of magnetostriction but opposite sign of anisotropy constants, hence the alloy made with the combination of Tb and Dy, reduced the magnetocrystalline anisotropy and this material in single crystal form showed magnetostriction of ~1600ppm at room temperature [3]. The main drawback of this material is poor mechanical strength and high cost of production. To solve this problem composite of Terfenol-D was prepared with polymers and $NaPO_3$ gas matrix. Here the problem of mechanical strength and cost was solved but at the cost of magnitude of magnetostriction coefficient [4].

Limitations of Terfenol-D were solved with the development of alloy made from Fe and Ga. Clark et. al reported the magnetostriction of ~400ppm at very low field (100Oe) for $Fe_{1-x}Ga_x$ (x = 0.2 to 0.35). Magnetostriction studies on FeAl and FeBe alloys were also studied [5, 6]. FeAl alloys exhibited lower value of magnetostriction compared to Galfenol. FeBe alloys showed almost comparable value with FeGa alloy, but are limited due to the toxic nature of Beryllium. Magnetic annealing and magnetic compaction were performed to further

improve the magnetostriction property of Terfenol-D [1, 7, 8]. Kellogg et. al. [6] reported high tensile strength for Galfenol alloy [9, 10].

Oxidation of rare earth alloys is the severe concern for several applications and this problem has partially been solved by replacing Terfenol-D with oxide based materials such as hexagonal ferrites, garnets, spinels. $Tb_3Fe_5O_{12}$, $DyFe_5O_{12}$ and $Ho_3Fe_5O_{12}$ single crystal garnets showed magnetostrictions of 2400, 875 and 450ppm respectively at -290˚C and it is observed to vanish at room temperature [11]. Spinel materials have exhibited high magnetostrictions at room temperature compared to rare earth based alloys and garnets. With the substitution of Ni from x = 0 to 1 in $Zn_{1-x}Ni_xFe_2O_4$, magnetostriction is observed to increase from zero to 35ppm [12]. Sm and Ho substituted $NiFe_2O_4$ have showed the magnetostriction coefficients of -34 and -24ppm respectively, against the value -25ppm for nickel ferrite [13].

Cobalt ferrite exhibits distinguishable magnetic and magnetoelastic properties (High curie temperature, high resistance, high coercivity, positive magnetocrystalline anisotropy, moderate magnetization) compared to other spinel ferrites ($ZnFe_2O_4$, $NiFe_2O_4$, $MnFe_2O_4$, etc) [14,15,16,17]. Cobalt ferrite has mixed spinel structure (Random distribution of Fe^{+3} and Co^{+2} ions in A- and B- sites in spinel lattice) and the degree of inversion depends on the synthesis method, chemical substitution, processing and annealing conditions [18]. Slonczewski and Tachiki [19, 20] reported that at lower concentrations Co^{+2} ions in the octahedral site is surrounded by Fe^{+3} ions, which produces a trigonal crystal field and the axis of symmetry lies along one of the body diagonals of the spinel cubic crystal. This trigonal crystal field distorts the symmetry of the cubic octahedral field produced by the oxygen ions resulting in lifting the degeneracy of the d-orbitals of cobalt ions and produces unquenched orbital moments. Magnetostriction and anisotropy energy results from the coupling of cobalt ion spin with its angular momentum.

Bozorth et. al. reported the magnetostriction of ~-600 and 190ppm before field annealing for the single crystal cobalt ferrite having the composition $Co_{0.8}Fe_{2.2}O_4$, when the measuring field applied parallel and perpendicular to <100> direction respectively. After field annealing along <100> direction magnetostriction measured in parallel and perpendicular directions of <100> are observed to be ~-5 and 800ppm respectively. It is also observed from the same study that magnetostriction not only depends on the measurement direction it also depends on composition. Magnetostriction of $Co_{1.1}Fe_{1.9}O_4$ and $Co_{0.8}Fe_{2.2}O_4$ compositions measured along <100> directions was observed to be -250 and -600ppm [21]. Single crystals

are limited due to the cost of production and difficulty in growing along a particular direction; hence it is useful to develop polycrystalline materials for practical applications.

Muhammad et.al. have reported the effect of compaction pressure on magnetostrictive properties of cobalt ferrites [22]. Cobalt ferrite sample compacted at 150MPa and sintered at 1350˚C for 24h has showed maximum magnetostriction and strain sensitivity of ~-200ppm and -0.6 × 10^{-9} A^{-1}m. The redistribution of ions (Co^{+2} and Fe^{+3}) among the interstitial sites of spinel structure has been attributed to the larger magnetostriction values. Cobalt ferrite annealed at magnetic field of 10T for 3h showed the λ_{max} and $d\lambda_{max}/dH$ of -400ppm and -1.2 × 10^{-9} A^{-1}m and these are almost twice compared to that of unannealed sample. Nlebedium et. al. have studied the effect of processing parameters and heat treatment conditions on magnetostriction property of cobalt ferrite. They have reported that samples compacted at 127 MPa and sintered at 1350˚C showed the λ_{max} of ~-210 ppm [23].

Lo et. al. studied the effect of magnetic annealing on magnetic and magnetostrictive properties of polycrystalline cobalt ferrite and the authors have reported that the magnetostriction is seen to increase from -200ppm to -250ppm after annealing [24]. From the parallel and perpendicular magnetization curves they have confirmed that uniaxial anisotropy is induced along annealing direction. Kaja Mohaideen and P.A. Joy reported [25] that the low temperature (1100˚C) sintered and magnetically annealed (magnetic field of 400 kA/m for 30mins and at 300˚C) polycrystalline cobalt ferrite samples showed high magnetostriction and strain derivative of 380ppm and 2.7 × 10-9 A-1m and it is claimed as the maximum magnetostriction so far reported in the literature.

In a recent study by Wang et. al. [26] they have applied the magnetic field during shaping of the pellet and after that sample was sintered at 1623K for 6h. 90% enhancement in maximum magnetostriction is observed for oriented sample (~270ppm) compared to non-oriented CFO (~142ppm) and strain sensitivity is increased from 2.2 × 10^{-9} A^{-1}m (for non-oriented sample) to 7.7 × 10^{-9} A^{-1}m (for oriented sample), which is the highest value compared to any other unsubstituted and substituted cobalt ferrite.

Magnetostrictive properties of metal bonded cobalt ferrites are reported by McCallum et.al. and the results were compared with Terfenol-D [27]. Magnetostriction and strain derivative of -220ppm and -1.3 × 10^{-9} A^{-1}m are observed for the cobalt ferrite composite and are higher than that observed for Terfenol-D at lower fields. And also it is reported that these materials exhibit better mechanical properties than Terfenol-D.

Sekhar et. al. reported the magnetostrictive properties of $Co_{1-x}Cu_xFe_2O_4$ [28]. Maximum magnetostriction of ~-170ppm is observed for x = 0.025 composition and maximum strain sensitivity of ~4.52 × 10^{-9} $A^{-1}m$ is observed for x = 0.15 composition compared to pure (~0.25 × 10^{-9} $A^{-1}m$). Nlebedim et. al. studied the effect of Zn substitution ($Co_{1-x}Zn_xFe_2O_4$) on magnetoelastic properties of cobalt ferrite [29]. Unlike $Co_{1-x}Cu_xFe_2O_4$ system, continuous decrease in λ_{max} and $d\lambda_{max}/dH$ is observed with progressive Zn substitution (-150ppm, ~0.5 × 10^{-9} $A^{-1}m$) compared to pure cobalt ferrite (-183ppm, ~0.7 × 10^{-9} $A^{-1}m$). From the observation of both Cu and Zn substituted cobalt ferrite systems, even though the Cu and Zn are substituted for Co^{+2} ion, variations in magnetoelastic properties were observed, which indicates that ion size and site preference strongly affects the magnetostriction property. Similar effect was observed for $CoMg_xFe_{2-x}O_4$ and $CoZn_xFe_{2-x}O_4$ systems [30].

Magnetostrictive properties of Mn, Cr, Al, Ga substituted cobalt ferrite samples have been studied by Jiles group [31-34]. $CoT_xFe_{2-x}O_4$ (T = Mn, Cr, Al, Ga) samples are synthesized by solid state method and sintered at 1350˚C for 24h. The authors have reported the λ_{max} of -180, -78, -140, -100ppm and $d\lambda_{max}/dH$ of 2.5 × 10^{-9} $A^{-1}m$, 2 × 10^{-9} $A^{-1}m$, 2.9 × 10^{-9} $A^{-1}m$, 3.2 × 10^{-9} $A^{-1}m$ for the respective substituted cobalt ferrites. From the observation of results they have reported that positive magnetostriction at lower fields might be due to the change in sign of anisotropy of the compositions, which affected the magnetostriction. Khaja et.al. reported the magnetostrictive properties of $CoMn_xFe_{2-x}O_4$ (x = 0 to 0.3) [35]. Maximum magnetostriction of ~232ppm was observed for x = 0.2 composition and is further increased to -262ppm with magnetic annealing. P.N. Anantharamaiah et. al. studied the effect of magnetic annealing and substitution of Al and Ga on magnetic and magnetostrictive properties of cobalt ferrite [36, 37]. Magnetostriction and strain sensitivity of $CoAl_xFe_{2-x}O_4$ are observed to increase from -217ppm and 1.4 × 10^{-9} $A^{-1}m$ for x = 0 to -230ppm and 2.4 × 10^{-9} $A^{-1}m$ for x = 0.1 and with magnetic annealing is observed to increase from -225ppm and 3.3 × 10^{-9} $A^{-1}m$ for x = 0 to -306ppm and 4.5 × 10^{-9} $A^{-1}m$ for x = 0.1. M_S, H_C, K_1, T_C are observed to decrease with increasing concentration of Al in spinel lattice. Similarly, with Ga substitution λ_{max} is observed to decrease from -250ppm for x = 0 to -100ppm for x = 0.3 and with magnetic annealing is observed to increase from -22ppm to -306ppm for x = 0.1. The magnetostriction reported in this study is larger than that of same composition reported by Jiles group.

Nlebedim et. al studied the effect of Ti^{+4} substitution on magnetostriction properties of cobalt ferrite and the results were compared with the magnetostriction of Ge substituted cobalt ferrite reported by Ranvah et. al. [38, 39]. $Co_{1+x}Ti_xFe_{2-2x}O_4$ and $Co_{1+x}Ge_xFe_{2-2x}O_4$ samples

were prepared by conventional ceramic method and sintered at 1350˚C for 24h. Continuous decrease in magnetostriction was observed with increasing Ti^{+4} concentration from -220ppm for x = 0 to -20ppm for x = 0.1, whereas λ_{max} is observed to increase to from -241ppm with Ge substitution (x = 0.1) compared to pure (-220ppm). Strain sensitivity is also observed to increase with progressive Ge concentration from 2×10^{-9} $A^{-1}m$ for x = 0 to 2×10^{-9} $A^{-1}m$ for x = 0.1. Rao et. al. reported the magnetostriction properties of Si substituted cobalt ferrite, prepared by solid state method and sintered at 1250˚C for 4h. λ_{max} of all Si- substituted cobalt ferrites is observed to be nearly equal to the parent composition (-90ppm) [40].

In order to achieve better enhancement in magnetostriction and strain sensitivity, based on the knowledge acquired from the literature review, objective of this thesis work has been framed.

2.2. Objective:

The objective of the present investigation is to study the influences of magnetic field assisted compaction and co-substitution of Zr^{+4}/Co^{+2}, Ti^{+4}/Co^{+2}, Ce^{+4}/Co^{+2} for 2 Fe^{+3} in the CFO lattice on the structural, magnetic and magnetoelastic properties of cobalt ferrite. Zr^{+4}, Ti^{+4} and Ce^{+4} ions have been chosen to investigate the effect of site preferences and ionic sizes on magnetostrictive property of cobalt ferrite. Magnetic compaction technique has been chosen to study the magnetic domain orientation effect on magnetic and magnetoelastic properties of cobalt ferrite.

2.2. References

[1] G. Engdahl, Handbook of Gaint Magnetostrictive materials (Academic Press, Sandiego, 2000)

[2] A.E.Clark, Ferromagnetic Materials, E.P. Wohlfarth(Ed.), Vol.1, North-Holland Publishing Co., Amsterdam, (1980)

[3] R. Abbundi, A.E.Clark, IEEE Trans. Magn. 13, 4510 (1977)

[4] M.R.J. Gibbs, Modern Trends in Magnetostriction Study and Applicaton (Kluwer Academic, Dordrecht, 2001)

[5] J.R. Cullen, A.E. Clark, M. Wun-Fogle, J.B. Rostorff and T.A. Lograsso, J.Magn.Magn. Mater. 226, 948 (2002)

[6] A.E. Clark, M. Wun-Fogle, J.B. Rostorff, T.A. Lograsso and G. Petculescu, J. Appl. Phys. 95, 6942 (2004)

[7] J. H. Yoo, S.M. Na, J.B. Rostorff, M. Wun-Fogle and A.B. Flatau, IEEE Trans. Magn. 45, 4145 (2009)

[8] N. Srisukhumbowornchai and S. Guruswamy, J.Appl. Phys. 90, 5680 (2001)

[9] R.A. Kellogg, A.M.Russel, T.A. Lograsso, A.F. Flautau, A.E. Clark, and M. Wun-Fogle, Act. Mater. 52, 5043 (2004)

[10] R.A. Kellogg, Ph.D. Thesis, Engineering Mechanics, Iowa State University, Iowa, 2003

[11] F. Sayetat, J.Magn.Magn. Mater. 58, 334 (1986)

[12] R. Adhikari, A. Sarkar, M.V. Limaye, S.K. Kulkarni and A.K. Das, J. Appl. Phys. 111, 073903 (2012)

[13] K.K.Bharathi, G. Markandeyulu and C.V. Ramana, J.Phys.Chem. C 115, 554 (2011)

[14] Cullity, B.D., Graham, C.D., Introduction to Magnetic Materials (2nd ed., Wiley) (New Jersey, 2009)

[15] P.N.Anantharamaiah, P.A.Joy, J. Appl. Phys. 121, 093904 (2017)

[16] H. Shenker, Phys. Rev. 107, 1246 (1957)

[17] F. J. Pedrosa, J. Rial, K.M. Golasinski, M.N. Guzik, A. Quesada, J.F. Fernandez, S. Deledda, J. Camarero and A. Bollero, Appl. Phys. Lett. 109, 223105 (2016)

[18] G.A.Sawatzky, F.V.D. Woude and A.H. Morrish, J. Appl. Phys. 39, 1204 (1968)

[19] J. Slonczewski, Origin of Magnetic Anisotropy in Cobalt-Substituted Magnetite, Physical Review, 110 (1958) 1341–1348

[20] M. Tachiki, Origin of the Magnetic Anisotropy Energy of Cobalt Ferrite, Progress of Theoretical Physics, 23 (1960) 1055–1072

[21] R.M. Bozorth, E.F. Tilden and A.J.Williams, Phys. Rev. 99, 1788 (1955)

[22] A. Muhammad, R. Sato-Turtelli, M. Kriegisch, R. Grossinger, F. Kubel and T. Konegger, J. Appl. Phys. 111, 013918 (2012)

[23] I.C. Nlebedimn, N. Ranvah, P.I. Williams, Y. Melikhov, F. Anayi, J.E. Snyder, A.J. Moses, D.C. Jiles, J. Magn. Magn. Mater 321 (2009) 2528–2532

[24] C. C. H. Lo, A.P.Ring, J.E. Snyder, D.C. Jiles, IEEE Trans. Magn. 41, 3676 (2005)

[25] Kaja Mohaideen K. and Joy P.A. J. Magn. Magn. Mater. 371 121–129 (2014)

[26] Jiquan Wang, Xiuexu Gao, Chao Yuan, Jiheng Li and Xiaoqian Bao, J. Magn. Magn. Mater. 401 662 (2007)

[27] R. W. McCallum, K. W. Dennis, D. C. Jiles, J.E.Synder and Y.H.Chen, Low Temp. Phys. 27, 266 (2001) J. Appl. Phys. 115 (2014) 17A519

[28] B.C.Sekhar, G.S.N.Rao,O.F.Caltun, B.D.Lakshmi, B.P.Rao, P.S.V.S. Rao, J.Magn.Magn. Mater. 398, 59 (2016)

[29] I. C. Nlebedim, M. Vinitha, P. J. Praveen, D. Das and D. C. Jiles, J. Appl. Phys., 113 (2013) 193904

[30] Nalla Somaiah, Tanjore V. Jayaraman, P.A. Joy, Dibakar Das, J. Magn. Magn. Mater. 324 (2012) 2286–2291

[31] J.A.Paulsen, A.P.Ring, C.C.H.Lo, R., J..E.Synder, and D. C. Jiles, J. Appl. Phys. 97, 044502 (2005)

[32] S.H.Song, C.C.H.Lo, S.J.Lee, S.T.Aldini, J..E.Synder, and D. C. Jiles, J. Appl. Phys. 101, 09C517 (2007)

[33] S.J.Lee, C.C.H.Lo, S.H.Song, Y. Melikov, J..E.Synder, and D. C. Jiles, J. Appl. Phys. 102, 073910 (2007)

[34] I. C. Nlebedim, N. Ranvah, Y. Melikhov, P. I. Williams, J. E. Snyder, A. J. Moses, and D. C. Jiles, IEEE Trans. Magn. 45 (2009) 4120-4123

[35] K.K.Mohaideen and P.A. Joy, Curr. Apl. Phys. 13, 1697 (2013)

[36] Anantharamaiah P.N and Joy P.A., J. Mater. Sci. 50 6510-6517 (2015)

[37] Anantharamaiah P.N and Joy P.A., Mater. Lett., 192, 169 (2017)

[38] N. Ranvah, I. C. Nlebedim, Y. Melikhov, J. E. Snyder, D. C. Jiles, A. J. Moses, and S. H. Song, IEEE Trans. Magn. 44, 3013 (2008)

[39] I. C. Nlebedim and D. C. Jiles, Smart Mater. Strut., 24, 025006 (2015)

[40] G.S.N. Rao, O.F.Caltun, K.H.Rao, B.P.Rao, H.L.Wamocha and H.H. Hamdeh, Hyperfine Interact. 184, 179 (2008)

Chapter – 3

Experimental Techniques

In this chapter details of synthesis method and various characterization techniques carried out in this work are reported

3.1. Preparation of samples

In the present study conventional solid state method was used to synthesize the material. A solid state reaction is also called a dry media reaction and has a high reaction rate. Synthesis of polycrystalline ceramic materials using wet chemical solution method increases the better control over particle size, stoichiometry and chemical homogeneity compared to solid state reaction method. But industrial application point of view solid state reaction is the most appropriate method to produce large scale quantity of materials and properties of the material changes when it varies from nano to micron level. By considering it as a major issue, in the present study solid state reaction method was used to synthesize the material. In this method carbonates and oxides precursors are mainly used, hence it is also called as mixed oxide route. The precursors are taken in stoichiometric quantities and ball milled for several hours to achieve better homogeneous mixture of the oxides and reduction in particle sizes and subsequently these precursor powders were heat treated at elevated temperatures for the complete phase formation.

In the present investigation a series of Zr, Ti and Ce-substituted polycrystalline cobalt ferrite samples with nominal compositions, $Co_{1+x}(Zr/Ti)_xFe_{2-2x}O_4$ (where x = 0.0 to 0.4) and $Co_{1+x}Ce_xFe_{2-2x}O_4$ (where x = 0.0 to 0.04) were synthesized by conventional solid-state method using Fe_2O_3, ZrO_2, TiO_2, CeO_2 and Co_3O_4 powders as precursors. These precursor powders in appropriate ratios were subjected to ball milling for 3hrs to ensure proper mixing followed by calcination at 1000°C for 24 hours to impart the phase formation. The calcined powders were subsequently ball milled for 5 hrs to reduce the particle sizes. After repeated calcination and grinding the powders were pressed into pellets using uniaxial compaction in the presence and absence of applied magnetic field. The green samples, after appropriate drying, were sintered at 1300°C for 12 hours in a resistive heating muffle furnace. These sintered pellets were used for further structural and magnetic characterizations.

Calcination: Calcination is a heat treatment method in which the partial or complete phase formation occurs. In this process interaction between the constituents takes place by the inter diffusion of ions and atoms and as a result homogeneous material will be obtained. Calcination parameters are the key factors, which control the shrinkage during sintering.

Calcination temperature must be below the melting point of the material and the yield after calcination consists of a very consistent product in which 70-75% phase will be formed.

Granulation: The process of Calcination increases the particle size and it results in the formation of lumps. . Particle size of calcined powder was reduced via the process of ball milling and it was sieved 2 to 3 times using a mesh to obtain a homogeneous powder. The process in which granules (greater units of powder) are formed from the fine and homogenous size powder is called granulation. This process is very important since the granulated powder has a better flow compared to fine powder and it also adds strength to the compacts. Mixing the fine powder with polymer binder in small quantity resulted in granulated powder. In the present investigation it was achieved by adding 1wt% of polyvinyl alcohol (PVA). Polyvinyl alcohol binds the powder thoroughly and intense mixing forms spherical granules.

Pelletization: The process of application of pressure on granulated powder to form compact pellets is called pelletization. During this process the $CoFe_2O_4$ (CFO) granulated powder was loaded into a die of desired size and shape and then pressed using appropriate pressure in a uniaxial press. Cylindrical pellets of 10mm thickness and 10mm diameter were formed during the process of Pelletization. Green density of pellets is observed to increase with increase in applied pressure, as shown in Fig. 3.1.

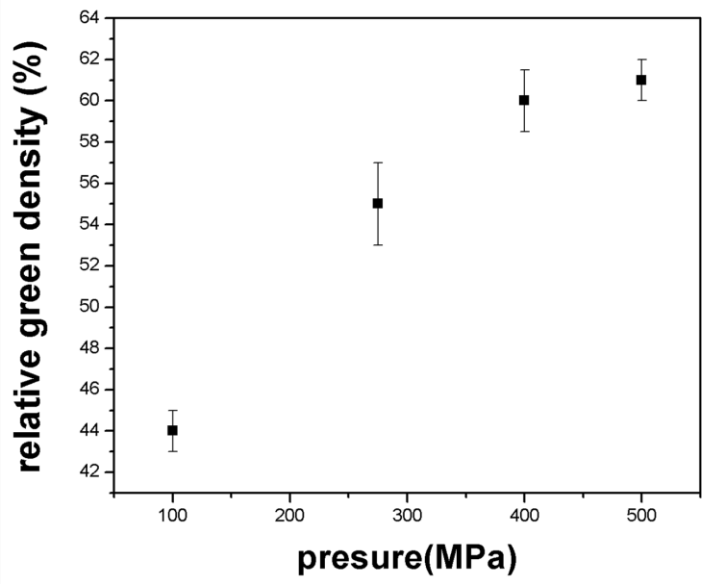

Figure 3.1 Relation between applied pressure and green density of CFO pellets

But as the amount of load is increased beyond a certain point the surface of the pellet begins to crack. This was observed when the applied pressure was increased to 400 to 500 MPa. Since lower applied pressure produces lower green density as observed in fig

3.1, the applied pressure was varied and fixed at a value of 275 MPa to get optimized green density. The required amount of powder was pressed at an optimized pressure of 275MPa for 2-5 minutes using uniaxial press.

Magnetic compaction:

Compaction is one of the key parameters in the processing of CFO and if it is performed in the presence of magnetic field is expected to enhance the magnetic properties. Therefore, one more set of pellets were prepared using the calcined powders of CFO. Required amount of powders were taken in a non-magnetic die and pressed into pellets in the presence of magnetic field (~ 1 Tesla). Magnetic field was applied approximately for 2sec along the axial direction. Schematic of magnetic compaction is shown in Fig. 3.2.

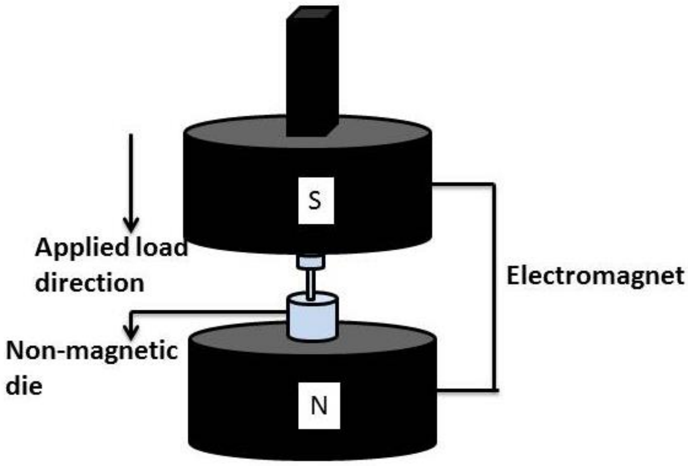

Fig. 3.2. Schematic of magnetic compaction

The Green density of the pellets was measured using the dimensional method after the pellets were dried at 100°C in an oven for 12 hrs. In the dimensional method the average thickness (h) and diameter (2r) of the sample were measured using vernier calipers and weight (m) of the sample was measured by weighing balance. The density of the sample measured by the dimensional method (D_M) can be expressed as,

$$D_M = m/\pi r^2 h \ldots\ldots\ldots(1)$$

Theoretical density of cobalt ferrite was calculated as follows,

The molecular weight of one mole of $CoFe_2O_4$ is ~234.62g, which is used as a base to calculate the theoretical density. Unit cell of spinel lattice consists of eight formula units.

Molecular weight of one $CoFe_2O_4$ molecule = $(234.62/N_A)$ g

Molecular weight of a unit cell (m) = $8 \times (234.62/N_A)$ g,

where 'N_A' is the Avogadro's number. The volume of each unit cell of a spinal ferrite is a^3, where 'a' is the side of a cubic unit cell. Each edge 'a' (A˚) of a cubit unit cell of $CoFe_2O_4$ is 8.37 Å.

Volume (V) = a^3

Density (D_{th}) = m/V = $(8 \times 234.62)/([6.023 \times 10^{23}][8.37]^3 \times [10^{-24}])$

= 5.3 g/cm^3

The ratio of measured density divided by the theoretical density calculated from the structure parameters gives the relative density of the sample.

$$\%\text{Relative density (gm/cm}^3) = (D_M/D_{th}) \times 100 \ldots\ldots\ldots\ldots\ldots\ldots (2)$$

Binder burn out and sintering

The PVA binder, which was used during the process of granulation, is removed from the sample through evaporation by heating the sample. A rapid heating rate results in the development of cracks in the sample and hence the green pellet was initially subjected to slow heating process at 100°C for 12 hrs in a hot air oven. The Binder burn out is then carried out at 500°C for 3 hrs to completely evaporate the PVA out of the sample. The process of sintering should then be carried out as soon as the binder is evaporated. Both grain growth and densification occur during the process of sintering. The process of reducing the porosity of the sample is called densification. The grain boundary motion occurs during the grain growth which resulted in larger grain size. Fig. 3.3 shows the schematic of sintering schedule.

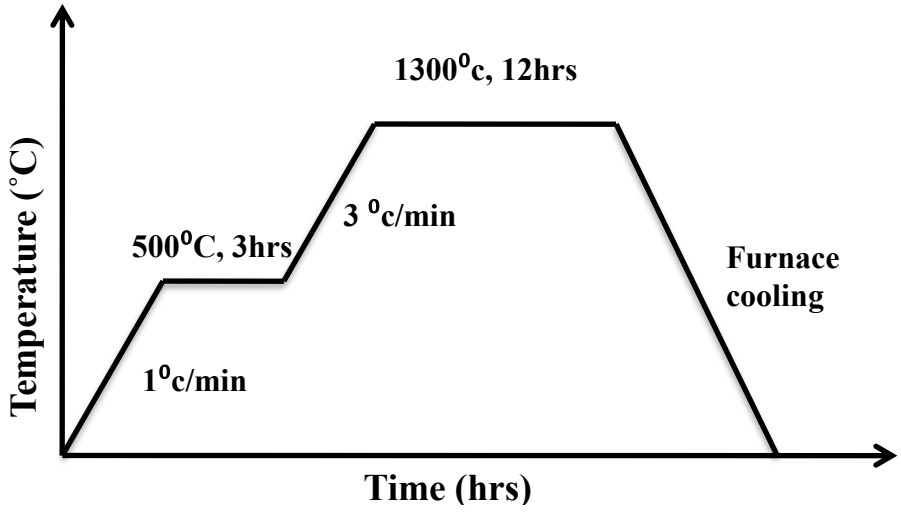

Figure 3.3 Sintering schedule

During the process of sintering atoms diffuse, in the sample from a region of high chemical potential to a region of lower chemical potential. Different sintering mechanisms

cause the atoms to diffuse from one location to another in different paths. These different mechanisms are categorized as densifying and non-densifying mechanisms.

Non-densifying mechanism: Atoms diffusing within the same surface or onto another surface is categorized as non-densifying mechanism. Basically atoms rearrange themselves on the surface without causing the pores to shrink.

- Surface diffusion – Atoms diffuse along the surface of a particle
- Vapor transport – Atoms evaporate and then condense on a different surface
- Lattice diffusion from surface – atoms diffuse from surface through lattice

Densifying mechanism: Atoms moving from the bulk to the surface of the pores is categorized as densifying mechanism. This mechanism increases the density as the porosity of the sample is eliminated.

- Lattice diffusion from grain boundary – atom from grain boundary diffuses through lattice
- Grain boundary diffusion – atoms diffuse along grain boundary
- Plastic deformation – dislocation motion causes flow of matter

Grain growth: The interface or the transition area between adjacent crystallites of same lattice and chemical composition is a grain boundary. Due to the diffusion, the atoms shift positions in the grain boundary thereby having higher energy state compared to atoms in crystal lattice of the grain. Because of the difference in energies of the grain and grain boundaries etching (thermal or chemical) helps in revealing the microstructure of the ceramic samples. Normal grain growth results in microstructure with uniform grain sizes, whereas abnormal grain growth produces microstructure with random sizes of the grains. In the present work sintering has been carried out in fast firing furnace at 1300°C for 12 hrs. Results of sintered sample will be discussed in the following chapter.

Density measurement

Densities of sintered pellets were calculated both by dimensional and Archimedes methods. The geometric sintered density of each cylindrical pellet was calculated on the basis of mass and volume measurements, using a precision balance (accuracy 0.0001 g) and vernier calipers (accuracy 0.01 mm), respectively. Weight of the as sintered sample was taken as Dry weight (D).

The density measurement using Archimedes method is carried out as follows using the ASTM standards (ASTM-C37-C38). The sintered samples were subjected to boiling for 5hours and soaking in distilled water for 24hours. Using density measurement apparatus weights of the sample in air (saturated weight (W)) and water (suspended weight (S)) were measured.

Density = D/(W-S)……...(3)

3.2. Characterization techniques

In the present investigation the sintered pellets were characterized for structural, microstructural and magnetic properties using the methods described below.

3.2.1. X-RAY DIFFRACTION (XRD)

X-ray diffraction technique can be used to determine the crystal structure of crystalline materials and also the information on phase purity can be obtained from the X-ray diffraction pattern. When X-rays interacts with a crystal, the scattering of x-rays occur in all directions. The diffraction is generated, when a large number of scattered rays mutually reinforce each other. The specific condition for diffraction to occur can be described by the well-known Bragg's law, i.e.

$2d \sin\theta = n\lambda$……..(4)

Where 'θ' is the angle between the incident X-ray and the diffraction plane, 'd' and 'λ' are the inter planar spacing and incident X-ray wavelength respectively, and 'n' is an integer corresponding to the order of diffraction. By indexing several sets of diffraction peaks in the XRD spectra, the phase identification is possible in terms of the unique sets of 'd' spacing for a particular material. The process for measuring the lattice parameters by X-ray diffraction is indirect as it is derived from the measured parameters, such as Bragg angle of the diffraction planes. For cubic materials, such as spinel cobalt ferrite, the lattice parameter (a) is proportional to the spacing (d) of any particular set of (hkl) Bragg plane, i.e.

$$a = d\sqrt{h^2 + l^2 + k^2}\,. \quad \text{……..……(5)}$$

By measuring the Bragg angle θ and using the Bragg law $2d\sin\theta = \lambda$ the lattice parameter 'a' can be calculated from equations 4 and 5 mentioned above.

In the present investigation X-ray diffraction pattern of the sintered pellets were recorded on Bruker D8 Advance diffractometer using Cu-k_α radiation of wavelength

1.5406 Å. Cu-k_α radiation with wavelength 1.5406 Å was generated using an acceleration voltage of 40kV and current of 30mA.

Generally, diffraction line broadening has three contributions; instrumental effect, crystallite size and micro strain. Therefore, the total experimental line broadening (β_{exp}) can be expressed as,

$$\beta_{exp} = \beta_{ins} + \beta_{size} + \beta_{strain} \quad \ldots\ldots\ldots\ldots (6)$$

Where β_{exp} is the experimentally measured line broadening, i.e. full width at half maximum of the diffraction peaks (FWHM); β_{ins}, β_{size}, β_{strain} are FWHM due to the instrumental broadening, crystallite (grain) size broadening and strain-induced broadening respectively. The separation of grain-size broadening and strain broadening can be obtained by Williamson-Hall plot. The plot of $\beta\cos\theta$ vs $\sin\theta$ is known as Williamson-Hall plot. If there is no micro strain present in the grain $\beta\cos\theta$ will show no dependence on $\sin\theta$, and thus a flat and linear plot will appear. If strain shows an important contribution to the broadening of diffraction peak, $\beta\cos\theta$ will have a linear dependence on $\sin\theta$, and the strain can be estimated from the slope of the plot. Contribution from instrumental broadening can be eliminated by the following equation,

$$\beta^2 = (\beta_{exp})^2 - (\beta_{ins})^2 \quad \ldots\ldots\ldots\ldots (7)$$

3.2.2. MICROSTRUCTURE ANALYSIS:

Microstructure analysis of the sintered pellets was carried out using HITACHI S-3400N Scanning Electron Microscope (SEM).

Working Principle:

SEM is a microscope that works with electrons (particles with a negative charge) instead of light. Electrons are liberated from a field emission source and accelerated in a high electrical field gradient. Within the high vacuum column these so-called primary electrons are focused and deflected by electronic lenses to produce a narrow scan beam that bombards the object. As a result secondary electrons are emitted from each spot on the object. The angle and velocity of these secondary electrons relates to the surface structure of the object. A detector catches the secondary electrons and produces an electronic signal. This signal is amplified and transformed to a video scan-image that can be seen on a monitor or to a digital image that can be saved and processed further.

Sample Preparation:

Sintered pellets were polished using grade-B alumina slurry (particle size ~ 1µm) and diamond paste (particle size ~ ¼ µm) to get scratch free smooth surface. These polished samples were sonicated using acetone for 20mins. And these samples were thermally etched at 1250˚c for 15mins and then cooling down to room temperature using normal cooling rates. The samples have to be conductive for SEM viewing. The samples were dried thoroughly to get rid of any physically adsorbed water on the sample surface before loading into the SEM chamber. The samples were made conductive by coating them with an extremely thin layer (1.5 - 3.0 nm) of gold or gold-palladium.

3.2.3. Magnetic Properties Measurement

A Quantum design physical property measurement system (PPMS-6000) was used to study the magnetic properties of the samples at different temperatures (~5, 150, 300K) at an applied magnetic field upto ~4000 kA/m. Magnetization was measured on sample size of 2mm x 2mm x 1mm.

(a) Working principle

The vibrating sample magnetometer (VSM) option in PPMS is used to measure magnetization. The working principle of VSM is based on the magnetic induction measurements, involving observation of the voltage induced in a detection coil by a flux change when the applied magnetic field or sample position is changed. According to Faraday's law of electromagnetic induction, the voltage induced is proportional to the rate of change of magnetic flux, i.e.

$$V = d\phi/dt \quad \text{.....(8)}$$

where Φ is the magnetic flux enclosed by the pickup coil. Voltage for a sinusoidally oscillating sample position is given by

$$V = 2\pi fCmA \sin(2\pi ft) \quad \text{.....(9)}$$

Here 'f' and 'A' are the frequency and amplitude of oscillation respectively. 'C' is the coupling constant and 'm' is the DC moment of the sample.

3.2.4. Torque magnetometer:

Anisotropy constant of a crystalline material can be estimated from the torque curves. Torque curve basically represents the torque required to rotate the magnetization direction away from easy axis of magnetization as a function of angle of rotation. Torque curves can be measured using torque magnetometer.

Principle:

In the torque magnetometer a sensitive torsion fiber is used to place the sample in a saturating magnetic field. Other end of torsion fiber is connected to the sensing circuit, which senses the torque produced in the fiber. When the sample is rotated in the magnetic field about the axis passing through its center, the sensing circuit measures the torque developed in the fiber. If the magnetic field is strong enough to saturate the sample, the energy required to rotate the saturation magnetization from its easy direction is known as anisotropy energy. The first derivative of anisotropy energy (E) with respect to angle of rotation(θ) gives the torque (L).

$$L = dE/d\theta \quad \ldots\ldots(10)$$

In the present investigation during the torque measurements were, amplitude of the applied magnetic field was kept constant, whereas the direction was changed from 0° to 360° (clockwise) then back from 360° to 0° (counterclockwise) with a step of 5°.

3.2.5. Magnetoelastic property measurement

The magnetostriction was measured on flat surfaces of samples by using standard strain gauges at room temperature. Magnetostriction setup contains an electromagnet, Hall probe, strain indicator and strain gauge. An external magnetic field of ~800kA/m was applied to the sample and the resultant strain was measured from strain indicator.

Principle

Resistance of metallic material changes when it undergoes dimensional changes. So by measuring the change in resistance the strain developed in the specimen can be estimated, which is the basic principle of strain gauge. Strain gauge is tightly bonded on the specimen to measure the change in length (contraction or elongation). The change in resistance of the strain gauge (ΔR) to the original resistance R is related to the dimensional change (ΔL/L) of the sample,

$$\frac{\Delta R}{R} = \frac{k\,\Delta L}{L} \quad \ldots\ldots(11)$$

Where, k is called gauge factor related to the strain gauge sensitivity, ΔL is change in length, and L is the original gauge length. Change in resistance of strain gauge will be measured using the Bridge circuit. Bridge circuit is built by combination of four resistors and the bridge get balanced when

$$R_1 \times R_3 = R_2 \times R_4 \quad \ldots\ldots(12)$$

In this case irrespective of input voltage (E) output is zero. When one of these resistors is replaced with the strain gauge in the circuit, it loses its balance, hence the output voltage changes.

$$e = \frac{\frac{1}{4}.k.\Delta L}{L.E} \quad \text{.....(13)}$$

by knowing the output voltage the strain produced in the sample can be determined.

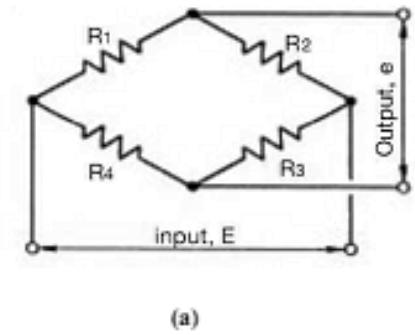

(a)

Fig 3.4 (a) Basic wheat stone bridge

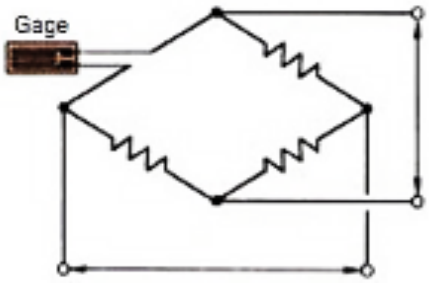

(b)

Fig 3.4 (b) R_1 substituted by strain gauge

3.3. References

[1] Chin, T.S., Hung, M.P., Tsai, D.S., Wu, K.F., Chang, W.C., Compaction and sintering behaviors of a Nd-Fe-B permanent magnet alloy *J. Appl. Phys.* **64**, 5531 (1988)

[2] Cullity, B.D., Graham, C.D., Introduction to Magnetic Materials (2nd ed., Wiley) (New Jersey, 2009)

[3] Srinivas, A., Karthik, T., Gopalan, R., Chandrasekaran, V. Improved magnetoelectricity by uniaxial magnetic field pressed and sintered composites in $BaTiO_3(x)–BaFe_{12}O_{19}(1−x)$ system (x= 0.8, 0.6). *Materials Science and Engineering B* **172**, 289 (2010)

Results and discussion

Effect of non-magnetic ion (Zr and Ti) substitution on structural, magnetic and magnetostrictive properties of cobalt ferrite

Magnetostriction (λ) and its sensitivity to applied magnetic field (dλ/dH) depend mainly on the amount of Co^{+2} ion in the B-site and the super exchange interaction between the A-B sub-lattices in the spinel structure. The valency of the dopants (di-, tri-, tetra-valant), their amount (degree of doping) and site preferences (tetra- or octahedral coordination) largely decide the overall distributions of the cations in the A and B sites of the ferrite crystal structure. Therefore, to study the effect of site preference on magnetic and magnetoelastic properties, substitution of Zr^{+4} and Ti^{+4} ions into CFO lattice, which are known to have preference for tetra and octahedral sites, respectively, have been studied. Chapter 4 describes the structural, magnetic and magnetoelastic properties of Zr^{+4} and Ti^{+4} substituted cobalt ferrite samples and the results have been compared.

4.1. Structural properties

Figures 4.1 and 4.2 show the x-ray diffraction patterns of the sintered Zr and Ti-substituted cobalt ferrite samples ($Co_{1+x}M_xFe_{2-2x}O_4$ ($0 \leq x \leq 0.4$ and M = Zr, Ti)), confirming the single-phase spinel structure except for $x = 0.4$ sample. An overall increase (from ~8.375 Å for $x = 0$ to ~8.392 Å for $x = 0.4$) and decrease (from ~8.375 Å for $x = 0$ to ~8.358 Å for $x = 0.4$) in lattice parameter, as shown in Fig. 4.3, have been observed with progressive substitution of Zr and Ti in the cobalt ferrite lattice, respectively. The lattice parameter obtained for pure cobalt ferrite is in good agreement with reported literature [1].

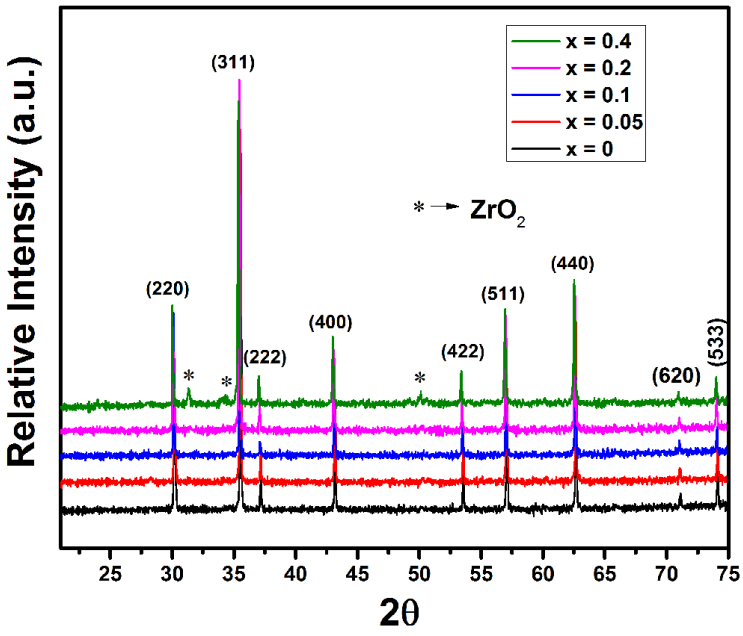

Figure.4.1. X-ray diffraction pattern of $Co_{1+x}Zr_xFe_{2-2x}O_4$ ($0 \leq x \leq 0.4$) sintered at 1300°C for 12 hrs.

$CoFe_2O_4$ is known to have partial inverse spinel structure and the inversion factor depends on sample synthesis method, annealing temperatures and heat treatment schedule [2-7]. Based on the cation distribution in tetra- and octahedral sub lattices, lattice parameter of ferrite material varies [8-11]. Zr^{+4} and Ti^{+4} ions are known to occupy tetrahedral (A) and octahedral (B) sites respectively due to their strong preference for respective coordination [1, 12, 13].

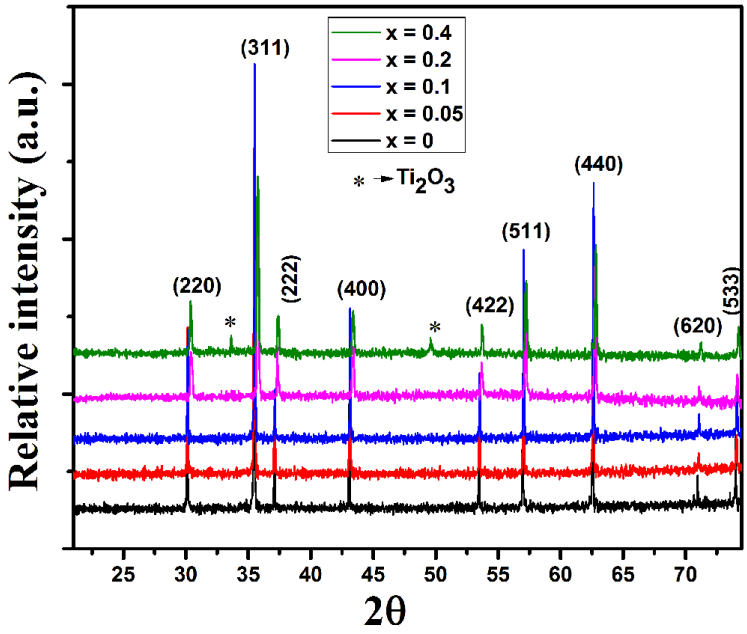

Figure.4. 2. X-ray diffraction pattern of $Co_{1+x}Ti_xFe_{2-2x}O_4$ ($0 \leq x \leq 0.4$) sintered at 1300°C for 12 hrs

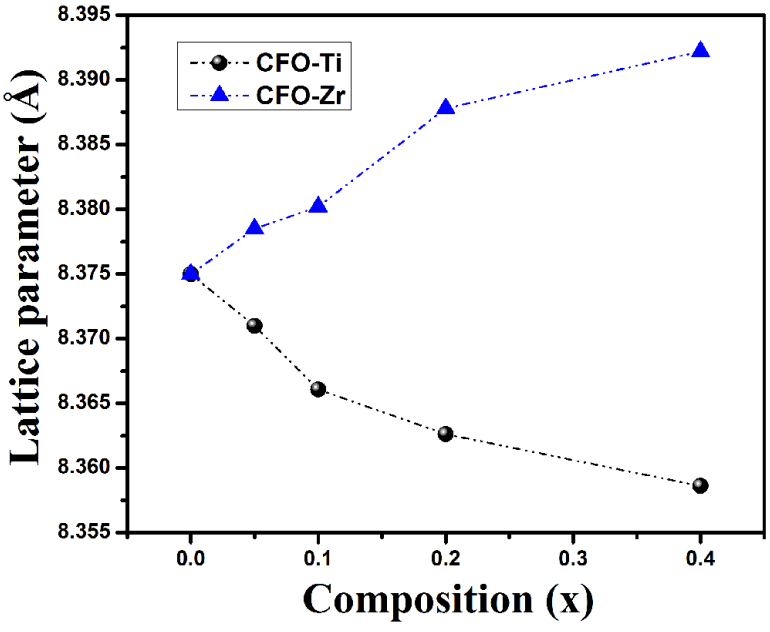

Figure. 4.3. Variation in lattice parameter of $Co_{1+x}(Zr/Ti)_xFe_{2-2x}O_4$ ($0 \leq x \leq 0.4$) samples with respect to temperature and composition.

Lattice parameter of $Co_{1+x}Zr_xFe_{2-2x}O_4$ ($0 \leq x \leq 0.4$) is observed to increase, based on the fact that the ionic radii of Zr^{+4} in tetrahedral co-ordination is greater than those of Fe^{+3} ion with similar coordination. The decrease in lattice parameter for Ti^{+4} substitutions could be due to the smaller ionic radius of Ti^{+4} ion than Fe^{+3} ion in octahedral site. Similar trend in lattice parameter was observed in previously reported literature for Zr and Ti substituted samples [1, 12].

4.2. Microstructural properties

Figure 4.4 and 4.5 shows the SEM images of the polished surface of the sintered $Co_{1+x}M_xFe_{2-2x}O_4$ ($0 \leq x \leq 0.4$ and M = Zr, Ti) samples.

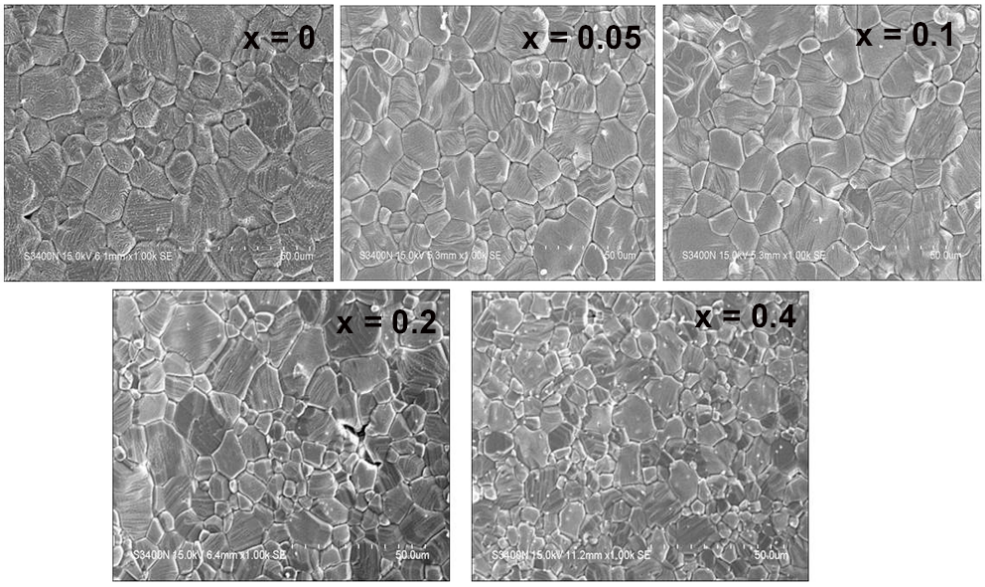

Figure.4.4. Scanning electron micrographs of the sintered pellets of $Co_{1+x}Zr_xFe_{2-2x}O_4$

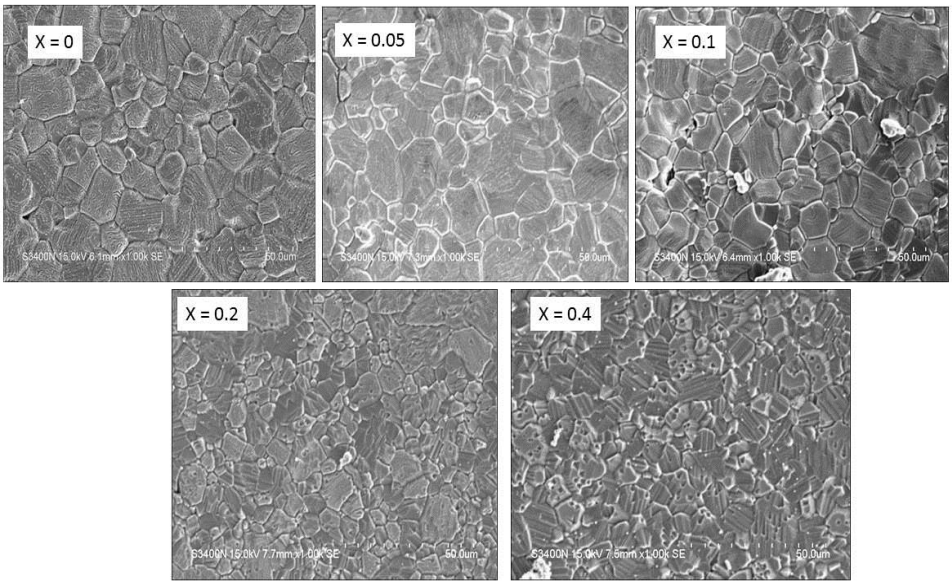

Figure.4.5. Scanning electron micrographs of the sintered pellets of $Co_{1+x}Ti_xFe_{2-2x}O_4$

The average grain sizes estimated using line intercept method of all the Zr and Ti substituted cobalt ferrite samples have been found to be ~ 10 μm, except for x = 0.4 composition of both the dopants. Slight reduction in grain size was observed for $Co_{1.4}M_{0.4}Fe_{1.2}O_4$ (M = Zr, Ti) samples and this could be due to the presence of extra phases ZrO_2 and Ti_2O_3 in the respective samples, which were act as grain growth inhibitors.

4.3. Magnetic properties

Filed dependent M-H hysteresis loops of $Co_{1+x}M_xFe_{2-2x}O_4$ ($0 \leq x \leq 0.4$ and M = Zr, Ti) measured at 5K, 150K and 300K temperatures are shown in Fig. 4.6 and 4.7. As the temperature decreases an expansion in hysteresis curves of all the compositions is observed.

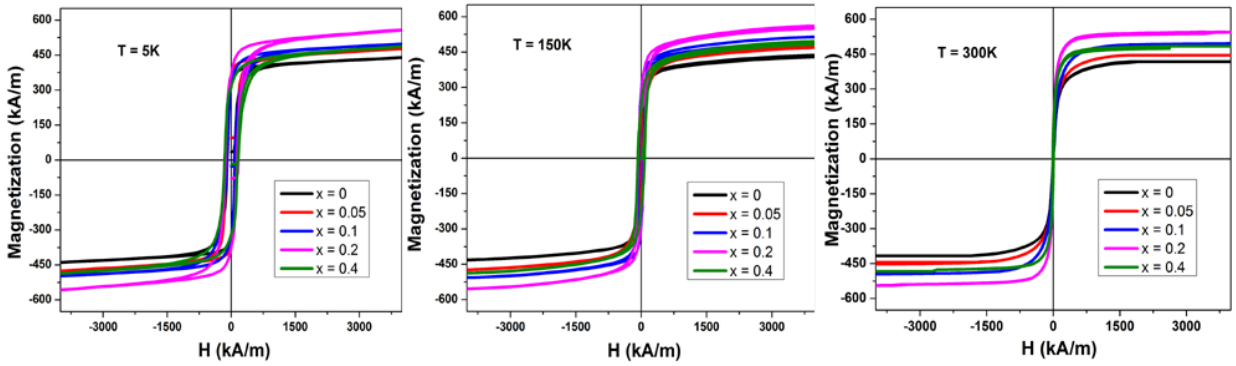

Figure.4.6. Magnetization vs magnetic field plots of Zr substituted $Co_{1+x}Zr_xFe_{2-2x}O_4$ ($0 \leq x \leq 0.4$) samples measured at 5, 150, 300 K.

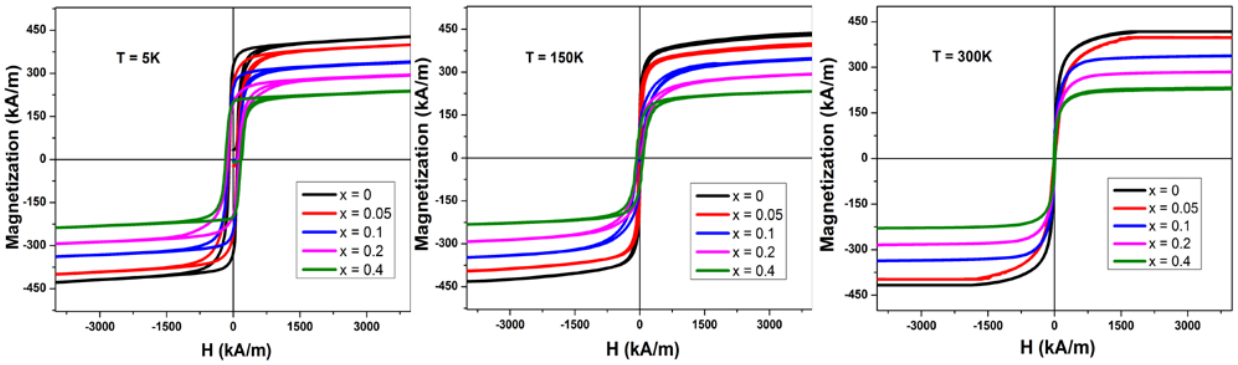

Figure.4.7. The M-H curves of Ti substituted $Co_{1+x}Ti_xFe_{2-2x}O_4$ ($0 \leq x \leq 0.4$) cobalt ferrites measured at 5, 150, 300 K

From the magnetization curves of all the compositions it is observed that, magnetization measured at room temperature (~300K) is seen to approach saturation but at lower temperatures (~150K and ~5K) slight increment in magnetization with increasing magnetic field is observed, which indicates that maximum applied field of ~4000 kA/m is not sufficient to saturate the magnetic moments.

a. Magnetization:

Figure. 4.8 shows the explicit dependence of maximum magnetization (M_{max}), obtained at maximum applied field of ~4000 kA/m, on temperature and composition. From Fig. 4.8. the maximum magnetization (M_{max}) is seen to increase and decrease as the temperature decreases from 300 K to 5 K for all the Zr and Ti substituted samples, respectively. Similar variation in magnetization around ~150 K is observed in the previously reported literature on cobalt ferrite [14].

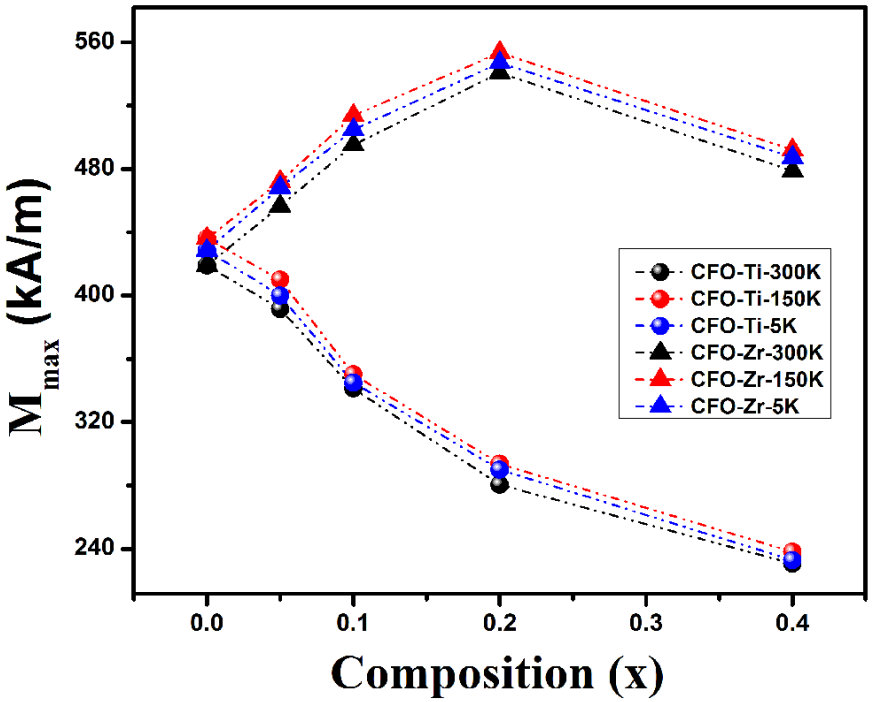

Figure. 4.8. Magnetization of $Co_{1+x}M_xFe_{2-2x}O_4$ ($0 \leq x \leq 0.4$ and M = Ti, Zr) samples as a function of temperature and composition. (Circle and triangle shapes indicate Ti and Zr substitution; black, red and blue colors indicate 300, 150, 5K temperatures, respectively)

As the temperature decreases from ~300 to 150 K, because of the presence of lower thermal energies randomness in the spin alignment decreases, which results in effective alignment of magnetic moment with increasing applied magnetic field at ~150 K. Further decrease in temperature from ~150 to 5 K induces large anisotropies in the system. Martin et.al [15] reported that the second order anisotropy constant K_2 of $CoFe_2O_4$ single crystal increases significantly around 150 K, which consequently changes the easy axis of magnetization from (100) to (111). In this temperature region magnetization behavior can be explained based on two factors, thermal energy and anisotropy energy. Due to the reduced thermal energies at ~5 K temperature, the applied magnetic field is the only key to align magnetic moments against the increased anisotropy energy, resulting in lowering of maximum magnetization (M_{max}).

From Fig. 4.8, M_{max} is observed to increase and decrease as the Zr and Ti concentration increases, respectively. For pure cobalt ferrite maximum magnetization is observed to be ~402 kA/m, this is in agreement with the literature [1]. The overall magnetization in ferrite materials depends on the antiparallel magnetic interaction between the moments of cations in tetrahedral and octahedral sites. Therefore, the net magnetization comes from the difference between the magnetization of the A and B sites. Cobalt ferrite is known to have mixed spinel structure and the magnetic properties of cobalt ferrite material vary based on the site occupancy of different cations in cobalt ferrite lattice [16, 17]. In case of $Co_{1+x}Zr_xFe_{2-2x}O_4$ ($0 \leq x \leq 0.2$) samples, due to the occupancy of non-magnetic Zr^{+4} ions in tetrahedral site, magnetic moment of the respective site is expected to decrease, which in turn resulted in increase in the total magnetic moment with the progressive Zr^{+4} substitution in cobalt ferrite lattice. In case of $Co_{1+x}Ti_xFe_{2-2x}O_4$ ($0 \leq x \leq 0.4$) samples, B-site magnetic moment is expected to decrease because Ti^{+4} ions have strong preference for octahedral site, hence resulted in decrease in net magnetic moment with increasing Ti^{+4} concentration in cobalt ferrite samples. For both the dopants M_{max} is observed to decrease for x = 0.4 composition, which could be due to the presence of extra ZrO_2 and Ti_2O_3 phases in the system.

b. Magneto crystalline anisotropy coefficient:

The magnetocrystalline anisotropy constant (K_1) of the substituted cobalt ferrite samples was determined according to the "Law of Approach" (LoA) to saturation magnetization. In the saturation region with increasing applied magnetic field domain rotation occurs against anisotropy energy. Therefore, the high filed region corresponding to the saturation magnetization can be considered to estimate the first order anisotropy constant. Magnetization processes at an applied field greater than coercive field ($H > H_c$) is expressed by the following equation [18],

$$M = M_S (1- a/H – b/H^2 - . . .) + \kappa H \ldots\ldots\ldots\ldots\ldots\ldots\ldots\ldots (1)$$

where M, M_S and H are the magnetization, saturation magnetization, applied field respectively and κ is the forced magnetization coefficient, which represents the linear increment in spontaneous magnetization at high applied magnetic fields. This forced magnetization term 'κH' can be neglected for the magnetization measurements performed at temperatures far below the Curie temperature. The coefficient 'a' is related to the inclusions and microstress in the system and coefficient 'b' describes the magnetocrystalline anisotropy

of the sample. For the magnetization measurement carried out at ambient temperature and ignoring the contribution of coefficient '*a*', equation (1) can be expressed as,

$$M = M_S (1- b/H^2) \quad \text{(2)}$$

Anisotropy constant was estimated from the M-H data by fitting the LoA in the form of y = mx - c, as given below

$$M/M_s = 1- b/H^2 \quad \text{(3)}$$

Slope of the plot of M/M_s vs $1/H^2$ is equal to the coefficient 'b'. For cubic structured randomly oriented polycrystalline samples, the coefficient '*b*' is given as,

$$b = (8/105) (K_1^2/\mu_0^2 M_S^2) \quad \text{(4)}$$

where μ_0 is the permeability of free space. In the present study '*M*' values corresponding to the applied fields above ~2800 kA/m were used to fit equation (2).

Fitted plots, using equation (3), of $Co_{1+x}M_xFe_{2-2x}O_4$ (x = 0, 0.2 and M = Zr, Ti) compositions are shown in Fig. 4.9. 'K_1' was estimated from equation 4, by equating the slope to the coefficient 'b'.

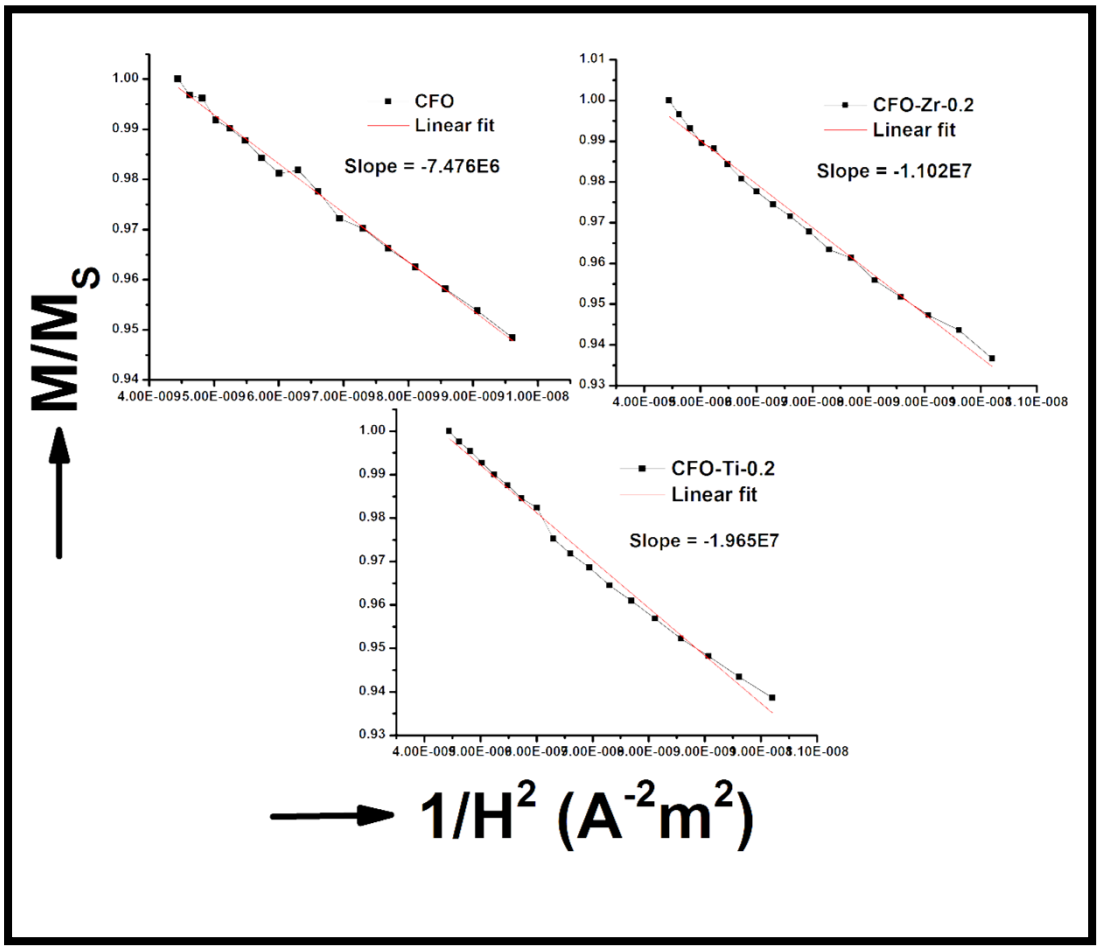

Figure. 4.9. LoA fitted plos of $Co_{1+x}M_xFe_{2-2x}O_4$ (x = 0, 0.2 and M = Zr, Ti) samples

The variation in anisotropy coefficient (K_1), estimated from equations 2 and 3, with respect to temperature and composition is shown in Fig 4.10. K_1 of pure cobalt ferrite (~4.1 x 10^5 J/m^3) estimated from the magnetization curve measured at room temperature (~300 K) is in good agreement with the previously reported literature [1].

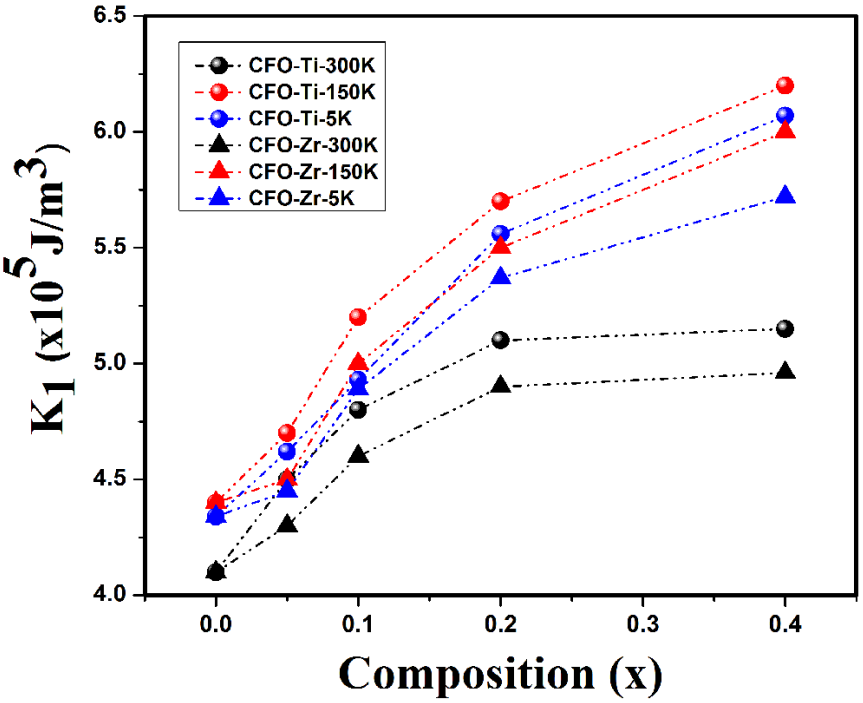

Figure.4.10. Variation of anisotropy constant (K_1) as a function of temperature and composition. (Circle and triangle shapes indicate Ti and Zr substitution; black, red and blue colors indicate 300, 150, 5K temperatures, respectively)

K_1 is observed to increase (~4.45 x 10^5 J/m^3) and decrease (~4.27 x 10^5 J/m^3) with decrease in temperature from ~300 to ~150 K and subsequent decrease from ~150 to 5 K respectively. Similar type of peaking behavior was observed in the reported literature [14]. In general, anisotropy constant has to increase with decrease in temperature due to reduced thermal energies but in the present study it is not in agreement with the expectation. Significant contribution of K_2 around 5 K increases the anisotropy energy; hence the maximum applied field (~4000 kA/m) was insufficient to saturate the magnetic moments. Therefore, the estimated K_1 values from the unsaturated magnetization data around 5 K are not reliable. Similar type of peaking behavior around ~150 K was observed for all Zr and Ti substituted samples.

From Fig. 4.10 the anisotropy constant (K_1) is observed to increase with increase in substitution of Zr^{+4} and Ti^{+4}. Slonczewski [19] proposed that large positive

magnetocrystalline anisotropy of Cobalt ferrite compared to magnetite is ascribed to the presence of Co^{+2} ions at octahedral site of spinel lattice. Tachiki [20] reported that, at lower substitution levels of Co^{+2} in magnetite, it occupies the center of the threefold symmetry (trigonal field) of charge distribution produced by the next nearest neighbor B-site metal ions. In the presence of cubic crystalline field of oxygen neighbor ions ground state energy levels of Co^{+2} ion splits into doubly degenerate dγ levels (d_{x2-y2}, d_{z2}) and triply degenerate dε levels (d_{xy}, d_{yz}, d_{xz}). Due to the distortion of octahedral field in the presence of trigonal field, again these triply degenerate levels splits into singlet (higher energy) and doubly degenerate levels (lower energy). Spin-orbit coupling, which is the main origin of cubic crystalline anisotropy arise from the unquenched orbital angular momentum of Co^{+2} ion in the doubly degenerate level. As the concentration of Co^{+2} ions in B-site increases beyond $x > 0.7$, it further removes the degeneracy because of the crystalline field produced by the randomly distributed Fe^{+3} and Co^{+2} ions in B-site [20]. This subsequently results in quenching of the orbital angular momentum and thereby reduces the cubic crystalline anisotropy. Therefore, the concentration of Co^{+2} ions in B-site is the main key factor to decide the strength of magnetocrystalline anisotropy energy of substituted cobalt ferrite material. In the present investigation anisotropy coefficient is observed to increase with increasing Zr^{+4} and Ti^{+4} substitutions in the CFO lattice. In case of Zr^{+4} substitution, because of its strong preference for tetrahedral site, Fe^{+3} ions are expected to migrate from A- to B-site, which results in lowering of the crystal field distortion and as a consequence increase in magneto crystalline anisotropy is observed. Since Ti^{+4} ions have stronger preference for octahedral site it replaces the Fe^{+3} ions from B to A-site. Along with Ti^{+4} ion Co^{+2} ion prefers to occupy B- site, hence co- substitution of these two ions in CFO lattice increases the Co^{+2} concentration in the B-site. Increase in anisotropy in case of Ti^{+4} substitutions could be due to the increasing Co^{+2} concentrations within the limit of $x > 0.7$ in B-site. This observed variation in K_1 is not in agreement with the reported literature on Ti doped CFO [21]. Anisotropy constant mainly depends on amount of Co^{+2} ions present at B-site, which varies based on the heat treatment temperature and schedule and such study was already reported for pure cobalt ferrite [22, 23]. The difference in heat treatment conditions compared to existing literature may lead to the disagreement with the trend reported in literature.

c. Coercivity:

Figure. 4.11 shows the dependence of coercive field (H_C) on temperature and composition. As the temperature decreases coercivity is observed to increase for all

compositions. Coercivity of a system mainly depends on the anisotropy energy. The observed increase in coercivity could be due to the presence of large anisotropy energy at lower temperatures. From Fig.4.11 it is also seen that the coercive field increases with increasing Zr^{+4} and Ti^{+4} substitutions into CFO lattice. Coercive field for pure cobalt ferrite is observed to be ~4.5 kA/m, this is similar to the previously reported value [1]. The H_C in pure cobalt-ferrite is predominantly due to the single ion anisotropy of Co^{+2} ions in octahedral site. Therefore, increasing concentration of Co^{+2} ion in B-site with the progressive substitution of Zr^{+4} and Ti^{+4} ions lead to increase in magnetocrystalline anisotropy energy as well as coercive field.

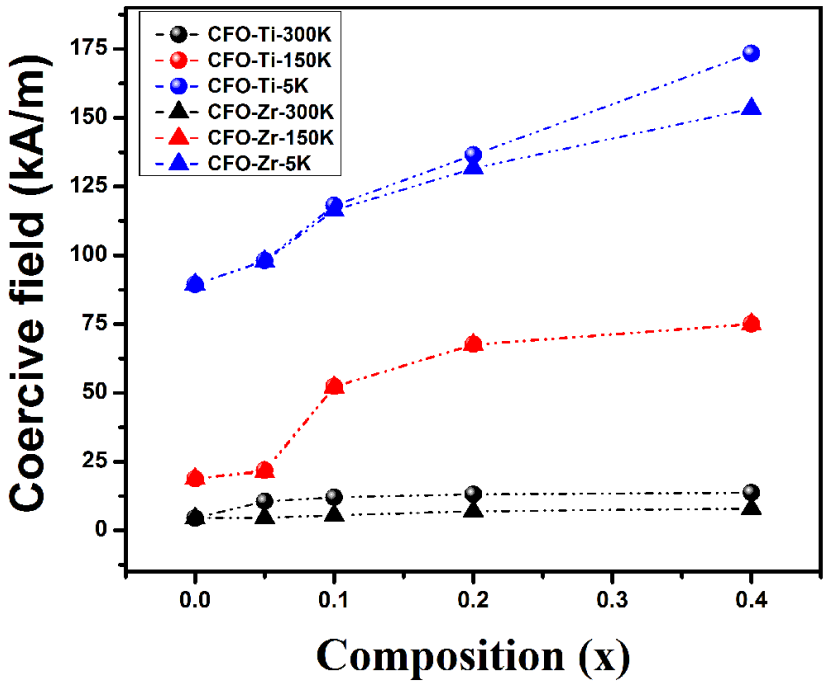

Figure. 4.11. Effect of temperature and composition on coercive field of $Co_{1+x}(Zr/Ti)_xFe_{2-2x}O_4$ ($0 \leq x \leq 0.4$) samples. (circle and triangle shapes indicate Ti and Zr substitution; black, red and blue colors indicate 300, 150, 5K temperatures, respectively)

The difference in reduction in exchange interaction due to the substitution in A and B site of spinel lattice results from the difference in the co-ordination number (C.N.) of ions in these sites. Zr^{+4} ion substitution into the A-sub lattice (C.N. 12) reduces the tetrahedral-octahedral exchange interaction more compared to Ti^{+4} ion substitution into the B- sub lattice (C.N. 6). This results in lower coercive fields for $Co_{1+x}Zr_xFe_{2-2x}O_4$ ($0 \leq x \leq 0.2$) compared to $Co_{1+x}Ti_xFe_{2-2x}O_4$ ($0 \leq x \leq 0.2$) samples at room temperature (~300 K).

As the exchange interaction reduces, spin arrangement will become more non collinear. Therefore, more non collinear spin arrangement is anticipated in Zr^{+4} substituted samples compered to Ti^{+4} substituted CFO. As the temperature decreases (~150 and 5 K) the collinear spin arrangement in a system increases. The superimposed coercive fields for Zr^{+4} and Ti^{+4} substituted systems at ~150 and 5 K, as depicted in Fig. 4.11, could result from similar spin arrangement of these systems at lower temperatures. But, a difference in coercive fields for x = 0.2 and 0.4 samples at ~5K was observed. As the temperature decreases beyond ~10K, the contribution from the second order anisotropy constant, K_2, dominates [20] and influences the magneto crystalline anisotropy constant (K_1). The observed variation in coercive fields for x = 0.2 and 0.4 at 5K could be due to the combined effect of K_1 and K_2.

d. Field sensitivity of magnetization:

Variation in field sensitivity of magnetization (*dM/dH*) obtained by differentiating the low field magnetization data (≤ 20 kA/m) as a function of temperature and composition is shown in Fig. 4.12.

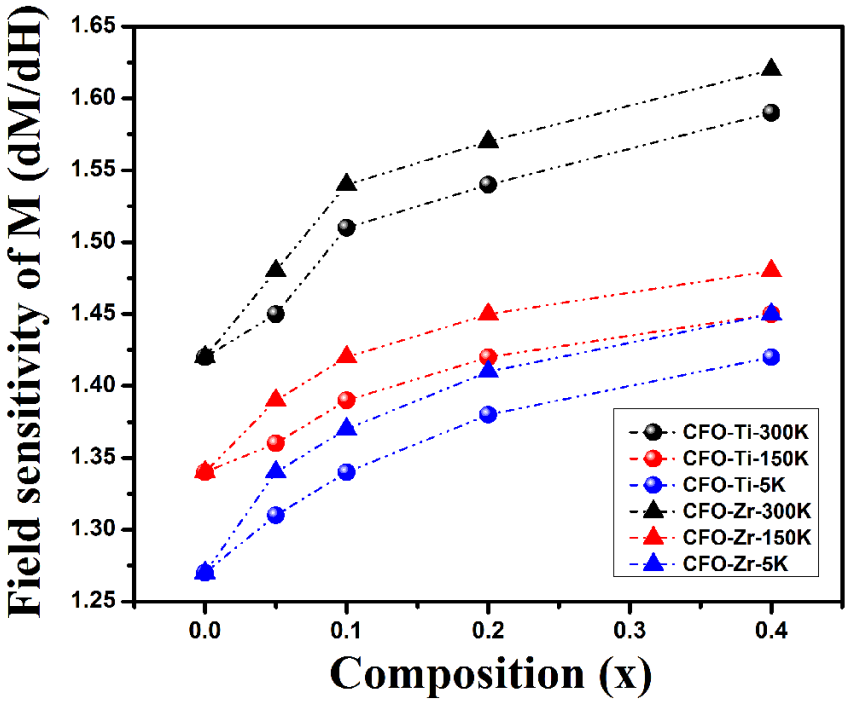

Figure. 4.12. Maximum differential susceptibility of $Co_{1+x}T_xFe_{2-2x}O_4$ ($0 \leq x \leq 0.4$ and T = Ti, Zr) samples at 40kA/m as a function of temperature and composition. (Circle and triangle shapes indicate Ti and Zr substitution; black, red and blue colors indicate 300, 150, 5K temperatures, respectively)

dM/dH indicates the easiness of material response to the applied magnetic field. From Fig. 4.12, *dM/dH* is observed to increase with increase in temperature; this could be due to increased thermal activation energy, which enables magnetic moments to orient easily in the direction of applied magnetic field. Fig. 4.12 also shows that *dM/dH* increases with the increasing substitution of Zr and Ti in the CFO lattice. Low field magnetization behavior is mainly related to the domain wall motion, which explicitly depends on exchange interaction energy [18]. Substitution of non-magnetic Zr^{+4} and Ti^{+4} ions in CFO lattice reduces the strength of the exchange interaction between tetrahedral and octahedral sub lattices. Strength of exchange interaction energy is known to have inverse relation with domain wall thickness. As the exchange interaction energy reduces it increases the domain wall thickness, which in turn decreases the angle between the spins within the wall [18]. Thus, magnetic response of the material increases towards the application of smaller amount of magnetic field.

e. Transition temperature:

Figure.4.13 shows the M-T curves of $Co_{1+x}M_xFe_{2-2x}O_4$ (x = 0, 0.2 and M = Zr, Ti) samples. As the doping concentration up to x = 0.2 reveals single phase structure and showed similar variation in other magnetic properties, hence x = 0.2 doping concentration has been chosen to investigate the magnetic transition temperature.

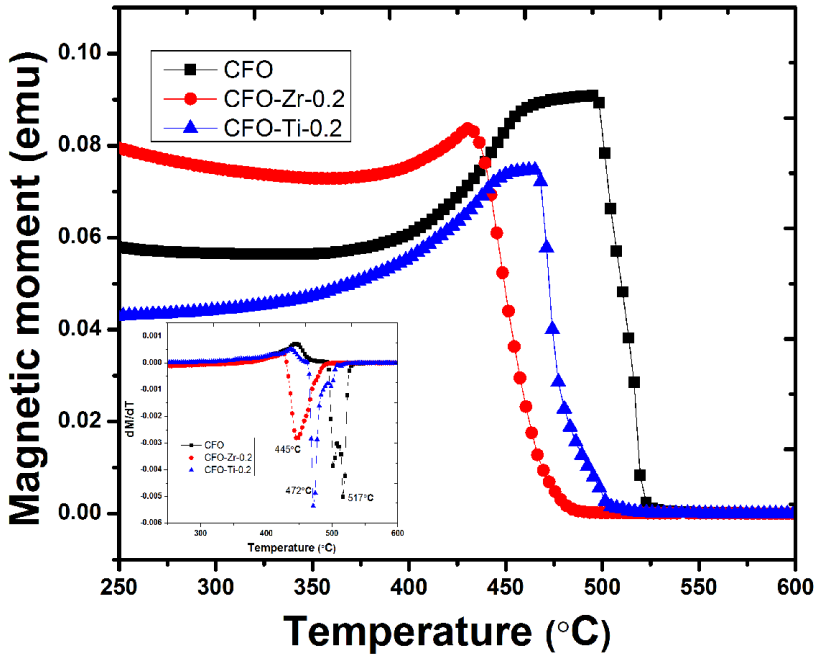

Figure.4.13. Magnetic moment of pure CFO, Zr and Ti doped CFO as a function of temperature, Inset: dM/dT as a function of temperature

Transition temperatures (T_C) were estimated from the plot of first derivative of magnetic moment with respect to temperature and are shown in inset of Fig. 4.13 as a function of temperature. Transition temperatures of $CoFe_2O_4$, $Co_{1.2}Zr_{0.2}Fe_{1.6}O_4$ and $Co_{1.2}Ti_{0.2}Fe_{1.6}O_4$ were observed to be 517, 445 and 472 ˚C. Measured T_C value of pure cobalt ferrite in the present study is in well agreement with the reported value [24]. In the spinel structure metal ions on A-sites are coupled strongly with 12 neighboring metal ions on B sites, while ions on the B-sites have strong exchange interaction with 6 neighboring metal ions in A-site. Therefore, Substitution of non-magnetic Zr^{+4} ions in A-site of CFO lattice is expected to reduce the exchange interaction relatively high compared to the substitution of non-magnetic Ti^{+4} ions in B-site, hence resulted in lower transition temperature for Zr^{+4} substituted samples compared to pure and Ti^{+4} substituted samples.

4.4. Magnetoelastic properties

Magnetostriction (λ) of $Co_{1+x}M_xFe_{2-2x}O_4$ ($0 \leq x \leq 0.4$ and M = Zr, Ti) samples, measured at room temperature, as a function of applied field (H) are shown in Fig. 4.14 and 15.

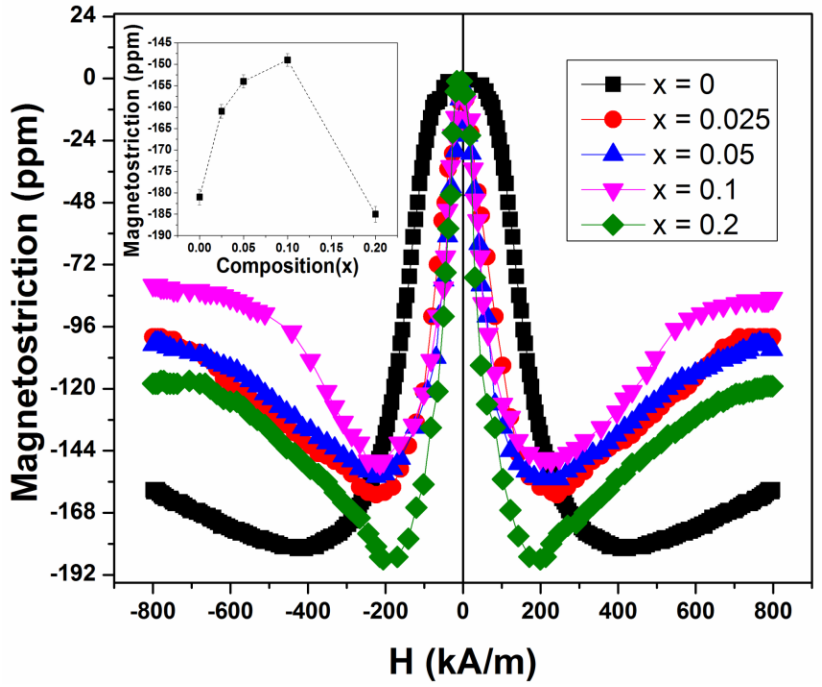

Figure. 4.14. Magnetostriction curves of $Co_{1+x}Zr_xFe_{2-2x}O_4$, ($0 \leq x \leq 0.2$) samples at room temperature. Inset: Variation of magnitude of maximum magnetostriction as a function of composition, x.

As the substitution levels of Zr^{+4} and Ti^{+4} concentrations in the CFO lattice increases, magnetostriction amplitude (λ) is observed to decrease up to $x \leq 0.1$ and increased for x = 0.2

composition and again is seen to decrease for x = 0.4 composition compared to pure CFO, as shown in inset of Fig. 4.14 and 4.15 respectively.

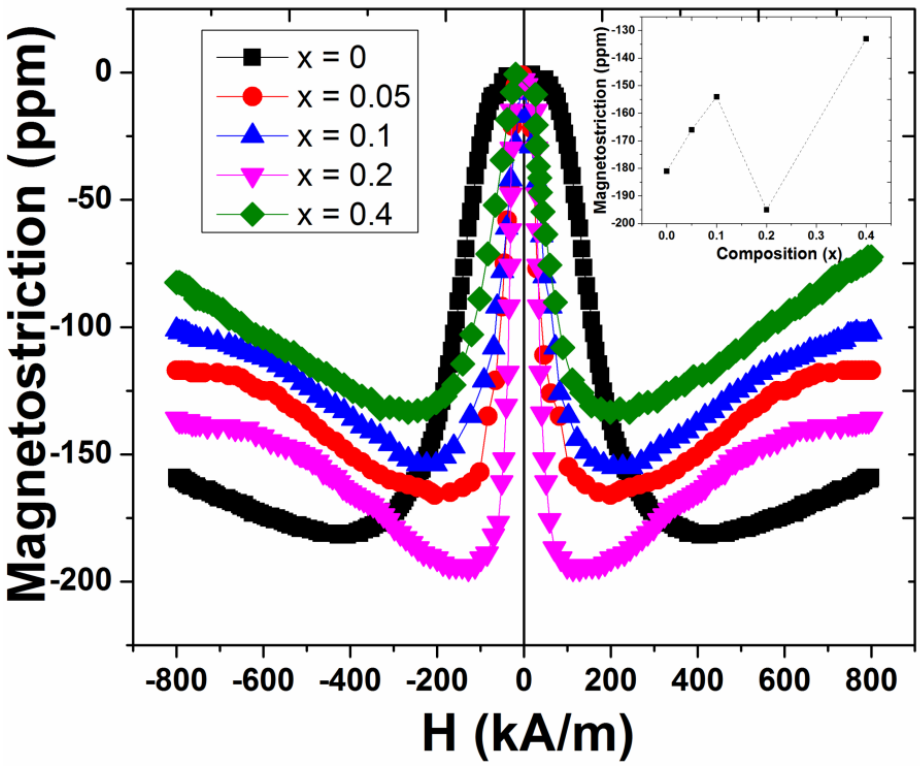

Figure 4.15. Magnetostriction curves of $Co_{1+x}Ti_xFe_{2-2x}O_4$, ($0 \leq x \leq 0.4$) samples at room temperature. Inset: Variation of magnitude of λ_{max} as a function of composition, x.

Maximum magnetostrictions (λ_{max}) of ~ -181, -186 and -195ppm were observed for $CoFe_2O_4$, $Co_{1.2}Zr_{0.2}Fe_{1.6}O_4$ and $Co_{1.2}Ti_{0.2}Fe_{1.6}O_4$ compositions. The λ_{max} of pure cobalt ferrite observed in the present investigation is in good agreement with the reported literature. With increasing concentration of tetravalent ions (Zr^{+4} and Ti^{+4} ions), FWHMs of the magnetostriction curves are observed to decrease, which could be due to the increased filed sensitivity of magnetization (dM/dH) with the substitution of non-magnetic ions into the CFO lattice, as discussed in the earlier section (Fig. 12). Low and high field regions of magnetostriction curve are mainly due to the dominant contribution of domain orientation along [100] and [111] directions, along which it has negative (λ_{100}) and positive magnetostrictions (λ_{111}) respectively.

High filed regions of magnetostriction curves of doped cobalt ferrites are more steeper compared to pure cobalt ferrite, as shown in Fig. 4.13 and 4.14, which indicates that substitution of Zr^{+4} and Ti^{+4} ions into the CFO lattice is increasing the λ_{111} contribution to the overall magnetostriction of the $Co_{1+x}M_xFe_{2-2x}O_4$ (M = Zr, Ti) samples. Tachiki proposed that anisotropy constant increase over a particular substitution level of Co^{+2} ions in B-site of CFO

lattice. Since spin-orbit coupling is the main origin of anisotropy and magnetostriction [25], the observed increase in λ_{max} for $Co_{1+x}M_xFe_{2-2x}O_4$ (x = 0.2 and M = Zr, Ti) samples compared to undoped cobalt ferrite could be due to the presence of optimum level of Co^{+2} ions in B-site of substituted CFO lattice. For x = 0.4 compositions of Zr and Ti substituted cobalt ferrites, due to the presence of extra phases (ZrO_2 and Ti_2O_3 respectively), magnetostriction is observed to decrease

Strain derivative ($d\lambda/dH$) of $Co_{1+x}M_xFe_{2-2x}O_4$ ($0 \leq x \leq 0.4$ and M = Zr, Ti) samples, estimated from the magnetostriction curves, as a function of applied magnetic field are shown in Fig 4.16 and 4.17.

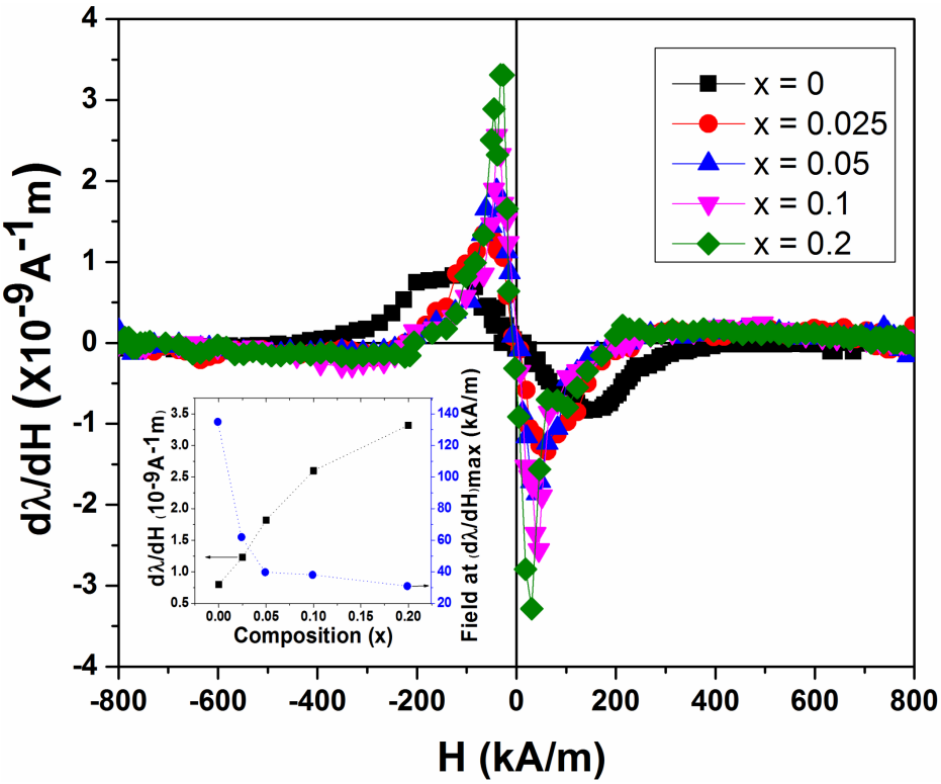

Figure 4.16: Magnetic field (H) dependence of strain derivative ($d\lambda/dH$) for $Co_{1+x}Zr_xFe_{2-2x}O_4$, ($0 \leq x \leq 0.2$) samples. Inset: Variation of maximum strain derivative ($d\lambda/dH$) and field (H) required to achieve that as a function of composition, x.

For both the series of samples $(d\lambda/dH)_{max}$ is observed to increase with increasing concentrations of Zr and Ti from x = 0 to x = 0.2, as shown in inset of Fig. 4.16 and 17, this could be due to the reduced exchange interaction strength between the cations in tetra and octahedral sub lattices with the substitution of non-magnetic ions (Zr^{+4} and Ti^{+4}) into the CFO lattice. Decrease in strain derivative observed for x = 0.4 composition of both the substituents could be due to the presence of extra phases (ZrO_2 and Ti_2O_3) at grain boundaries, as shown micrographs, which hindrances the domain wall motion. A remarkable

300 and 345 % enhancement in dλ/dH has been observed for $Co_{1.2}Zr_{0.2}Fe_{1.6}O_4$ and $Co_{1.2}Ti_{0.2}Fe_{1.6}O_4$ compositions respectively, compared to pure cobalt ferrite.

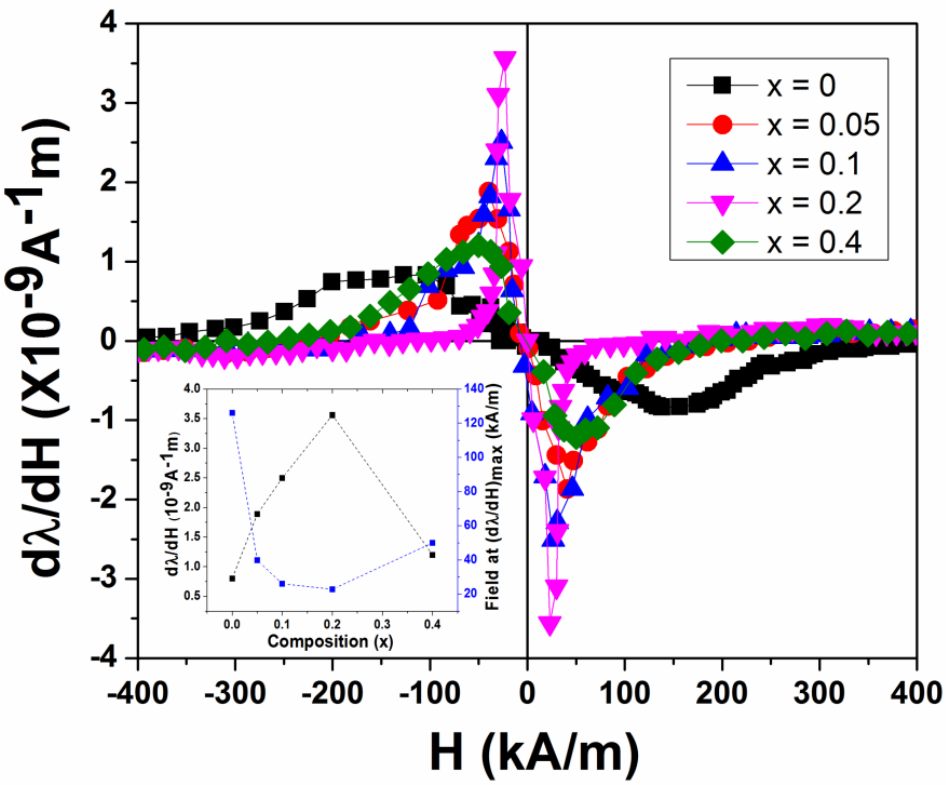

Figure 4.17. Magnetic field (H) dependence of piezomagnetic coefficient (dλ/dH) for $Co_{1+x}Ti_xFe_{2-2x}O_4$, ($0 \leq x \leq 0.4$) samples; Inset: Variation of maximum strain derivative (dλ/dH) and field (H) required to achieve that as a function of composition, x.

From the inset of Fig. 4.16 and 17, it is also observed that, along with increase in strain sensitivity, field required to achieve maximum strain sensitivity is found to decrease with increasing substitution levels of Zr and Ti in the CFO lattice, which is the main requirement for stress sensor applications. In the low field region magnetization process takes place mainly through domain wall motion, which depends on exchange interaction strength. Since exchange interaction energy is inversely related to domain wall thickness, reduction in strength of exchange interaction with Zr and Ti ions substitution increases the domain wall thickness, which in turn reduces the angle between the spin moments. Thus, the amount of filed required to get $(d\lambda/dH)_{max}$ decreases.

4.5. Conclusion:

- Transition temperatures (T_C) of $CoFe_2O_4$, $Co_{1.2}Zr_{0.2}Fe_{1.6}O_4$ and $Co_{1.2}Ti_{0.2}Fe_{1.6}O_4$ samples were observed to be 517, 445 and 472 ˚C, respectively.
- Maximum magnetostrictions (λ_{max}) and strain sensitivity ($d\lambda/dH$) of ~ -186 ppm and ~ 3.32 x 10^{-9} $A^{-1}m$ were observed for $Co_{1.2}Zr_{0.2}Fe_{1.6}O_4$ composition. ~300% increase in $d\lambda/dH$ is observed for $Co_{1.2}Zr_{0.2}Fe_{1.6}O_4$ compared to $CoFe_2O_4$ (~ 0.8 x 10^{-9} $A^{-1}m$).
- Approximately 8 and 345% increase in maximum magnetostriction (λ_{max}) and strain sensitivity ($d\lambda/dH$) is observed for $Co_{1.2}Ti_{0.2}Fe_{1.6}O_4$ (~ -195 ppm and ~3.56 X 10^{-9} $A^{-1}m$) compared to $CoFe_2O_4$ (~ -195 ppm and ~ 0.8 x 10^{-9} $A^{-1}m$).

4.6. References:

[1] Vinitha Reddy Monaji, Dibakar Das, Influence of Zr doping on the structural, magnetic and magnetoelastic properties of cobalt-ferrites, J. Alloys Compd. 634 (2015) 99–103

[2] S. D. Bhame and P. A. Joy, Enhanced magnetostrictive properties of Mn substituted cobalt ferrite $Co_{1.2}Fe_{1.8}O_4$, J. Appl. Phys. 99 (2006) 073901

[3] K. Kriebel, C. C. H. Lo, Y. Melikhov and J. E. Snyder, Investigation of Cr substitution in Co ferrite $(CoCr_xFe_{2-x}O_4)(CoCr_xFe_{2-x}O_4)$ using Mossbauer spectroscopy, J. Appl. Phys. 99 (2006) 08M912

[4] Y. Melikhov, J. E. Snyder, D.C. Jiles, A. P. Ring, J. A. Paulsen, C. C. H. Lo and K. W. Dennis, Temperature dependence of magnetic anisotropy in Mn-substituted cobalt ferrite, J. Appl. Phys. 99 (2006) 08R102

[5] Nalla Somaiah, Tanjore V. Jayaraman, P.A. Joy, Dibakar Das, Magnetic and magnetoelastic properties of Zn-doped cobalt-ferrites—$CoFe_{2-x}Zn_xO4$(x = 0, 0.1, 0.2, and 0.3), J. Magn. Magn. Mater. 324 (2012) 2286–2291

[6] W. Bayoumi, Structural and electrical properties of zinc-substituted cobalt ferrite, J. Mater. Sci. 42 (2007) 8254-8261

[7] M. R. De Guire, R. C. O'Handley and G. Kalonji, The cooling rate dependence of cation distributions in $CoFe_2O_4$, J. Appl. Phys. 65 (1989) 3167

[8] I. C. Nlebedim, M. Vinitha, P. J. Praveen, D. Das and D. C. Jiles, Temperature dependence of the structural, magnetic, and magnetostrictive properties of zinc-substituted cobalt ferrite, J. Appl. Phys., 113 (2013) 193904

[9] S. H. Song, C. C. H. Lo, S. J. Lee, S. T. Aldini, J. E. Snyder, and D. C. Jiles, Magnetic and magnetoelastic properties of Ga-substituted cobalt ferrite, J. Appl. Phys. 101 (2007) 09C517

[10] I. C. Nlebedim, N. Ranvah, Y. Melikhov, P. I. Williams, J. E. Snyder, A. J. Moses, and D. C. Jiles, Magnetic and Magnetomechanical Properties of $CoAl_xFe_{2-x}O_4$ for Stress Sensor and Actuator Applications, IEEE Trans. Magn. 45 (2009) 4120-4123

[11] N. Ranvah, I. C. Nlebedim, Y. Melikhov, J. E. Snyder, A. J. Moses, P. I. Williams, and D. Jiles, Temperature Dependence of Magnetostriction of $Co_{1+x}Ge_xFe_{2-2x}O_4$ for Magnetostrictive Sensor and Actuator Applications, IEEE Trans. Magn. 44 (2008) 3013

[12] I. C. Nlebedim, K. W. Dennis, R. W. McCallum and D. C. Jiles, Structural and magnetic properties of Ti4+/Co2+ co-substituted cobalt ferrite, J. Appl. Phys. 115 (2014) 17A519

[13] S. K. Banerjee, W. O'Reilly, T. C. Gibb, and N. N. Greenwood, The behaviour of ferrous ions in iron-titanium spinels, J. Phys. Chem. Solids 28 (1967) 1323

[14] Sateesh Prathapani, Tanjore V. Jayaraman, Eswara K. Varaprasadarao and Dibakar Das, Structural and ambient/sub-ambient temperature magnetic properties of Er-substituted cobalt-ferrites synthesized by sol-gel assisted auto-combustion method, J. Appl. Phys., 116 (2014) 023908

[15] M. Kriegisch, W. Ren, R. Sato-Turtelli, H. Muller, R. Grossinger and Z. Zhang, Field-induced magnetic transition in cobalt-ferrite, J. Appl. Phys. 111 (2012) 07E308

[16] I.C. Nlebedimn, N. Ranvah, Y. Melikhov, P.I. Williams, J.E. Snyder, A.J. Moses, and D.C. Jiles, Effect of temperature variation on the magnetostrictive properties of $CoAl_xFe_{2-x}O_4$, J. Appl. Phys. 107 (2007) 09C517

[17] L. Ben Tahar, A. Artus, S. Ammar, L. S. Smiri, F. Herbst, M. J. Vaulay, V. Richard, J. M. Greneche, F. Villian and F. Fievet, Magnetic properties of $CoFe_{1.9}RE_{0.1}O_4$ nanoparticles (RE=La, Ce, Nd, Sm, Eu, Gd, Tb, Ho) prepared in polyol, J. Magn. Magn. Mater. 320 (2008) 3242-3250

[18] B.D. Cullity and C.D. Graham, Introduction to Magnetic Materials, 2nd ed., (Wiley/IEEE, New Jersey, USA, 2009)

[19] J. Slonczewski, Origin of Magnetic Anisotropy in Cobalt-Substituted Magnetite, Physical Review, 110 (1958) 1341–1348

[20] M. Tachiki, Origin of the Magnetic Anisotropy Energy of Cobalt Ferrite, Progress of Theoretical Physics, 23 (1960) 1055–1072

[21] I.C. Nlebedimn and D.C. Jiles, Thermal effects on the magnetic properties of titanium modified cobalt ferrite, J. Appl. Phys. 117 (2015) 17A506

[22] I.C. Nlebedimn, N. Ranvah, P.I. Williams, Y. Melikhov, J.E. Snyder, A.J. Moses, D.C. Jiles, Effect of heat treatment on the magnetic and magnetoelastic properties of cobalt ferrite, J. Magn. Magn. Mater 322 (2010) 1929–1933

[23] I.C. Nlebedimn, N. Ranvah, P.I. Williams, Y. Melikhov, F. Anayi, J.E. Snyder, A.J. Moses, D.C. Jiles, Influence of vacuum sintering on microstructure and magnetic properties of magnetostrictive cobalt ferrite, J. Magn. Magn. Mater 321 (2009) 2528–2532

[24] S. J. Lee, C. C. H. Lo, P. N. Matlage, S. H. Song, Y. Melikhov, J.E. Snyder, D.C. Jiles, Magnetic and magnetoelastic properties of Cr-substituted cobalt ferrite, J. Appl. Phys. 102 (2007) 073910

[25] I. C. Nlebedim, M. Vinitha, P. J. Praveen, D. Das and D. C. Jiles, Jiles, Temperature dependence of the structural, magnetic, and magnetostrictive properties of zinc-substituted cobalt ferrite, J. Appl. Phys., 113 (2013) 193904

Chapter – 5

Results and discussion

Effect of non-magnetic ion (Zr and Ti) substitution and magnetic field assisted compaction on structural, magnetic and magnetostrictive properties of cobalt ferrite

Substitution of non-magnetic ion reduces the A-B sub lattice exchange interaction, which is known to influence the field dependent magnetization and in turn the strain sensitivity of the system. Presence of induced uniaxial anisotropy in a system enhances the magnetostriction, which has been observed in case of magnetic annealing. In this chapter magnetic compaction, which is routinely used to produce permanent magnets, has been used to induce uniaxial anisotropy in the substituted cobalt ferrites. Chapter 5 describes the structural, magnetic and magnetoelastic properties of magnetically compacted Zr^{+4} and Ti^{+4} substituted cobalt ferrites and the results were compared.

5.1. Structural properties

Figure 5.1(a) and (b) show the x-ray diffraction spectra (θ/2θ scan) of the magnetically compacted and sintered Zr and Ti-substituted cobalt ferrite samples ($Co_{1+x}M_xFe_{2-2x}O_4$ ($0 \leq x \leq 0.4$ and M = Zr, Ti), confirming the single-phase cubic spinel structure as revealed by the different crystallographic planes.

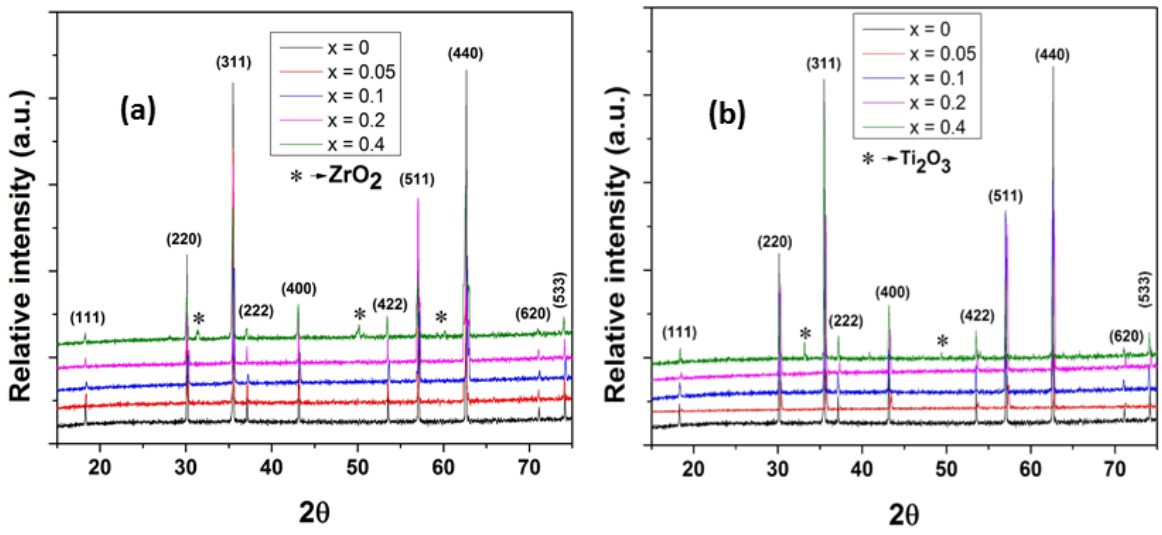

Figure 5.1: (a) and (b) X-ray diffraction spectra of sintered $Co_{1+x}M_xFe_{2-2x}O_4$ (M = Zr, Ti; $0 \leq x \leq 0.4$)-MC samples

An overall increase and decrease in lattice parameter, from ~8.375 Å for x = 0 to ~8.397 Å for x = 0.4 and ~8.375 Å for x = 0 to ~8.337 Å for x = 0.4 as shown in Fig. 5.2(a) and (b), has been observed with progressive Zr and Ti substitution in the cobalt ferrite lattice respectively. $CoFe_2O_4$ has partially inversed spinel structure and the inversion factor, which depends on the synthesis method and annealing temperature is expected to affect the lattice parameter. O'Neill and Navrotsky reported [1] the calculated lattice parameters of $(Co^{+2})[Fe^{+3}]O_4$ and $(Fe^{+3})[Co^{+2}Fe^{+3}]O_4$ as 8.4091 Å and 8.3702 Å

respectively. Sawatzky et al. [2] estimated the cation distribution of $CoFe_2O_4$ from mÖssbauer spectroscopy and reported it as $(Co_{0.3}^{+2}Fe_{0.7}^{+3})[Co_{0.7}^{+2}Fe_{1.3}^{+3}]O_4$.

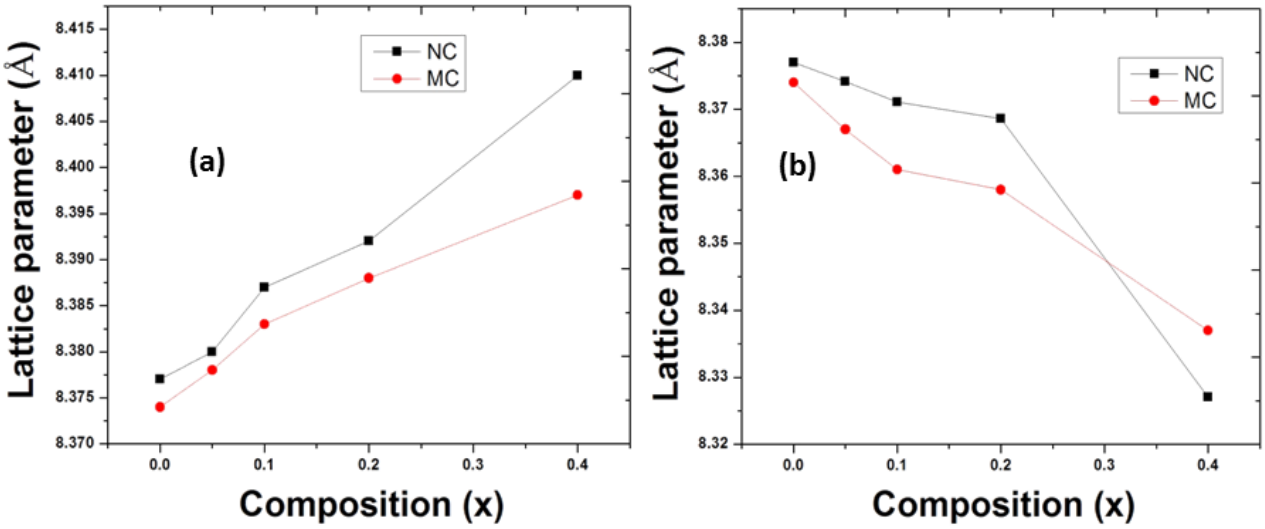

Figure.5.2. (a) and (b) The variation of lattice parameter as a function of Zr and Ti substitution, x and their comparison with normal compacted samples

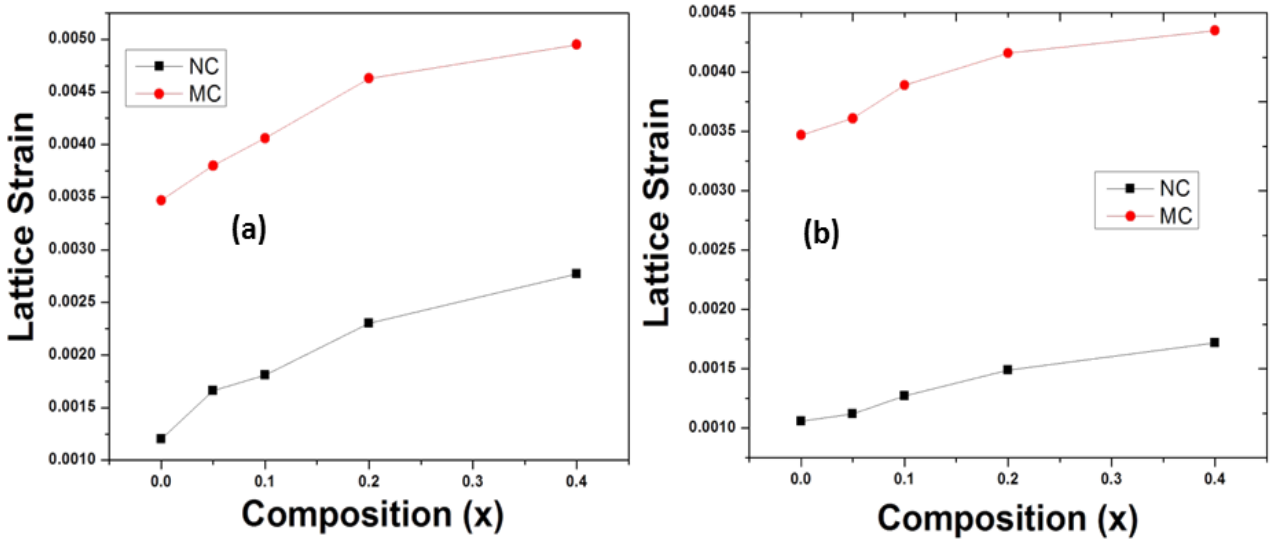

Figure 5.3. (a) and (b) The variation of lattice strain as a function of Zr and Ti substitution, x and their comparison with normal compacted samples

The lattice parameter obtained in this investigation (~ 8.3826 Å) is in excellent agreement with the value calculated by O'Neill and Navrotsky. Since Zr^{+4} and Ti^{+4} ions have strong preference for tetrahedral and octahedral coordination, they prefer to occupy the respective sites [3]. The observed increase and decrease in lattice parameter with progressive substitution of Zr^{+4} and Ti^{+4} ions in CFO lattice could be due to the fact that the ionic radius of Zr^{+4} and Ti^{+4} in tetrahedral and octahedral co-ordination, respectively,

is greater and smaller than those of Fe^{+3} ion with similar coordination numbers. Based on the calculated lattice parameters reported in ref.2, the increasing non-linearity in lattice parameters after x = 0.1 for normally compacted Zr^{+4} and Ti^{+4} substituted CFO samples, could be due to the occupation of more Co^{+2} ions in tetrahedral site of spinel lattice.

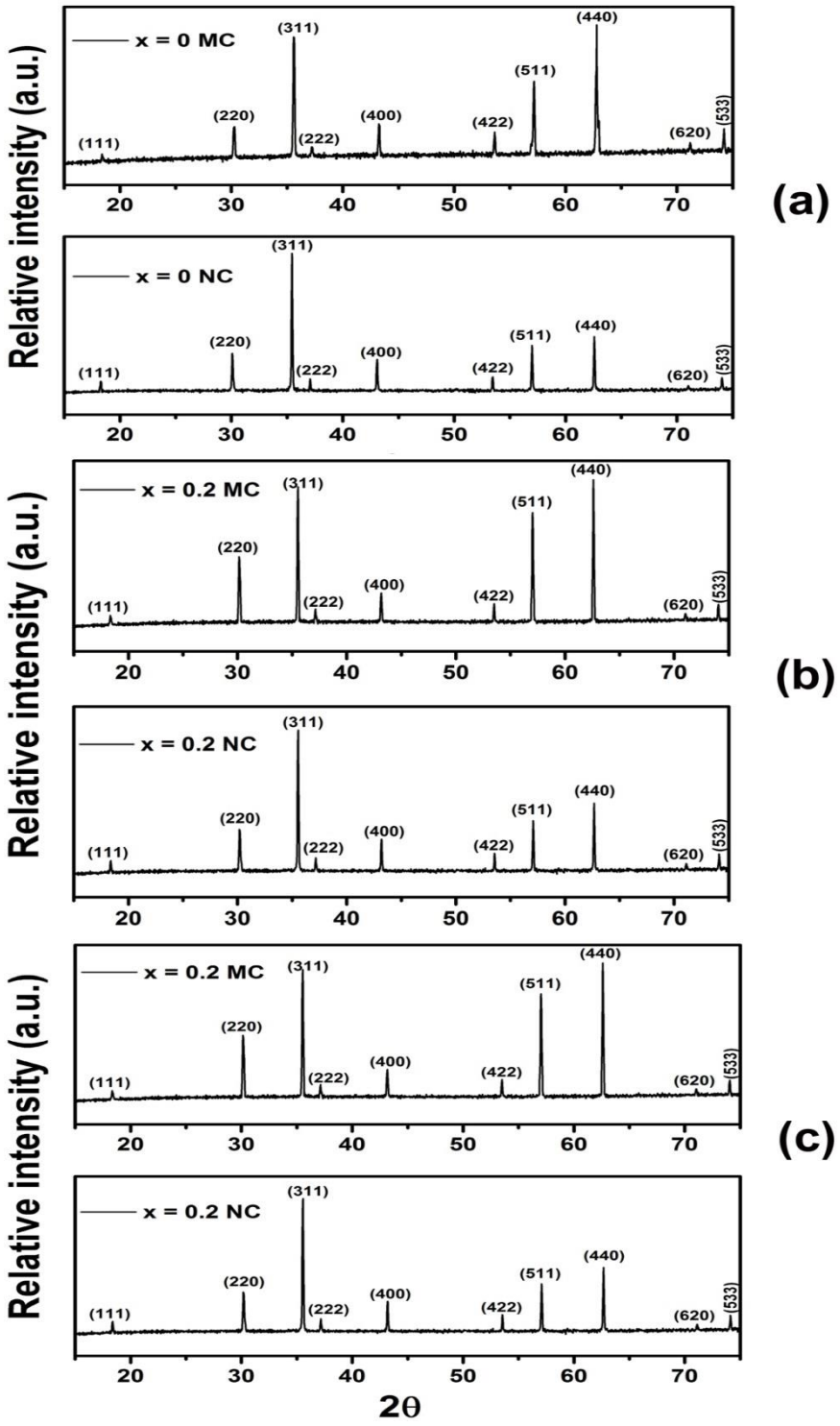

Figure 5.4. (a), (b) and (c) XRD patterns of NC and MC x = 0 and 0.2 compositions of Zr and Ti substituted cobalt ferrites

The lattice strain in $Co_{1+x}M_xFe_{2-2x}O_4$ (where x = 0.0 to 0.4, M = Zr, Ti) ceramic sample was estimated using the Williamson–Hall relation [4, 5]. The lattice strain was observed to increase with Zr and Ti substitution as shown in Fig. 5.3(a) and (b) respectively, which could be due to the difference in ionic radii of Zr^{+4} and Ti^{+4} ions compared to Co^{+2} and Fe^{+3} ions. Lattice parameter is observed to decrease and micro strain seems to increase in the magnetically pressed samples compared to normal compacted samples (reported in our earlier studies) as shown in Fig. 5.2 and 5.3 [6]. This observation confirms that there is a compressive strain present in the field assisted compacted samples [7]. From the comparison of XRD patterns of magnetic field and normal pressed x = 0 and 0.2 compositions of Zr^{+4} and Ti^{+4} substituted CFO samples, as shown in Fig. 5.4(a), (b), and (c) respectively, increase in intensity of the Bragg reflections is observed for (220), (511) and (440) planes in the magnetic field pressed sample, which indicates the formation of texture along those respective planes. The effect of texture on magnetostriction will be discussed in the respective section.

5.2. Microstructural properties

The SEM images of the sintered Zr and Ti substituted cobalt ferrite ($Co_{1+x}M_xFe_{2-2x}O_4$ ($0.0 \leq x \leq 0.4$), M = Zr, Ti) samples are shown in Fig. 5.5 and 5.6. Figures 5(a) and (b) represent the microstructures of normally and magnetically pressed (NC and MC respectively) pure cobalt ferrite samples. The average grain sizes, as estimated from the line intercept method, have been found to be around ~10 and 20 μm for CFO-NC and CFO-MC samples, respectively. In general, in the compacted samples some preferred orientation should take place at right angles to the direction of compaction [8]. In the case of samples compacted in presence of magnetic field, along with the effect of compaction, domains in the particles get aligned in the direction of the magnetic field and because of the high agglomeration of single domain particles during the pressing operation high green density was achieved, which resulted in high sintered density and increased grain growth compared to those obtained from normal compacted samples. With increasing Zr^{+4} and Ti^{+4} concentrations not much difference in the grain size was observed except for x = 0.4 composition of both the substituted CFO samples, as shown in Fig. 5.5 and 5.6. The observed decrease in grain size for x = 0.4, could be due to the presence of extra ZrO_2, Ti_2O_3 phases in the matrix, which impedes the grain growth.

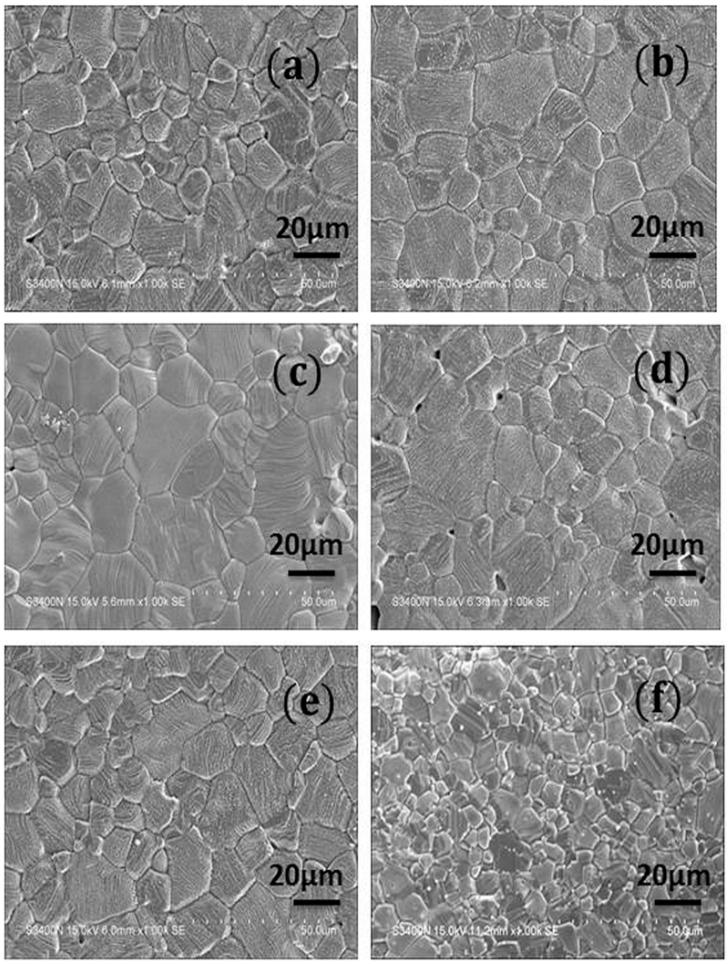

Figure 5.5: (a) and (b) SEM images of the NC and MC sintered cobalt ferrite samples respectively; (c), (d), (e), (f) Scanning electron micrographs of sintered pellets of x = 0.05, 0.1, 0.2, 0.4 samples respectively

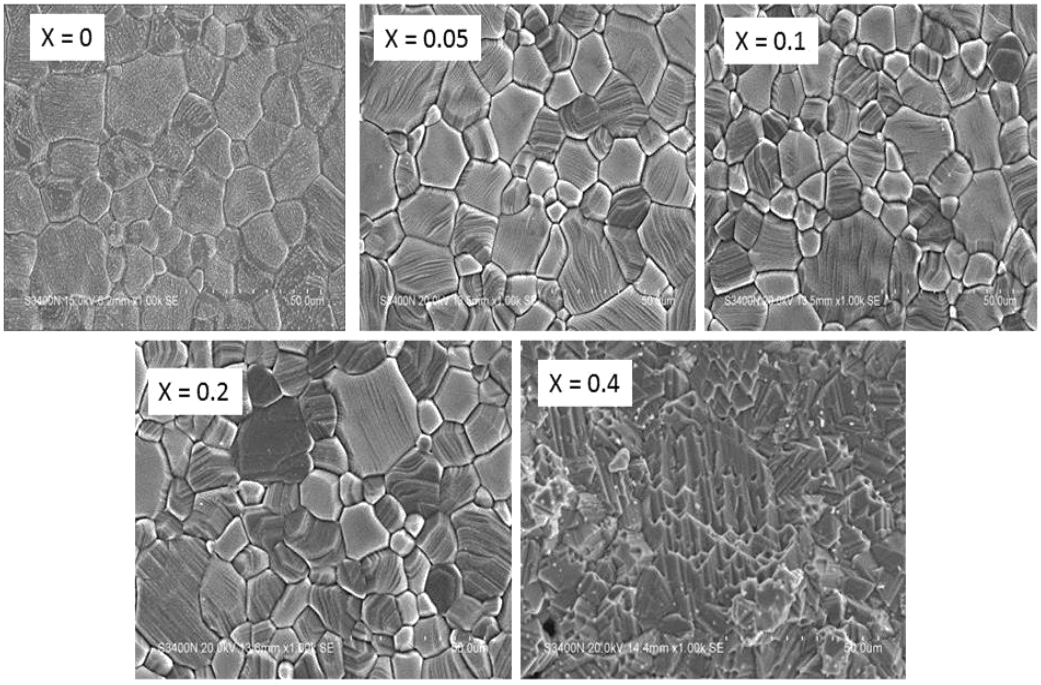

Figure 5.6. (a) to (e) Scanning electron micrographs of the MC sintered Ti- substituted cobalt ferrite samples respectively

5.3. Magnetic Properties

a. Magnetization:

Figure.5.7 shows the hysteresis loops of normally and magnetically pressed $CoFe_2O_4$ samples. Qualitative descriptions of domain alignment during magnetic pressing are shown schematically in Fig. 5.8. Direction of magnetization in a domain depends on the crystal structure, when the external stress and magnetic field are absent and these are the two main controlling factors to change the domain orientation. When the sample is compacted in the presence of magnetic field, magnetic strain energy (E_σ) and domain energy in the presence of applied magnetic field (E_H) come into picture and these energies are given by the following relations [9],

$$E_\sigma = \frac{3}{2}\lambda_s\, \sigma\, sin^2\theta \quad \text{.....(1)}$$

$$E_H = -H\, M_s\, cos\phi \quad \text{.....(2)}$$

Where λ_s, σ, H and M_s are the saturation magnetostriction, applied stress, field strength and saturation magnetization, respectively. Angles θ and ϕ represents orientation of magnetization in a domain with respect to stress and applied field, respectively.

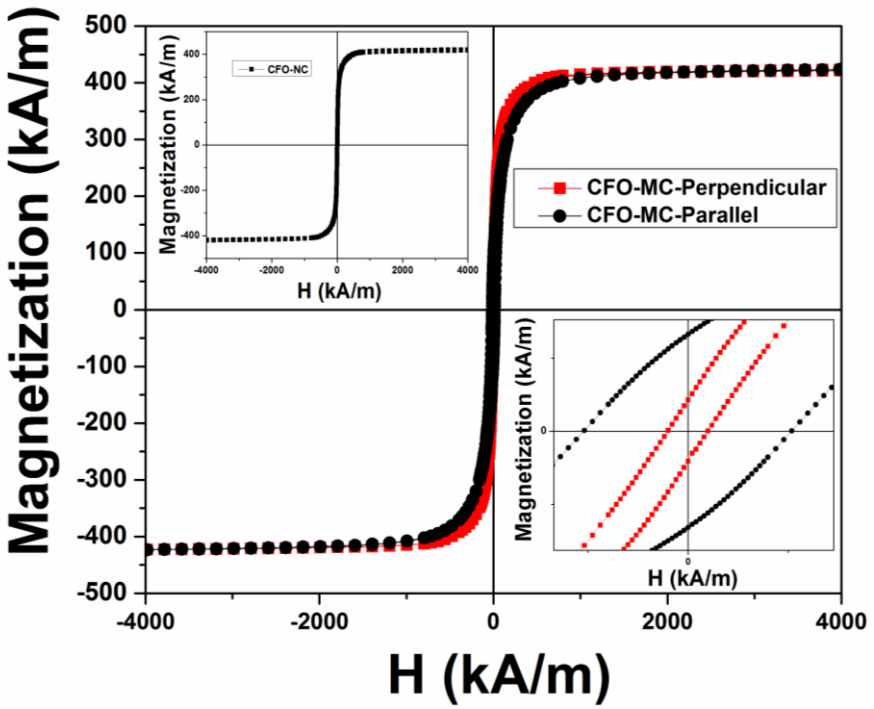

Figure.5.7. Parallel and perpendicular M-H curves of x = 0, inset of (a) shows magnetization curve of CFO-NC

During compaction (compressive stress) all the domains in the powder particles are oriented nearly to the direction of applied stress (θ = 0 or 180˚) due to the two-fold

symmetry of the uniaxial anisotropy generated by compaction. More precisely, the preferential direction of the magnetization will be close to the stress axis due to the negative magnetostriction (λ_s) of cobalt ferrite and compressive stress ('σ' negative) applied during compaction. Fig. 5.8(a) represents the ideal demagnetized state. To align the domains, compressive stress must be large enough compared to the forces due to crystal anisotropy, therefore from both the energy considerations the condition to orient the magnetization direction in a domain is

$$3/2\ \lambda_s\ \sigma > K_1 \quad \ldots\ldots(3)$$

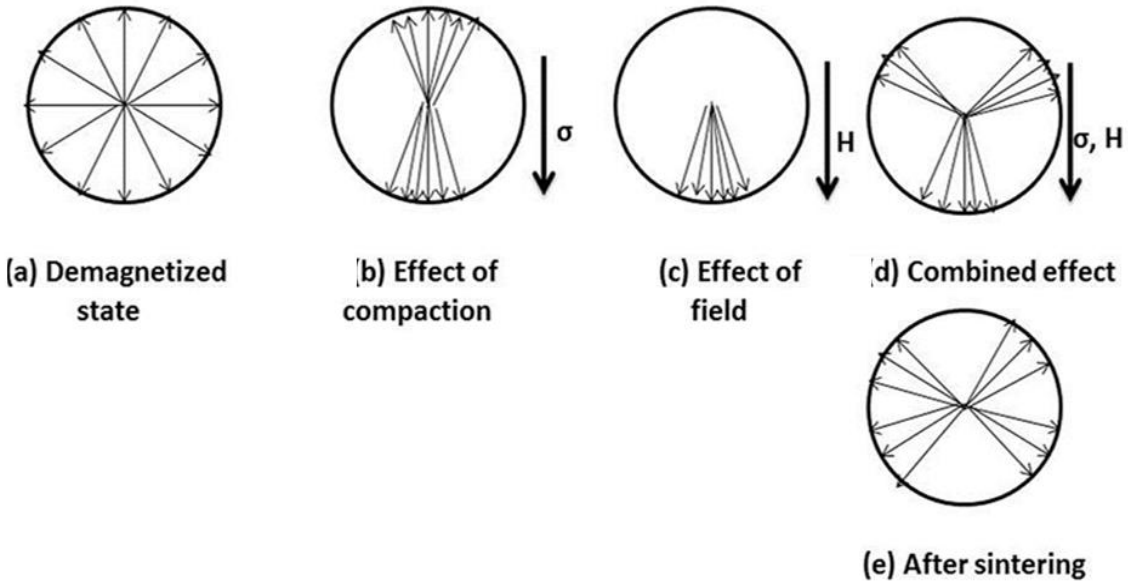

Figure 5.8. A schematic of domain alignment during magnetic compaction.

For cobalt ferrite the first order anisotropy constant K_1 is about 4×10^5 J/m^3. The energy of the applied stress (left side quantity in eq. 3) in the present investigation is greater than the crystal anisotropy; hence it orients the domain in the direction of compaction as shown in Fig.5.8(b) due to the two-fold symmetry of the stress field energy (eq. 1). Applied magnetic field during compaction tries to orient the domains in the field direction as shown in Fig.5.8(c) due to the one-fold symmetry of the Zeeman energy generated by the magnetic field (eq. 2). The resultant effect of these two energies orients the domains in the green compact as shown in Fig. 5.8(d). During sintering at 1300˚C, which is far greater than the Curie temperature (520˚C) of cobalt ferrite, spin orientations may get randomized but due to strong lattice-orbit coupling the resultant magnetization vectors align along the direction near to the initial stable magnetization direction after cooling, which is shown in Fig. 5.8(e). Here the perpendicular direction to the direction of compaction can be considered as induced easy axis or first easy axis. Intrinsic easy axes

for cobalt ferrite material are <100> axis, hence the <100> axes near 90˚ to the induced easy axes can be considered as second easy axes.

From the M-H loop of CFO-NC, which is shown in inset of Fig. 5.7 (left side top corner), it is observed that, initially with increasing applied magnetic field, alignment of domains takes place along the intrinsic easy axes through 180 and 90˚ domain wall motion if they are initially oriented at small and large angles, respectively, to the applied field direction. As the applied magnetic field further increases magnetization vector rotates along the field direction. The measured M-H loops of CFO-MC sample with the measuring field applied parallel and perpendicular to the compaction direction are shown in the main panel of Fig. 5.7. From the perpendicular magnetization data of CFO-MC, it is observed that with increasing magnetic field magnetization increases more quickly, that could be due to the initial alignment of most of the domains along the induced easy axes during magnetic compaction. Here, when the magnetic field increases domains get aligned along the induced easy axes only through 180˚ domain wall motion. In contrast, when magnetization of CFO-MC was measured in the parallel direction to that of pressing direction, magnetization process can be explained in three stages. In the first stage, with increasing magnetic field domains get oriented initially along the induced easy axes through 180˚ domain wall motion. In the second stage, further increment in magnetic field strength leads to a near 90˚ domain wall motion, which aligns the domains along the second easy axes (intrinsic easy axes). In the third stage, with increasing magnetic field magnetization of domains gradually rotates from the second easy direction to the direction of applied magnetic field. Increment in magnetization in all these stages is small compared to perpendicular magnetization measurement because initially the domains are oriented at large angles to the direction of applied field. Inset of Fig. 7 (right side down corner) will be discussed in the section of coercivity.

Figure. 5.9 and 5.10 show the field dependent perpendicular magnetization data of magnetically pressed $Co_{1+x}M_xFe_{2-2x}O_4$ ($0 \leq x \leq 0.4$, M = Zr, Ti) samples measured at room temperature. The maximum magnetization (M_{max}) obtained at maximum applied field of ~4000 kA/m is seen to increase and decrease marginally with increasing Zr^{+4} and Ti^{+4} substitution into CFO lattice, respectively, up to x = 0.2 composition, as shown in inset of Fig.5.9. and 5.10, respectively. For x = 0.4 composition of Zr substituted cobalt ferrite M_{max} is observed to decrease, this could be primarily due to the presence of extra ZrO_2 phase at the grain boundaries. Varying rate of decrease in maximum magnetization before

and after the Ti-substitution level of x = 0.2, could be due to the observed secondary phase of Ti_2O_3 at grain boundaries.

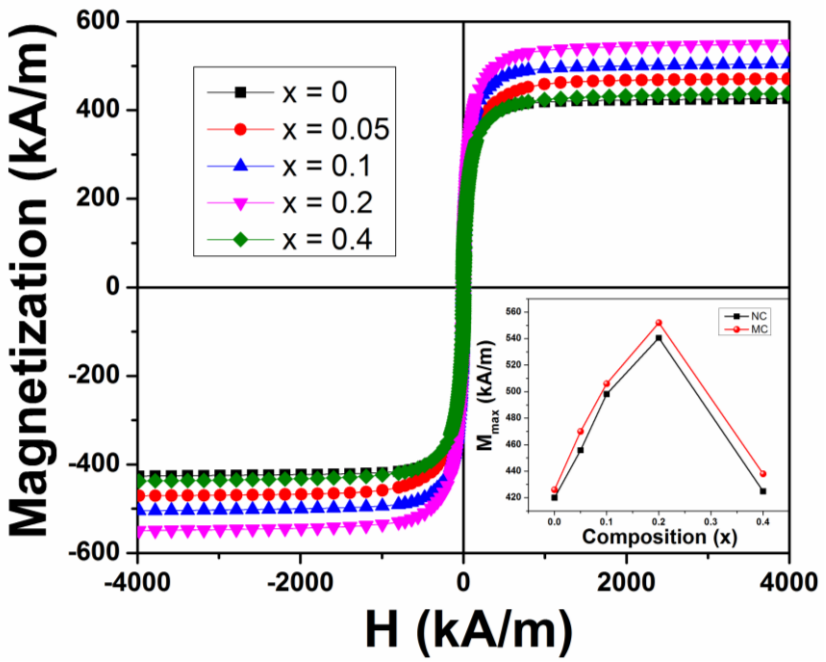

Figure 5.9: Magnetization (M-H) curves of $Co_{1+x}Zr_xFe_{2-2x}O_4$ ($0 \leq x \leq 0.4$)-MC samples at room temperature (~300 K); (inset) Variation of M_S with composition (x);

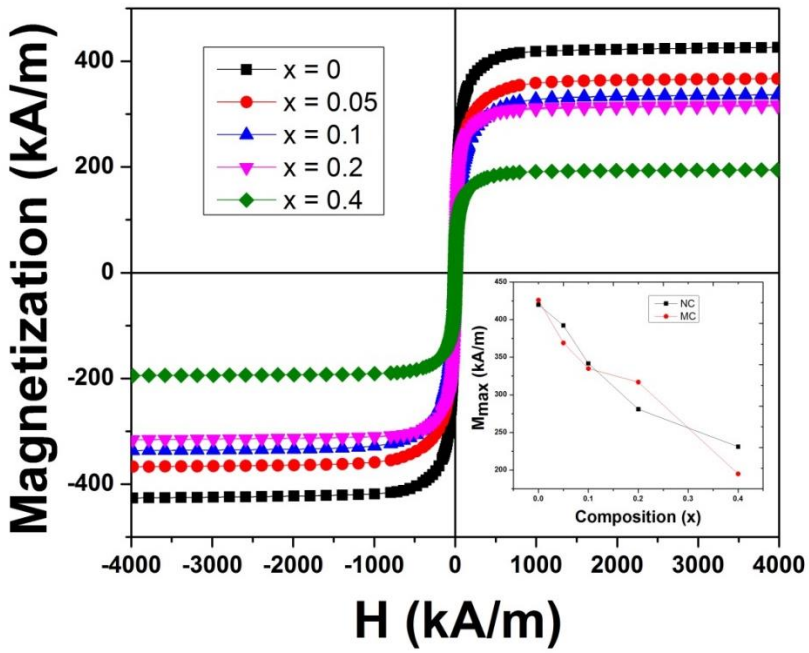

Figure 5.10: Magnetization (M-H) curves of $Co_{1+x}Zr_xFe_{2-2x}O_4$ ($0 \leq x \leq 0.4$)-MC samples at room temperature (~300 K); (inset) Variation of M_S with composition (x)

In spinel structure, super-exchange interaction between the cations in tetrahedral (A) and octahedral (B) sites is generally anti parallel. Therefore, the overall magnetization

is the difference in the magnetization of the A and B sub lattices. In general Co-ferrite has mixed spinel structure and the inversion factor mainly depends on the synthesis method, chemical substitution and annealing, since these processes redistribute the cations between the A- and B-sites. In case of $Co_{1+x}Zr_xFe_{2-2x}O_4$ ($0 \leq x \leq 0.2$), substitution of non-magnetic Zr^{+4} ions reduces the magnetic moment of tetrahedral sub lattice, since it has the strongest preference for the tetrahedral site, which resulted in increased net magnetization of the system. The observed decrease in magnetization in case of $Co_{1+x}Ti_xFe_{2-2x}O_4$ ($0 \leq x \leq 0.4$), could be due to the reduced moment of B-site in the presence of non-magnetic Ti^{+4} ions. Inset of Fig. 5.9 and 5.10, show the comparison of maximum magnetization of magnetically pressed (MC) to that of normally pressed (NC) Zr and Ti- substituted cobalt ferrites respectively.

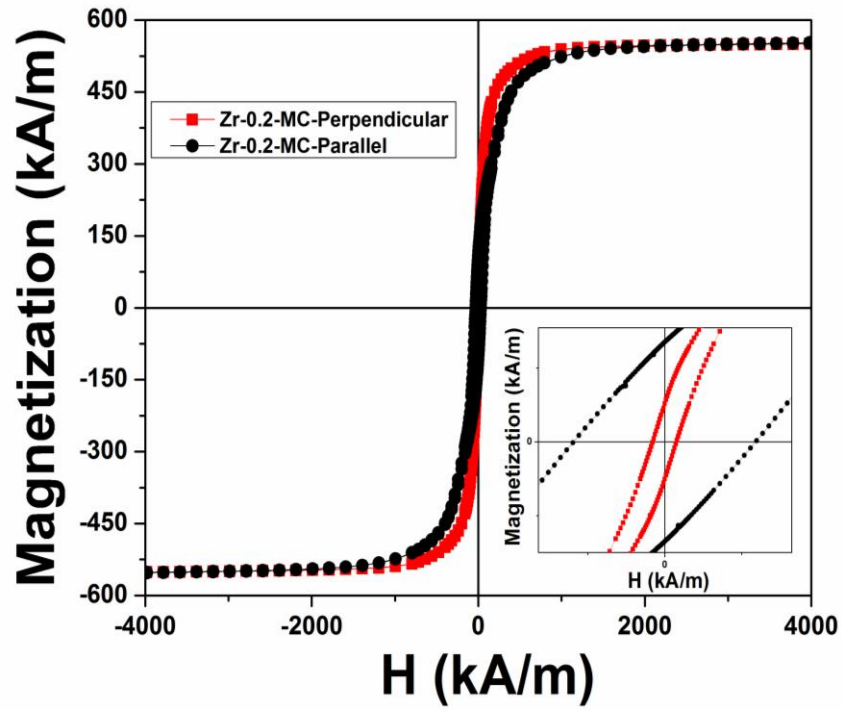

Figure 5.11: Parallel and perpendicular M-H curve of x = 0.2 composition of Zr-substituted cobalt ferrite

Marginal increment in magnetization is observed in the MC samples, which could be due to the presence of more aligned domain structure. Since the magnetization is increased up to x = 0.2, to see the effect of magnetic pressing, parallel magnetization measurement was also carried out on x = 0.2 composition of both the dopants. Fig. 5.11 and 5.12 show the parallel and perpendicular M-H loops of $Co_{1.2}Zr_{0.2}Fe_{1.6}O_4$ and $Co_{1.2}Ti_{0.2}Fe_{1.6}O_4$ samples respectively. From these figures it is clearly observed that perpendicular magnetization curve is steeper than the parallel magnetization curve.

Substitution of non-magnetic ion into the CFO-lattice reduces the strength of magnetic exchange interaction, which helps in aligning the domains easily along the direction of induced easy axis and thus should influence the magnetization behavior, which is clearly reflected in Fig. 5.11 and 5.12. Inset of Fig. 5.11 and 5.12 will be discussed in the section of coercivity

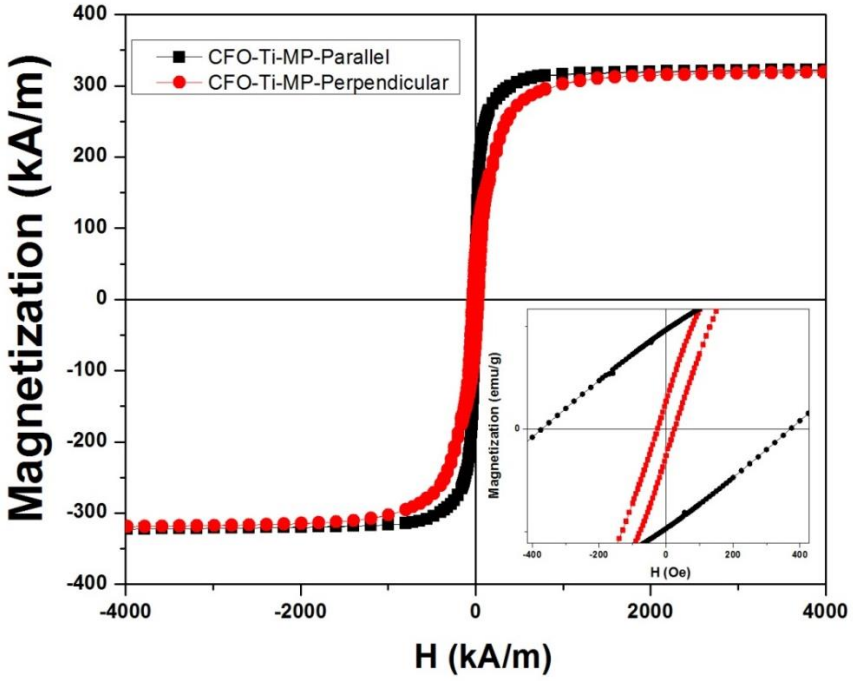

Figure 5.12: Parallel and perpendicular M-H curve of x = 0.2 composition of Ti-substituted cobalt ferrite

b. Anisotropy Constant estimated using Law of Approach to saturation:

It has already been reported that the cubic anisotropy constant of cobalt ferrite mainly depends on the concentration of Co^{+2} ions in B-site of spinel structure. Due to the cubic crystal field produced by the coulomb interaction between the oxygen ion and the electrons in the 3d orbitals, degenerate energy levels of Co^{+2} ion are split into t_{2g} (d_{xy}, d_{yz}, d_{xz}) and e_g ($d_{x^2-y^2}$, d_{z^2}) levels and the orbitals, which are situated along the cubic axes (e_g levels), are raised in energy compared to others (t_{2g} levels). For lower concentration of Co^{+2} ions in B site, neighboring iron ions produce trigonal field around Co^{+2} ion and the axis of three fold symmetry lies along one of the body diagonals ([111], [1-11], [-1-11], [-111]) of cubic crystal. This trigonal crystal field splits the t_{2g} levels further into singlet and a doublet by distorting the cubic crystal field produced by the oxygen ions. Occupation of seventh electron of Co^{+2} ($3d^7$) in one of these doubly degenerate levels produces unquenched orbital momentum and interaction of this orbital angular momentum

with total spin momentum of Co^{+2} ion gives rise to magneto crystalline anisotropy through spin-orbit coupling. In the previous study it is reported that the orbital degeneracy is further removed, when the Co^{+2} concentration in B-site increases beyond x > 0.7, due to the low symmetric crystalline field produced from the difference in charge between two metal cations (Co^{+2} and Fe^{+3}), which leads to quenching of the orbital angular momentum and subsequently reduces magnetocrystalline anisotropy. Hence, any variation in concentration of Co^{+2} ions in B-site results in change in the magnetocrystalline anisotropy of the system.

Anisotropy constant was estimated using LoA to saturation as explained in the previous chapter. Fitted plots, using equation (3), of $Co_{1+x}M_xFe_{2-2x}O_4$ (x = 0, 0.2 and M = Zr, Ti) compositions are shown in Fig. 5.13. 'K_1' was estimated by equating the slope to the coefficient 'b' in LoA.

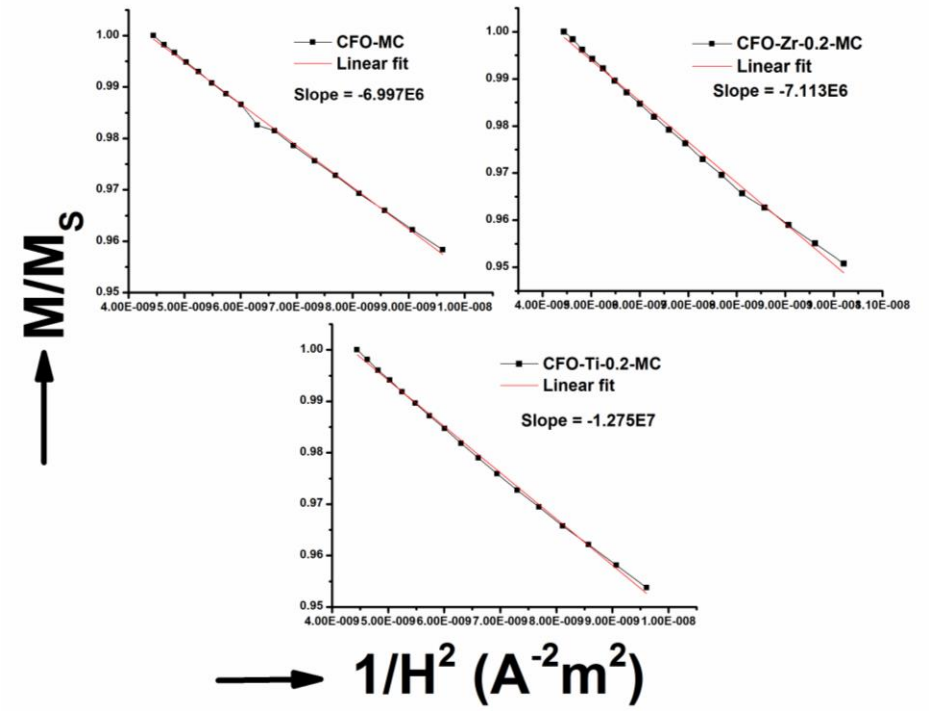

Figure. 5.13. LoA fitted plos of $Co_{1+x}M_xFe_{2-2x}O_4$ (x = 0, 0.2 and M = Zr, Ti) samples

The variation in anisotropy coefficient (K_1), estimated by fitting the magnetization data in the high field region , with Zr and Ti content are shown in Fig 5.14(a) and (b). The anisotropy constant (K_1) increases with increase in co-substitution of Zr^{+4}/ Co^{+2} and Ti^{+4}/ Co^{+2}, similar to the variation in coercive field (H_C) with composition of the samples, as shown in inset of Fig. 5.14(a) and (b).

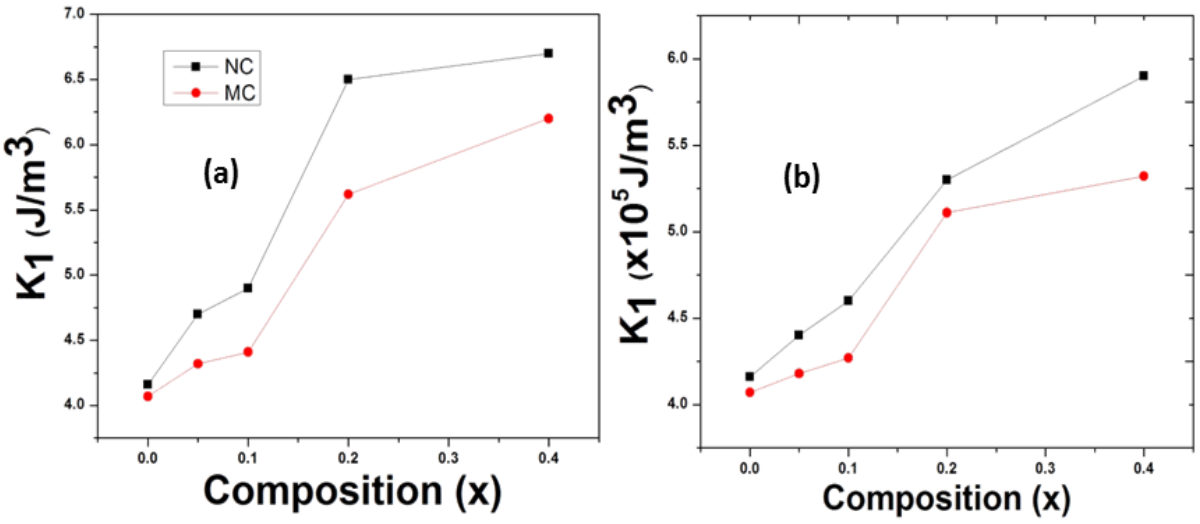

Figure 5.14: (a) and (b) Variation of anisotropy constant of Zr- and Ti- substituted cobalt ferrite as a function of composition and its comparison with NC samples

In the case of Zr^{+4} substituted CFO, Fe^{+3} ions are expected to migrate from A- to B-site with the substitution of Zr^{+4} ions in A-site. In the case of Ti^{+4} substituted CFO, co-substitution of Ti^{+4}/Co^{+2} ions in octahedral site is expected to displace the Fe^{+3} ions from B- to A- site up to x = 0.1 composition and after x = 0.1 due to the occupation of more Co^{+2} ions in tetrahedral site Fe^{+3} ions are expected to migrate from A- to B-site. The increase in anisotropy constant in both the substituent cases could be due to the enhanced trigonal field symmetry around Co^{+2} ion in B-site, resulting in increased spin-orbit coupling, which is the main origin of magneto crystalline anisotropy and magnetostriction. Figures 5.14(a) and (b) also depict that for all the magnetically pressed $Co_{1+x}M_xFe_{2-2x}O_4$ (M = Zr, Ti; $0 \leq x \leq 0.4$) samples; decrease in anisotropy constant is observed compared to normally pressed samples that might be due to the induced anisotropy along the first easy axis. In general, energy associated with the spin-orbit coupling at B-sites, which lie on the trigonal axis ([111], [1-11], [-1-11], [-111]) is equal, hence there is an equal probability for Co^{+2} ions to get distributed among these four B-sites. But, when the magnetic field is applied during compaction, resultant magnetization vector of spin-orbit interaction prefers to orient along the induced easy axis, therefore there is a probability of migration of Co^{+2} ions during heat treatment to the B-sites with its trigonal axes, which are nearer to induced easy axis and hence resulting in induced anisotropy.

C. Torque curves:

The torque measurement is an important technique to estimate the anisotropy constant. Torque curves of $Co_{1+x}M_xFe_{2-2x}O_4$ (M = Zr, Ti; x = 0 and 0.2) normally and

magnetically pressed poly crystalline samples are shown in Fig. 5.15 (a), (b) and (c). The figures clearly depict that the measured torque curves of both the systems are not periodic; hence Fourier analysis cannot be used to estimate the anisotropy constant. Fourier analysis requires oriented magnetic anisotropy for which the periodic torque curve can be decomposed in different harmonics with coefficients, which basically represent the different orders (first, second...) of magnetic anisotropy.

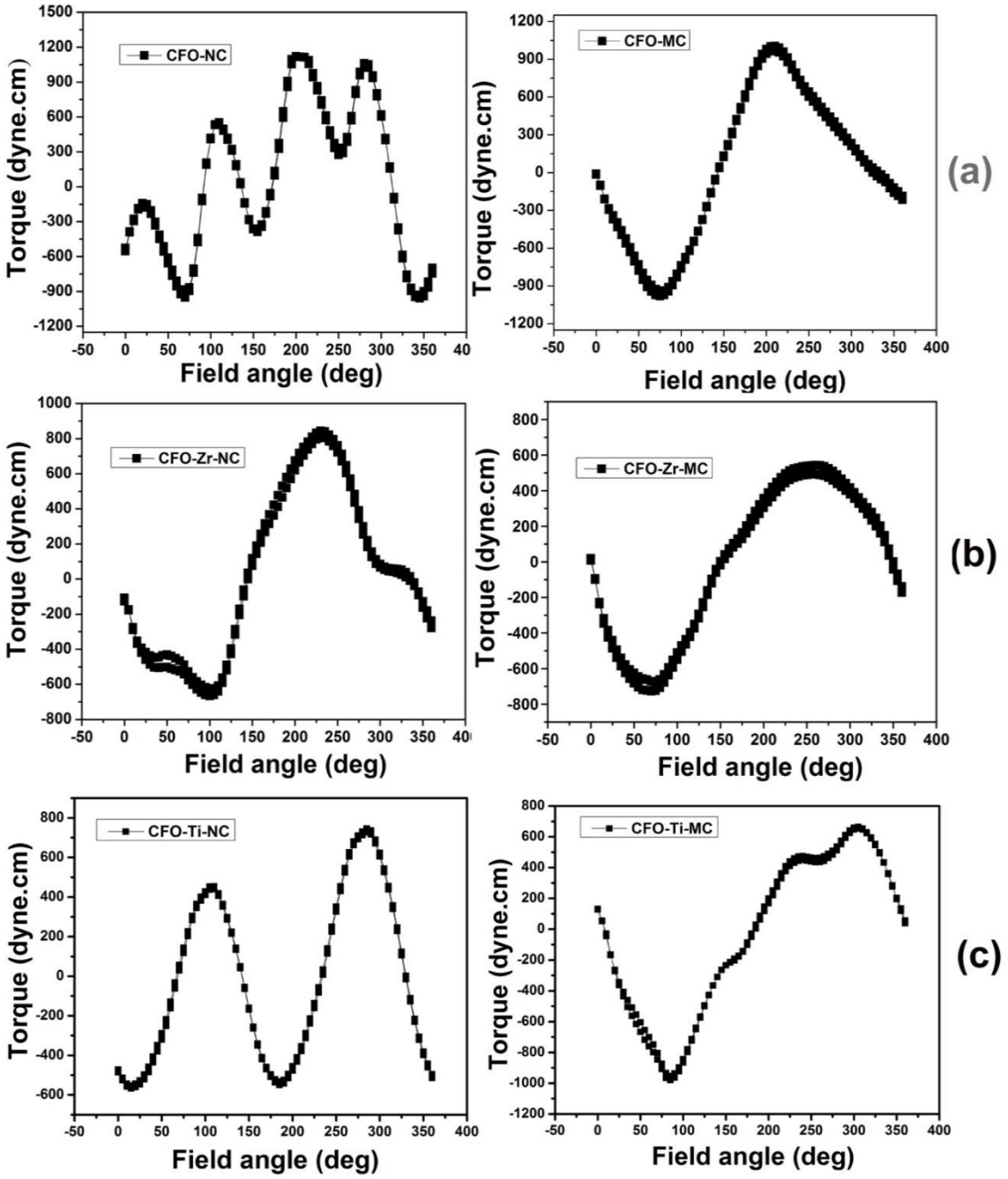

Figure 5.15: Torque curves of (a) x = 0 (b) CFO-Zr-0.2 (c) CFO-Ti-0.2 NC and MC Zr-substituted CFO samples

Table I: Comparison of anisotropy constants estimated from law of approach to saturation and torque curves

Composition	**$K_1 = [(105/8)(b\mu_0^2 M_S^2)]^{1/2}$ ($\times 10^5$ J/m^3)**	**$K_1 = H_a M_s/2$ ($\times 10^5$ J/m^3)**
CFO-NC	**4.16**	**2.14**
CFO-MC	**4.07**	**2.09**
CFO-Zr-0.2-NC	**6.51**	**5.52**
CFO-Zr-0.2-MC	**5.62**	**5.41**
CFO-Ti-0.2-NC	**5.32**	**4.63**
CFO-Ti-0.2-MC	**5.11**	**4.08**

d. Coercivity:

M-H loops of CFO-MC, shown in Fig. 5.7, clearly indicate that uniaxial anisotropy is induced along the perpendicular direction (induced easy axis) to that of compaction. Magnetic field induced uniaxial anisotropy during compaction reduces the magneto crystalline anisotropy. As a result, 5 times reduction in coercivity (H_c) has been observed along the perpendicular direction compared to parallel as shown in the inset of Fig. 5.7 (right side down corner of Fig. 5.7), which indicates that material has become magnetically soft along that direction. Similarly, coercivities of $Co_{1.2}Zr_{0.2}Fe_{1.6}O_4$ and $Co_{1.2}Ti_{0.2}Fe_{1.6}O_4$ samples along the perpendicular direction (induced easy axis) are observed to reduce by 7 and 8 times respectively, to that of measured along the parallel direction, as shown in inset of Fig. 5.11 and 5.12, which could be due to the presence of large induced uniaxial anisotropy in the substituted sample compared to pure one. Dependence of coercivity (Hc) on composition of Zr- and Ti- substituted NC and MC samples are shown in Fig 5.16 (a) and (b) respectively. Coercivity is observed to increase with increasing co-substitution of Co^{+2}/Zr^{+4} and Co^{+2}/Ti^{+4} for 2 Fe^{+3} ions in the CFO lattice because it is strongly related to the anisotropy of the system, which is mainly dependent on the amount of Co^{+2} ions present in the octahedral sites. Coercivity of MC samples is observed to be smaller than the NC samples, which is mainly attributed to the

presence of larger grains in the MC samples (~20μm) compared to that of NC samples (~10μm), since apart from anisotropy microstructure also affects the coercivity.

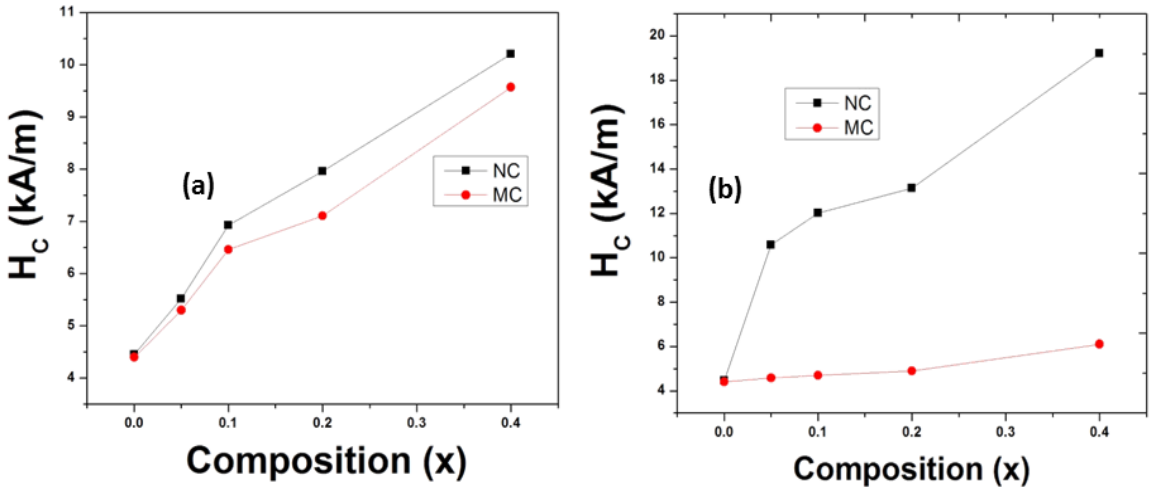

Figure 5.16: (a) and (b) Variation of coercivity as a function of composition of Zr and Ti substituted cobalt ferrite and its comparison with NC samples

5.4. Magnetoelastic properties:

Magnetostriction:

The magnetostriction value of magnetically pressed pure $CoFe_2O_4$ is shown in Fig.5.17. From Fig. 5.17 it is observed that, for normal pressed pure CFO (CFO-NC), longitudinal magnetostriction (λ_l) reaches the maximum of -181 ppm, when the applied magnetic field increases to ~400 kA/m and decreases marginally at higher applied magnetic field, which indicates the anisotropic nature of magnetostriction. The maximum transverse magnetostriction (λ_t) value (~88 ppm) is approximately one half of that for the longitudinal, which is in good accordance with the following relation,

$$\lambda = \frac{3}{2}\lambda s\,(\cos^2\theta - \frac{1}{3}) \quad \text{.....(5)}$$

where 'θ' is the angle between direction of magnetization and direction in which the magnetostriction is measured. θ = 0˚ and 90˚ denote the longitudinal (λ_l) and transverse magnetostriction (λ_t) respectively. If these two 'θ' values are substituted in the above equation it reduces to $\lambda_t = \lambda_l/2$. Direction dependence of magnetostrictions of magnetically pressed pure CFO (CFO-MC) is shown in Fig. 5.17. Significant improvement in magnetostriction is observed in comparison with CFO-NC. The corresponding values of λ_l and λ_t are ~ -360 ppm and ~ 44 ppm for the longitudinal and transverse measurements, respectively. It is interesting to note that the 2:1 relation of longitudinal and transverse

magnetostriction is no longer applicable for CFO-MC sample. In this case the above equation (5) is no longer valid and the dependency of magnetostriction on initial domain orientation can be explained based on the following equation,

$$\lambda = \frac{3}{2}\lambda_s \left(< \cos^2\theta >_t - < \cos^2\theta >_0\right) \ldots\ldots\ldots\ldots\ldots\ldots\ldots(6)$$

Here $<\cos^2\theta>_0$ and $<\cos^2\theta>_t$ represent the initial domain orientation and domain orientation at any time 't', respectively. Even though for a polycrystalline material it is difficult to mention the orientation direction, by relating the observed λ_l and λ_t values of CFO-MC sample with eq. 6 it can be concluded that initially oriented domains were present in the sample along the transverse direction to that of compaction.

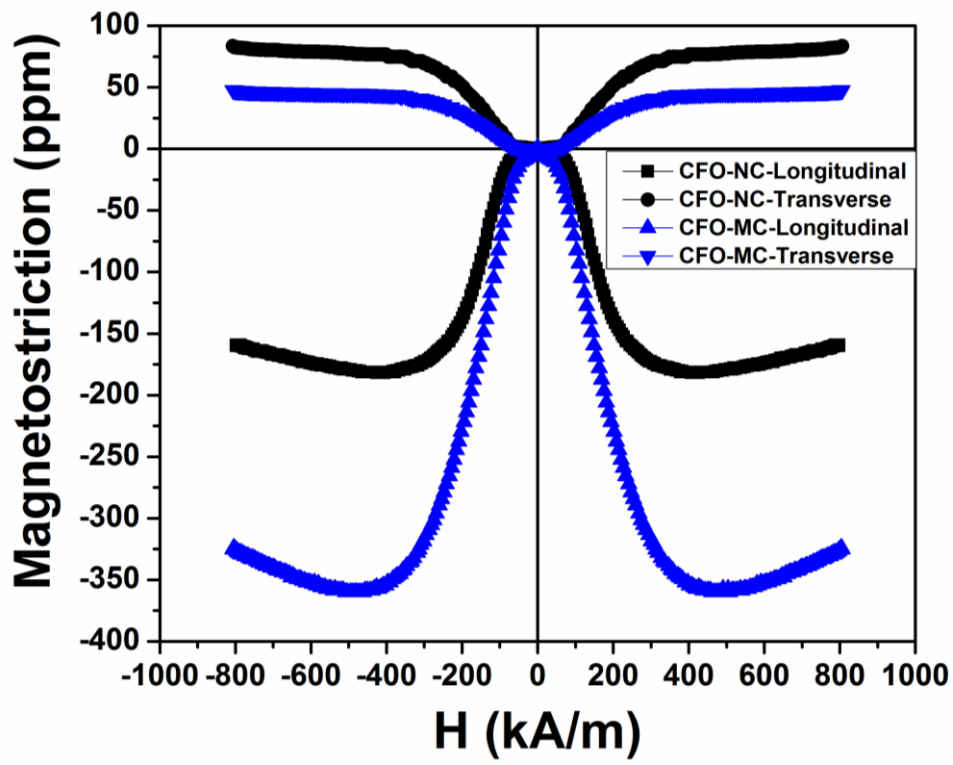

Figure 5.17: Longitudinal and Transverse magnetostriction curves of CFO - NC and MC samples

From Fig. 5.17, it is also observed that λ_t of CFO-MC is smaller than that of CFO-NC. If we relate this observation with the magnetization data measured in the same direction (induced easy axis), it is seen that the magnetization increased more rapidly with the application of field due to the initial domain orientation along the induced easy axis. Even though the magnetization increases it may not contribute to dimensional changes, since the domain orientation with the applied magnetic field takes place through 180° domain wall motion. The observed small transverse magnetostriction (λ_t) could be due to

the lack of complete alignment of domains in the magnetically pressed sintered sample. Two-fold increment in longitudinal magnetostriction (λ_l) is observed for CFO-MC sample compared to CFO-NC. This can be explained from the parallel magnetization measurement of CFO-MC sample. In this case, as explained in the previous section, with increasing applied magnetic field domains get aligned through 180˚ and 90˚ domain wall motion and domain rotation. Here 90˚ domain wall motion and domain rotation lead to the dimensional changes and these processes occur more in the magnetically pressed sample compared to CFO-NC, because of the presence of oriented domains along the induced easy axis.

Figures 5.18 and 5.19 show the longitudinal magnetostriction (λ_l) of magnetically pressed $Co_{1+x}M_xFe_{2-2x}O_4$ (M = Zr, Ti; $0 \leq x \leq 0.4$) samples. λ_l is seen to decrease with increasing Zr^{+4} and Ti^{+4} concentrations except for x = 0.2, as shown in inset of Fig. 5.18 and 5.19.

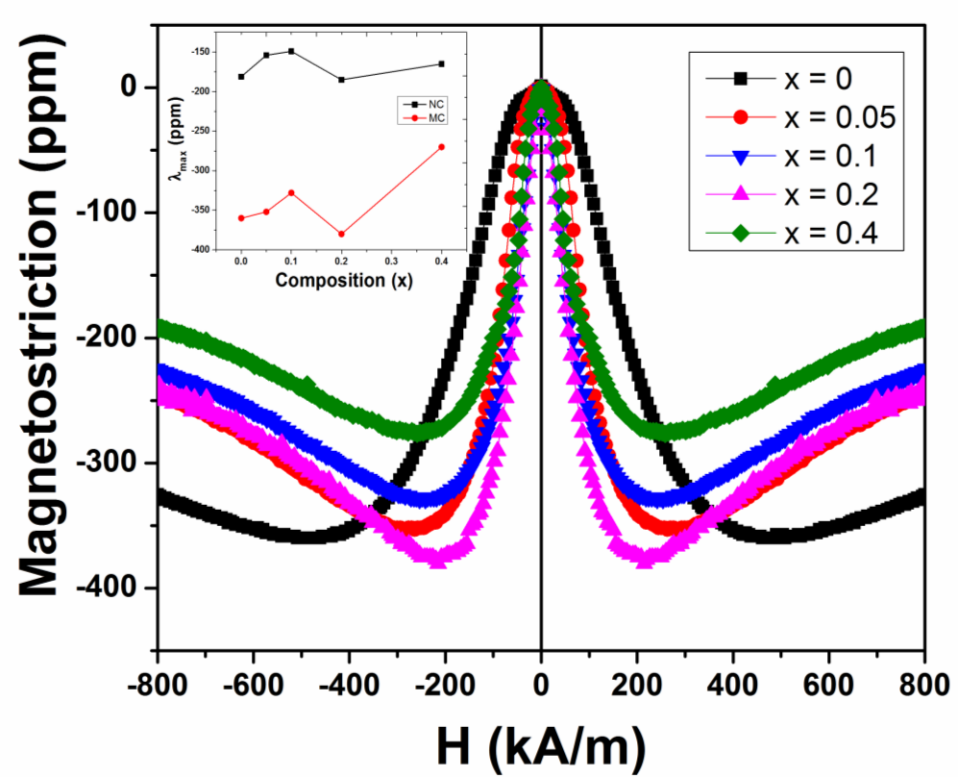

Figure 5.18: Longitudinal magnetostriction curves of $Co_{1+x}Zr_xFe_{2-2x}O_4$, ($0 \leq x \leq 0.4$)-MC samples; Inset: Variation of magnitude of maximum magnetostriction as a function of composition, x and their comparison with NC samples

Magnetostriction and cubic anisotropy of cobalt ferrite originate from spin-orbit coupling, which arises from the unquenched orbital momentum of Co^{+2} ions in octahedral site. Tachiki reported that, quenching of orbital momentum of Co^{+2} ion depends on the

amount of Co^{+2} ions present in the octahedral site of spinel lattice. The observed marginal increase in magnetostriction for x = 0.2 composition compared to pure is attributable to the presence of optimal concentration of Co^{+2} ions in the octahedral site with the co-substitution of Zr^{+4}/Co^{+2} and Ti^{+4}/Co^{+2} ions.

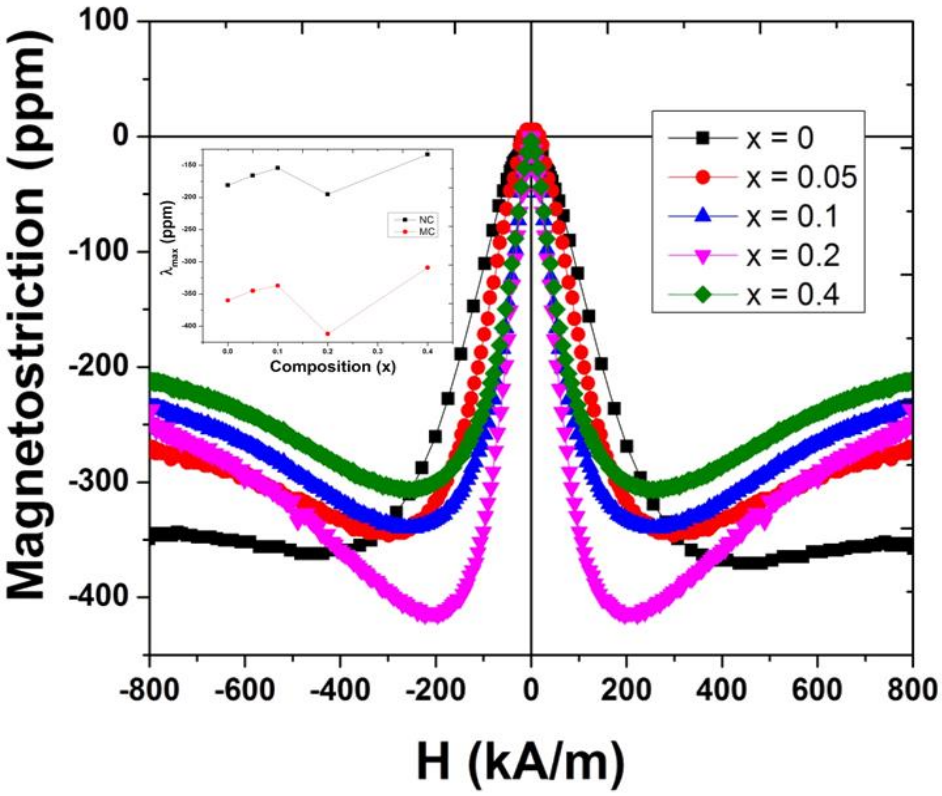

Figure 5.19: Longitudinal magnetostriction curves of $Co_{1+x}Ti_xFe_{2-2x}O_4$, ($0 \leq x \leq 0.4$)-MC samples; Inset: Variation of magnitude of maximum magnetostriction as a function of composition, x and their comparison with NC samples

Decrease in magnetostriction for x = 0.4 is attributed to the presence of secondary phases (ZrO_2 and Ti_2O_3) in the sample. From a careful review of the XRD data of magnetically compacted x = 0 and 0.2 samples (Fig. 3(a), (b) and (c)) it is seen that, texturing was observed along [220], [511] and [440] directions and out of these three, maximum crystal orientation was observed along [440] direction. By correlating this observation with the parallel and perpendicular data of magnetization and magnetostriction, it can be inferred that [440] direction could be the induced easy axis in the magnetically compacted samples. From the quantitative analysis of domain alignment, as discussed in magnetization section, it has been concluded that the perpendicular direction (to that of pressing direction) could be the induced easy axis. Therefore, the direction, which is perpendicular to the [440] direction could be the pressing direction.

Magnetically pressed $Co_{1+x}Zr_xFe_{2-2x}O_4$ ($0 \leq x \leq 0.4$) samples have shown large negative magnetostriction values, therefore [001] direction might be the pressing direction, since it is perpendicular to [440] direction and is one of the easy axes (<100>) of cobalt ferrite, along which $CoFe_2O_4$ has well known negative magnetostriction. The maximum magnetostriction values observed at lower fields could be due to the low angle alignment of [100] direction (one of the easy axes of cobalt ferrite) to [511] and [440] directions. Inset of Fig. 5.18 and 19 depict the variation in magnetostriction of normally and magnetically pressed $Co_{1+x}M_xFe_{2-2x}O_4$ (M = Zr, Ti; $0 \leq x \leq 0.4$) samples respectively. Approximately 111 and 129% increment in longitudinal magnetostriction is observed for magnetically pressed $Co_{1.2}Zr_{0.2}Fe_{1.6}O_4$ and $Co_{1.2}Ti_{0.2}Fe_{1.6}O_4$ samples respectively, compared to CFO-NC.

Strain sensitivity:

Strain sensitivity ($d\lambda_l/dH$) of magnetically compacted $Co_{1+x}M_xFe_{2-2x}O_4$ (M = Zr and Ti; $0 \leq x \leq 0.4$) samples as a function of applied magnetic field are shown in Fig. 5.20 and 5.21 respectively. Progressive Zr^{+4} and Ti^{+4} ions substitution into the CFO lattice resulted in increasing $(d\lambda_l/dH)_{max}$ up to x = 0.2 composition, which is ascribed to the reduced super exchange interaction between tetra and octahedral sub-lattices in the presence of non-magnetic Zr^{+4} and Ti^{+4} ions in the spinel lattice. For x = 0.4, $(d\lambda_l/dH)_{max}$ is observed to decrease due to the hindrances produced by the extra phase to the domain wall motion and also might be due to the magnetic dilution induced by the presence of more amount of Zr^{+4} and Ti^{+4} ions in the spinel lattice. Effective magnetostriction at lower fields results from the domain orientation through non-180˚ domain wall motion and as explained earlier these processes occur more and quickly in magnetically compacted samples due to the initial orientation of domains along first (induced) easy axis. Hence, large enhancement in strain derivative was observed for magnetically pressed Zr- and Ti-substituted cobalt ferrites compared to normally pressed samples. Inset of Fig. 5.20 and 5.21 (top right corner) shows the comparison of $(d\lambda_l/dH)_{max}$ of magnetically and normally pressed samples as a function of composition. From these figures ~55% increment in $(d\lambda_l/dH)_{max}$ is observed for CFO-MC sample (1.25×10^{-9} $A^{-1}m$) compared to that of CFO-NC (0.8×10^{-9} $A^{-1}m$) but with the combined effect of non-magnetic ion substitution (Zr and Ti) and magnetic field applied during compaction a dramatic 435 and 625% enhancement in strain sensitivity has been observed for $Co_{1.2}Zr_{0.2}Fe_{1.6}O_4$ (4.3×10^{-9} $A^{-1}m$) and $Co_{1.2}Ti_{0.2}Fe_{1.6}O_4$ (5.8×10^{-9} $A^{-1}m$) respectively, compared to CFO-NC (0.8×10^{-9} A^{-}

^{1}m). Inset of Fig 5.20 and 5.21 (lower left corner) show the filed at maximum strain sensitivity of normally and magnetically pressed samples. From the plot it is observed that slight decrease in field at $(d\lambda/dH)_{max}$ is observed for magnetically compacted sample compared to normally compacted CFO.

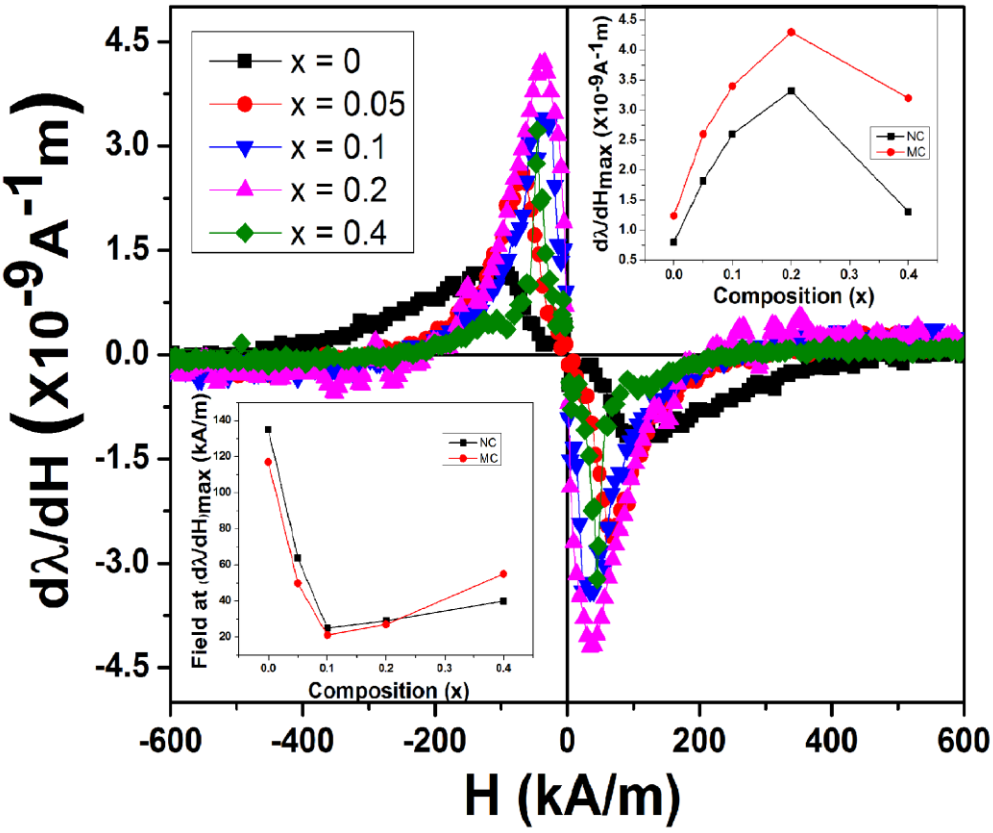

Figure 5.20: Magnetic field (H) dependence of strain derivative (dλ/dH) for $Co_{1+x}Zr_xFe_{2-2x}O_4$, ($0 \leq x \leq 0.4$)-MC samples. Inset: Variation of maximum strain derivative, $(d\lambda/dH)_{max}$ (Top right corner) and field (H) required to achieve that (lower left corner) as a function of composition, x.

The magnetostriction and strain sensitivity values obtained in the present investigation are almost similar to the values reported in existing literature on magnetic annealing [10, 11]. The larger stain sensitivity (7.7×10^{-9} A^{-1}m) reported by Wang et.al. compared to the value achieved in our study (4.3×10^{-9} A^{-1}m) could be due to the larger magnetic fields (~2T) applied during shaping of the samples compared to the fields applied (~1T) in our study. From this result we can conclude that effect of substitution of non-magnetic ion into the spinel lattice is more compared to the effect of compaction in the presence of magnetic field in enhancing the strain sensitivity. But, in the case of magnetostriction (λ_{max}) maximum effect is observed with magnetic compaction rather than

the non-magnetic ion substitution. It has also been observed that substitution of non-magnetic ion in octahedral site of spinel lattice has shown larger effect in enhancing the magnetostriction and strain sensitivity. Therefore, Ti substituted cobalt ferrite ($Co_{1.2}Ti_{0.2}Fe_{1.6}O_4$) processed by magnetic field assisted compaction can be considered as potential material for stress sensor application.

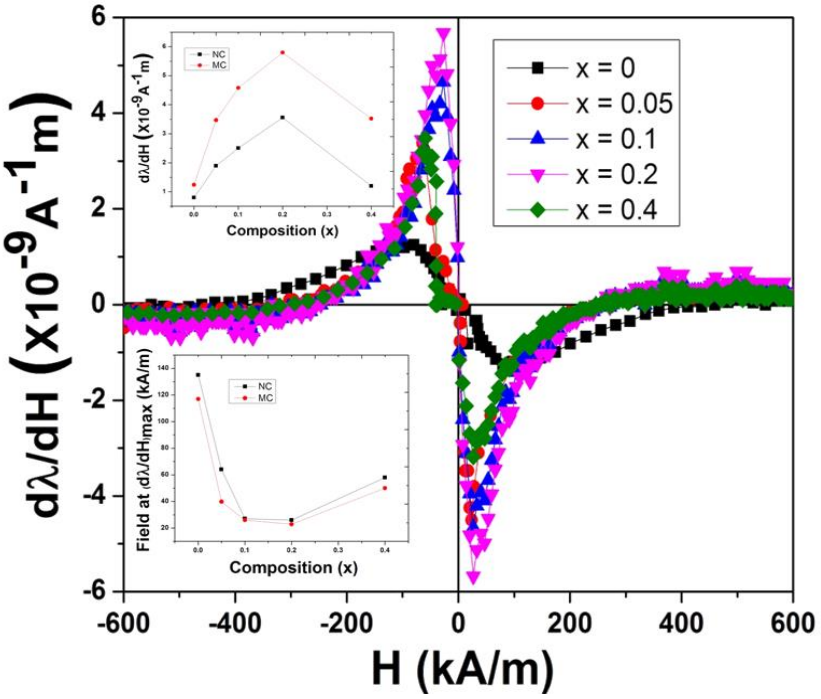

Figure 5.21: Magnetic field (H) dependence of strain derivative (dλ/dH) for $Co_{1+x}Ti_xFe_{2-2x}O_4$, ($0 \leq x \leq 0.4$) MC samples. Inset: Variation of maximum strain derivative, $(d\lambda/dH)_{max}$ (Top left corner) and field (H) required to achieve that (lower left corner) as a function of composition, x.

5.5. Conclusion:

- Approximately 99 and 55% increment in $(d\lambda_l/dH)_{max}$ is observed for CFO-MC sample (1.25×10^{-9} $A^{-1}m$) compared to that of CFO-NC (0.8×10^{-9} $A^{-1}m$)
- Approximately 111% and 128% increment in longitudinal magnetostriction are observed for magnetically pressed $Co_{1.2}Zr_{0.2}Fe_{1.6}O_4$ (~ -385 ppm) and $Co_{1.2}Ti_{0.2}Fe_{1.6}O_4$ (~ -412 ppm) sample compared to CFO-NC (~ -181 ppm).
- Due to the combined effect of non-magnetic ion (Zr^{+4} and Ti^{+4}) substitution and magnetic field applied during compaction a dramatic 435% and 625% enhancement in strain sensitivity have been observed for $Co_{1.2}Zr_{0.2}Fe_{1.6}O_4$ (4.3×10^{-9} $A^{-1}m$) and $Co_{1.2}Ti_{0.2}Fe_{1.6}O_4$ (5.8×10^{-9} $A^{-1}m$) compared to CFO-NC (0.8×10^{-9} $A^{-1}m$).

5.6. References

1) O'Neill, Hugh St. C., Alexandra Navrotsky Simple spinels: crystallographic parameters, cation radii, lattice energies and cation distribution. *American Mineralogist* **68**, 181-194 (1983).

2) Sawatzky, G. A., Van Der Woude, F., Morrish, A. H. Mossbauer study of several ferrimagnetic spinels. *Phys. Rev* **187**, 747-757 (1969)

3) Monaji Vinitha Reddy, Praveen Paul, J., Shara Sowmya, N., Srinivas, A., Dibakar Das Magneto-electric properties of in-situ prepared $xCoFe_2O_4$-$(1-x)(Ba_{0.85}Ca_{0.15})(Zr_{0.1}Ti_{0.9})O_3$ particulate composites. *Ceramics International* **42**, 17827-17833 (2016)

4) Paulsen, J.A., Ring, A.P., Lo, C.C.H., Snyder, J.E., Jiles, D.C. Manganese-substituted cobalt ferrite magnetostrictive materials for magnetic stress sensor applications. *J. Appl. Phys.* **97**, 044502 (2005)

5) Greenough, R. D., Lee, E. W. The magnetostriction of cobalt-manganese ferrite. *J. Phys. D.* **3**, 1595 (1970)

6) Sateesh Prathapani, Jayaraman, Tanjore V., Varaprasadarao, Eswara K., Dibakar Das Structural and ambient/sub-ambient temperature magnetic properties of Er-substituted cobalt-ferrites synthesized by sol-gel assisted auto-combustion method. *J. Appl. Phys.* **116**, 023908 (2014)

7) Vinitha Reddy Monaji, Srinivas Indla, Sudhindra Rayaprol, Shara Sowmya, Srinivas, A., Dibakar Das Temperature dependent magnetic properties of $Co_{1+x}T_xFe_{2-2x}O_4$ (T = Zr, Ti). *J. Alloys Compd.* **700,** 92 (2017)

8) Jiquan Wang, Xiuexu Gao, Chao Yuan, Jiheng Li and Xiaoqian Bao Magnetostriction properties of oriented polycrystalline $CoFe_2O_4$. *J. Magn. Magn. Mater.* **401** 662 (2007)

9) Willamson, G.K., Hall, W.H. X-ray line broadening from filed aluminium and wolfram. *Acta Metall.* **1**, 22 (1953).

10) Kaja Mohaideen K. and Joy P.A. High magnetostriction parameters for low-temperature sintered cobalt ferrite obtained by two-stage sintering. *J. Magn. Magn. Mater.* **371** 121–129 (2014)

11) Anantharamaiah P.N and Joy P.A. Magnetic and magnetostrictive properties of aluminum substituted cobalt ferrite synthesized by citrate-gel method. *J. Mater. Sci.* **50** 6510-6517 (2015)

Results and discussion

Effect of Ce substitution (non-magnetic) and magnetic field assisted compaction on structural, magnetic and magnetostrictive properties of cobalt ferrite

In CFO lattice, Co^{+2} ions in the octahedral site are surrounded by Fe^{+3} ions, which produce a trigonal crystal field. This trigonal crystal field distorts the symmetry of the cubic octahedral field produced by the oxygen ions resulting in lifting the degeneracy of the d-orbitals of cobalt ions and produces unquenched orbital moments. Magnetostriction and anisotropy energy results from the coupling of cobalt ion spin with its angular momentum. Hence, the distortion induced in the lattice is expected to affect the magnetostriction property. The variation in ionic size induces distortion in the lattice, which in turn affects the magnetostriction property. Hence, in the present chapter to observe the effect of ionic size on magnetostrictive properties, substitution of Ce^{+4} ion into CFO lattice has been studied. Chapter 6 describes the structural, magnetic and magnetoelastic properties of normally and magnetically compacted Ce^{+4} substituted cobalt ferrite samples and the results were compared.

6.1. Structural properties

X-ray diffraction patterns of the normally and magnetically compacted $Co_{1+x}Ce_xFe_{2-2x}O_4$ ($0 \leq x \leq 0.04$) samples, as shown in Fig. 6.1 and 6.2, confirmed the single-phase cubic spinel structure up to x = 0.03 composition and an additional diffraction peaks corresponds to CeO_2 were observed with the respective substitutions of x = 0.04 concentration.

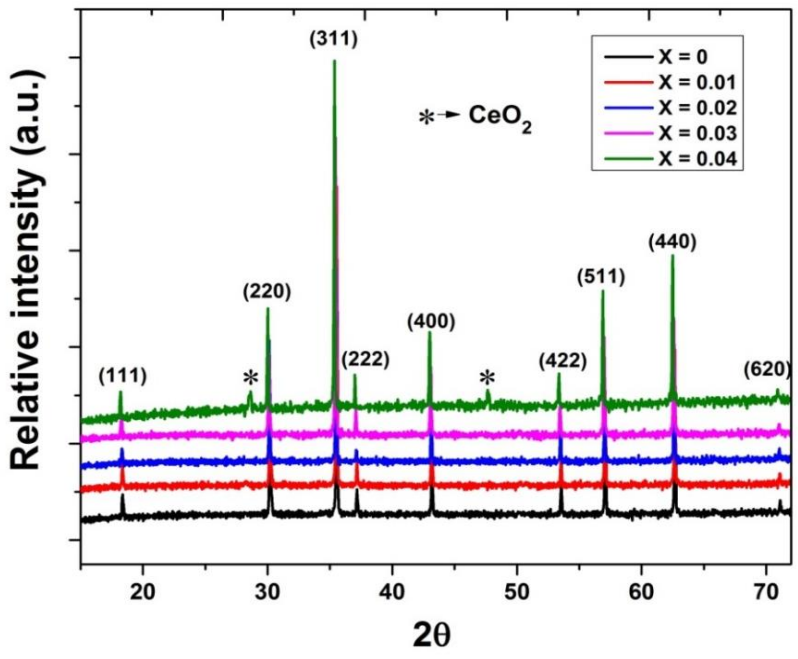

Figure.6.1. X-ray diffraction pattern of normally compacted $Co_{1+x}Ce_xFe_{2-2x}O_4$ ($0 \leq x \leq 0.04$) sintered at 1300°C for 12 hrs.

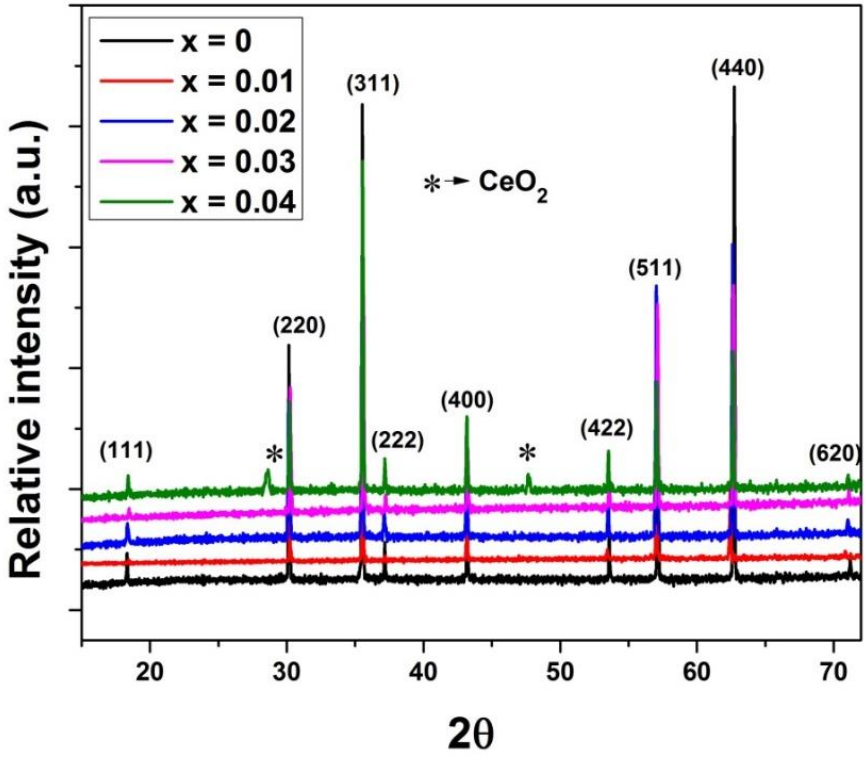

Figure. 6.2. X-ray diffraction pattern of magnetically compacted $Co_{1+x}Ce_xFe_{2-2x}O_4$ ($0 \leq x \leq 0.04$) sintered at 1300°C for 12 hrs

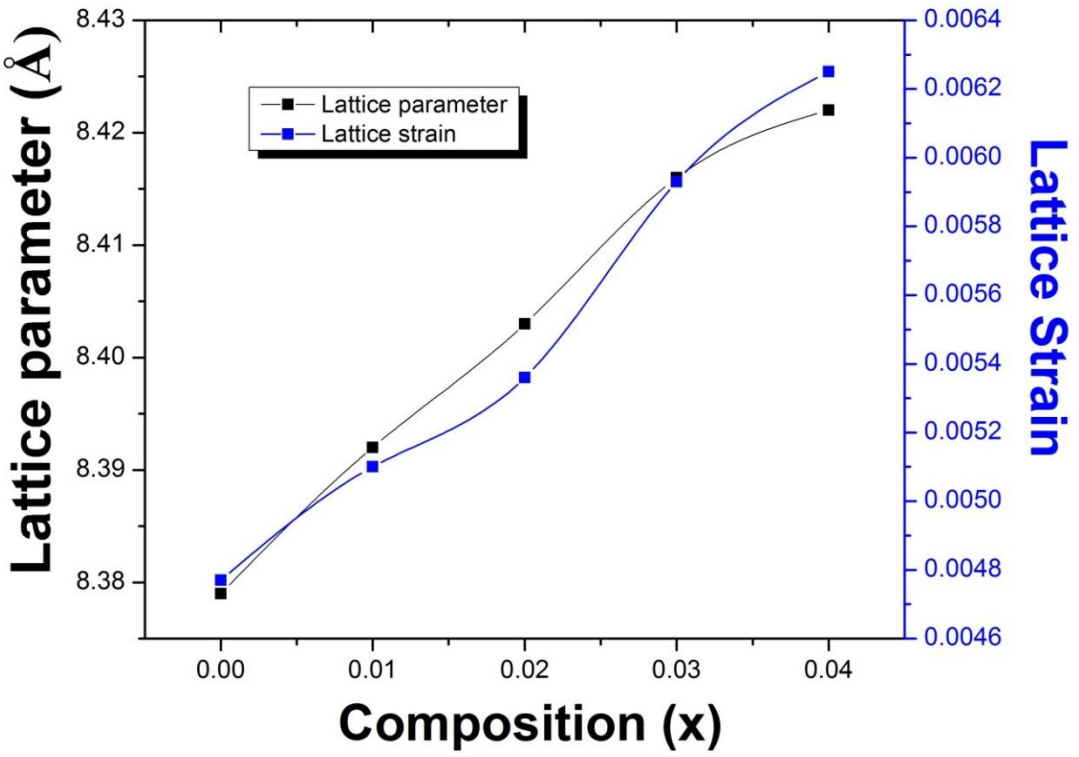

Figure.6.3. Variation in lattice parameter and lattice strain of normally compacted $Co_{1+x}Ce_xFe_{2-2x}O_4$ ($0 \leq x \leq 0.04$) samples with respect to composition.

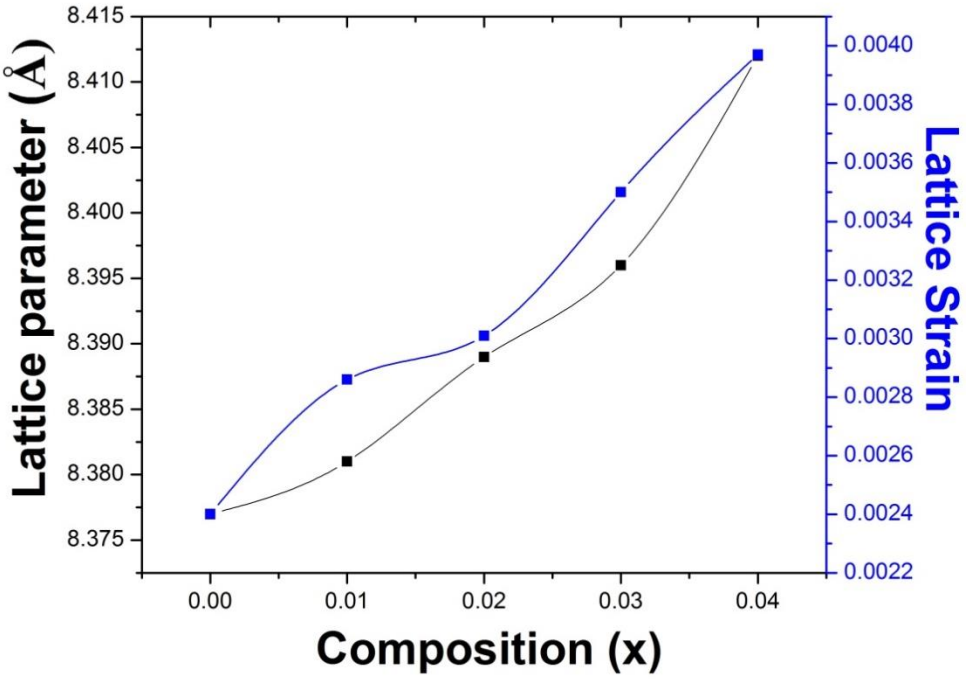

Figure.6.4. Variation in lattice parameter and lattice strain of magnetically compacted $Co_{1+x}Ce_xFe_{2-2x}O_4$ ($0 \leq x \leq 0.04$) samples with respect to composition.

From Fig. 6.3 and 6.4 lattice parameter and lattice strain are observed to increase with the progressive co-substitution of Ce^{+4}/Co^{+2} for 2 Fe^{+3} ions in the CFO lattice from ~8.378 Å for x = 0 to ~8.422 Å for x = 0.04 for NC samples and from ~8.374 Å for x = 0 to ~8.411 Å for x = 0.04 for MC samples. $CoFe_2O_4$ has partial inverse spinel structure and the cation distribution in both the sub lattices (tetra and octa), which directly affects the lattice parameter, depends on sample preparation method, chemical substitution, heat treatment temperature and schedule [1-6]. Ce^{+4} ions have strong tendency to occupy octahedral (B) sites. The increase in lattice parameter with increasing Ce^{+4} concentration could be due to the larger ionic radii of Ce^{+4} compared to Fe^{+3} and Co^{+2} ions in tetrahedral coordination. Decrease in lattice parameter with magnetic field assisted compaction suggests that compressive strains present in the system.

6.2. Microstructural properties

The SEM images of the normally and magnetically compacted and sintered Ce substituted cobalt ferrite ($Co_{1+x}Ce_xFe_{2-2x}O_4$ ($0.0 \leq x \leq 0.04$)) samples are shown in Fig. 6.5 and 6.6. The average grain size is observed to increase with CeO_2 substitution in both NC and MC samples. The average grain sizes, as estimated from the line intercept method, have been found to vary from ~10 to 15 μm and ~20 to 22 μm for NC and MC samples, respectively, with increasing Ce substitution. The observed

decrease in grain size for x = 0.04 composition, could be due to the presence of extra CeO_2 phase in the matrix, which impedes the grain growth.

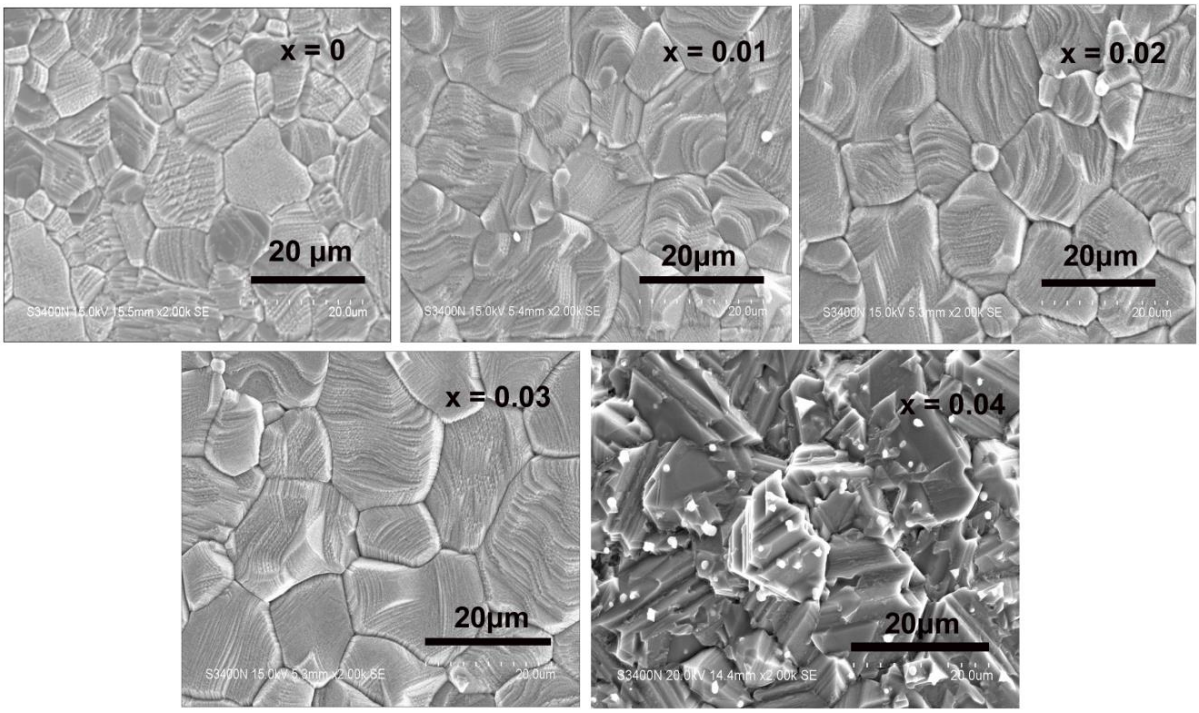

Figure 6.5. Scanning electron micrographs of $Co_{1+x}Ce_xFe_{2-2x}O_4$ ($0 \leq x \leq 0.04$) – NC samples respectively

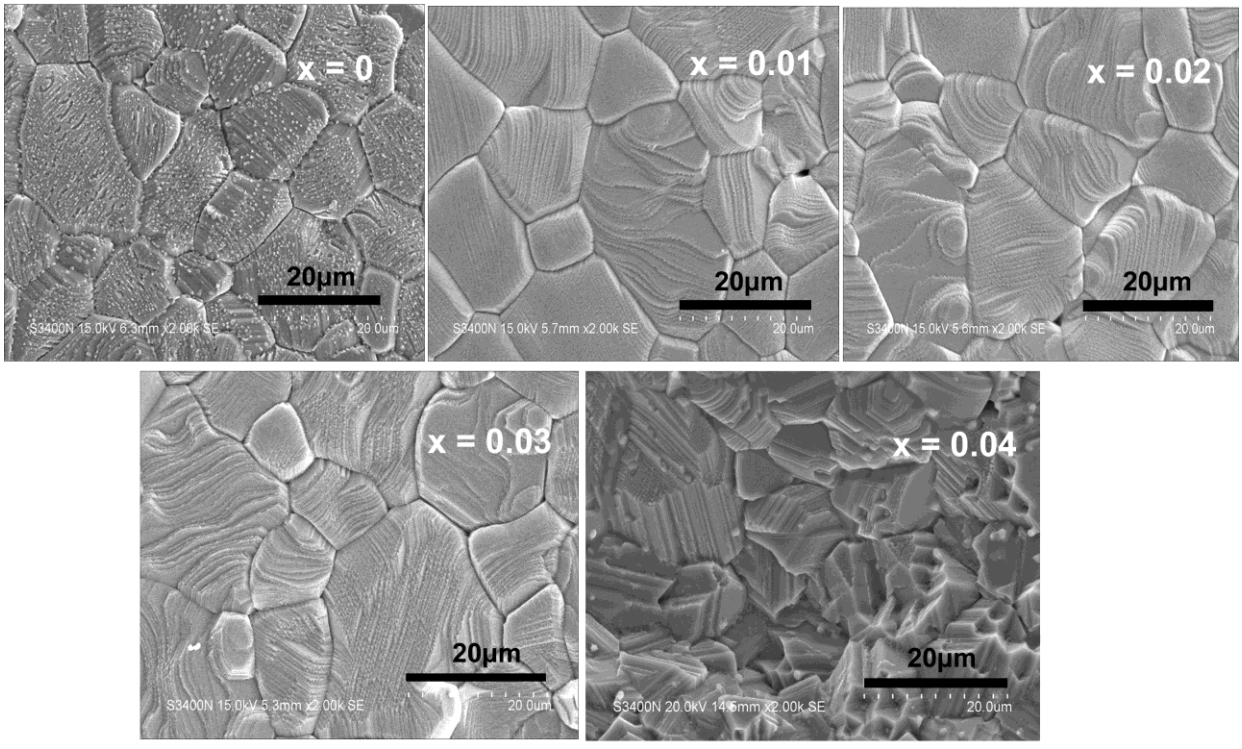

Figure. 6.6. Scanning electron micrographs of magnetically compacted and sintered Ce-substituted cobalt ferrite samples respectively

6.3. Magnetic properties

Field dependent M-H hysteresis loops of normally and magnetically compacted $Co_{1+x}Ce_xFe_{2-2x}O_4$ ($0 \leq x \leq 0.04$) measured at 300K temperatures are shown in Fig. 6.7 and 6.8. Therefore, the net magnetization can be considered as the result of A and B site magnetization difference. Since the cobalt ferrite has mixed spinel structure, its magnetic properties can vary based on the different metal cations present in the two interstitial sites (tetrahedral and octahedral) of cobalt ferrite lattice.

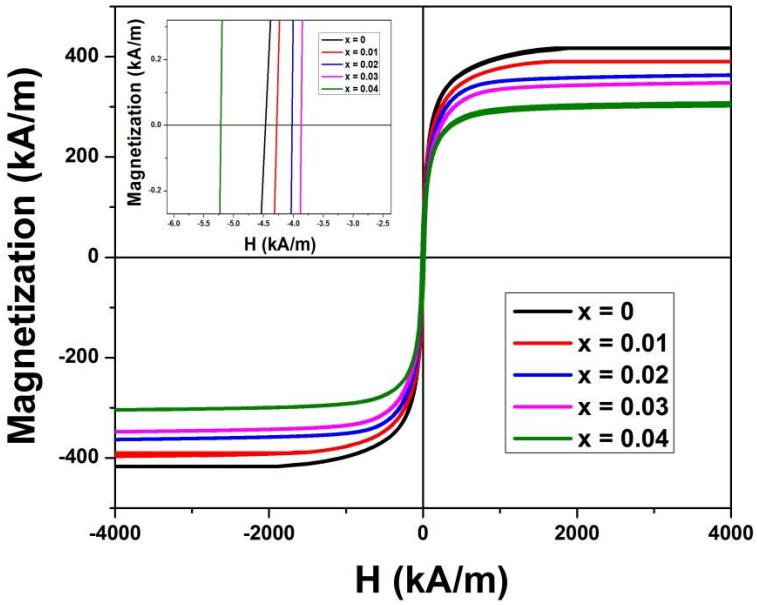

Figure. 6.7: Magnetization (M-H) curves of $Co_{1+x}Ce_xFe_{2-2x}O_4$ ($0 \leq x \leq 0.04$)-NC samples at room temperature (~300 K)

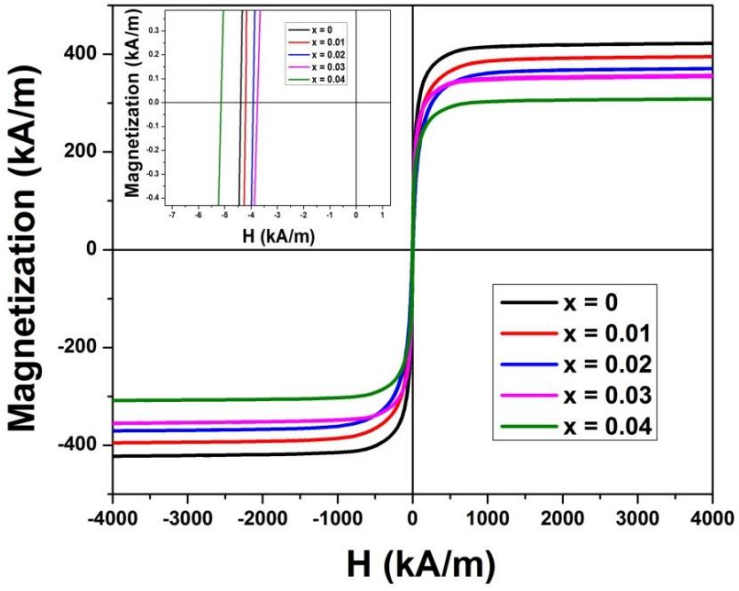

Figure. 6.8 Magnetization (M-H) curves of $Co_{1+x}Ce_xFe_{2-2x}O_4$ ($0 \leq x \leq 0.04$)-MC samples at room temperature (~300 K)

Since Ce^{+4} ions prefers to occupy octahedral site, magnetic moment of the respective site is expected to decrease, which in turn results in decreased net magnetic moment with increasing Ce^{+4} substitution in cobalt ferrite lattice. For x = 0.04 composition of Ce^{+4} substituted samples, M_{max} is seen to decrease, due to the presence of extra CeO_2 phase in the sample.

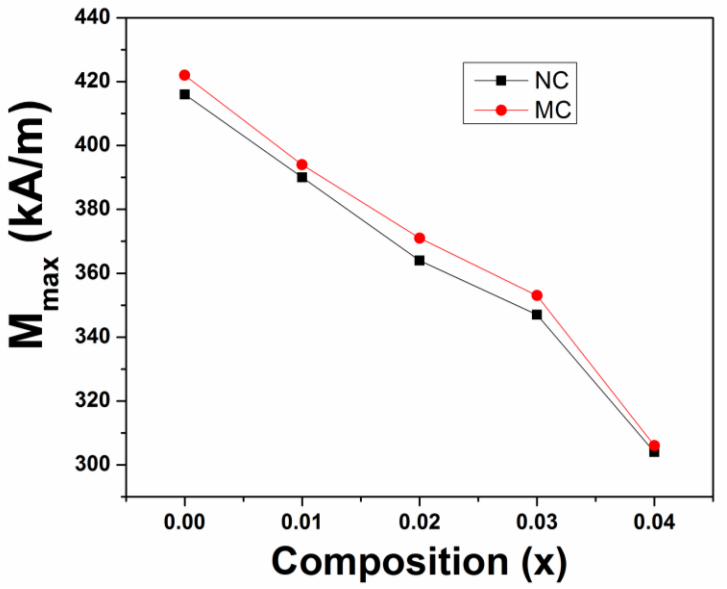

Figure. 6.9. Variation of M_{max} of NC and MC samples with composition (x)

Magneto crystalline anisotropy coefficient

Anisotropy constant was estimated using LoA to saturation as explained in the previous chapter. Fitted plots, using equation (3), of $Co_{1+x}Ce_xFe_{2-2x}O_4$ (x = 0, 0.03) compositions are shown in Fig. 6.10. 'K_1' was estimated by equating the slope to the coefficient 'b' in LoA.

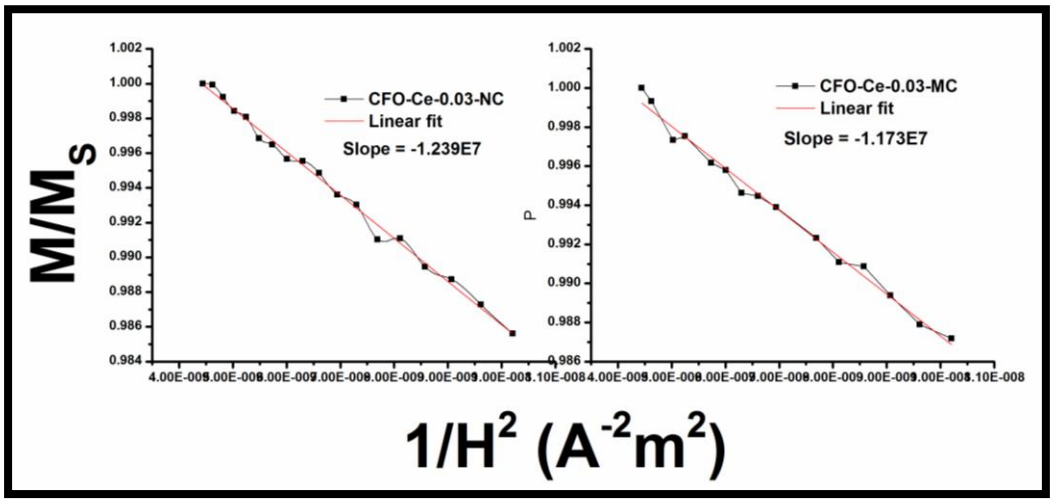

Figure. 6.10. LoA fitted plos of $Co_{1+x}Ce_xFe_{2-2x}O_4$ (x = 0, 0.03) samples

Figure.6.11 shows the variation in anisotropy coefficient (K_1) as a function of composition. The estimated 'K_1' from room temperature (~300 K) magnetization data of pure cobalt ferrite (~4.1 x 10^5 J/m^3) is in agreement with the reported literature [7]. From Fig.6.11 it is observed that substitution of Ce^{+4} ions into the CFO lattice increased the anisotropy constant (K_1) of the system.

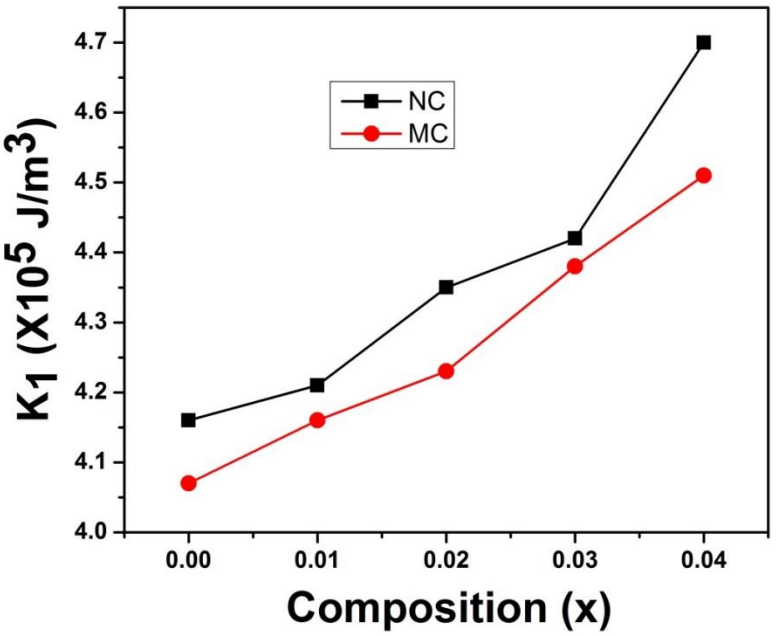

Figure.6.11. Variation of anisotropy constant as a function of composition and its comparison with NC samples

Slonczewski [8] reported that, cobalt ferrite has large positive magnetocrystalline anisotropy compared to magnetite (Fe_3O_4), which arises mainly due to the presence of Co^{+2} ions at B-site (Octahedral) of spinel crystal lattice. Tachiki [9] studied the dependence of anisotropy constant on the concentration of Co^{+2} ions in mixed Fe-Co ferrite and he reported that, Co^{+2} ions in octahedral site of magnetite spinel lattice are surrounded by oxygen ions (first nearest neighbors) and metal cations (second nearest neighbors), which produces cubic crystal field and trigonal crystal field respectively. In the presence of cubic crystal field, d-orbitals of Co^{+2} ion split into doubly (d_{x2-y2}, d_{z2}) and triply degenerate levels (d_{xy}, d_{yz}, d_{xz}). B-site metal cations produce charge distribution of threefold symmetry around Co^{+2} ion, at lower cobaltus ion concentrations. This trigonal field of three fold symmetry distorts the existing cubic crystal field and as a result, triply degenerate levels again split into singlet and doubly degenerate levels. Occupation of $3d^7$ electron into the doubly degenerate level produces unquenched orbital momentum to the system, which is the main origin of spin-orbit coupling and cubic crystalline anisotropy.

It is also reported that as the substitution level of Co^{+2} ion increases beyond $x > 0.7$, randomly distributed Fe^{+3} and Co^{+2} ions in octahedral site produces week crystalline field around, which further removes the degeneracy and thereby reduces the cubic crystalline anisotropy. Hence, Co^{+2} ion concentration in octahedral site of substituted cobalt ferrite is the main deciding factor for strength of the magnetocrystalline anisotropy energy. In case of Ce^{+4} substitutions, migration of Fe^{+3} ions from B to A-site is expected due to its strong preference for octahedral site. Increase in anisotropy for Ce^{+4} substituted cobalt ferrite samples could be due to the increasing amount of Co^{+2} ions within the limit of $x > 0.7$ in octahedral site. K_1 is observed to decrease in magnetically compacted samples compared to normally compacted substituted CFO, which might be due to the anisotropy induced in the system during the compaction in the presence of magnetic field.

Coercivity:

Variation in coercive field (H_C) of $Co_{1+x}Ce_xFe_{2-2x}O_4$ ($0 \leq x \leq 0.04$) samples, as a function of composition is shown Fig.6.12. Even though the coercivity of a system depends mainly on anisotropy energy, the decrease in coercivity could be related to the microstructural changes present in the system. In the present study, coercivity of undoped cobalt ferrite (~4.5 kA/m) is in good agreement with the reported value in the literature [7].

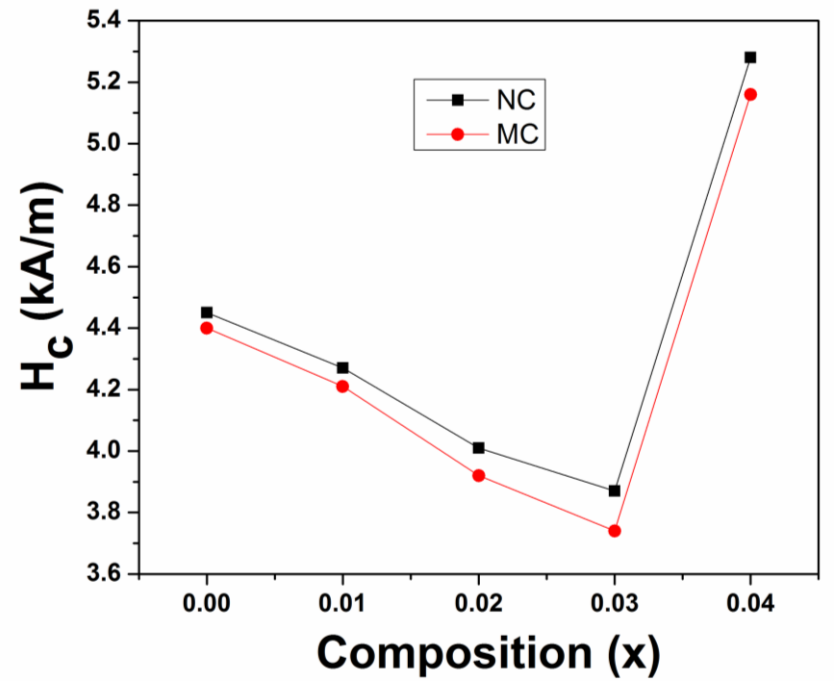

Figure.6.12. Variation of coercivity as a function of composition and its comparison with NC samples

6.4. Magnetoelastic properties

Magnetostriction (λ) curves of normally and magnetically compacted $Co_{1+x}Ce_xFe_{2-2x}O_4$ ($0 \leq x \leq 0.04$) samples, measured at room temperature, as a function of applied field (H) are shown in Fig. 6.13 and 6.14.

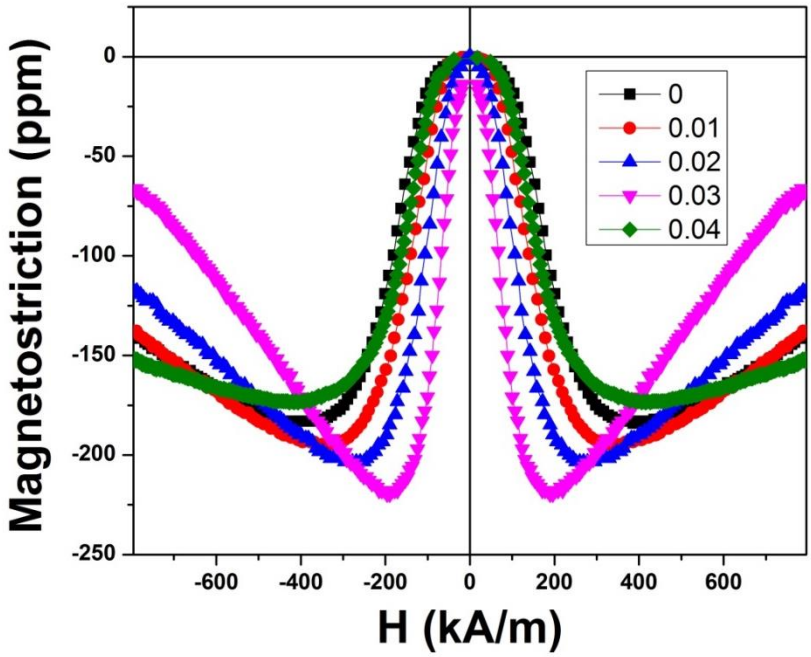

Figure 6.13. Longitudinal magnetostriction curves of $Co_{1+x}Ce_xFe_{2-2x}O_4$, ($0 \leq x \leq 0.04$)-NC samples

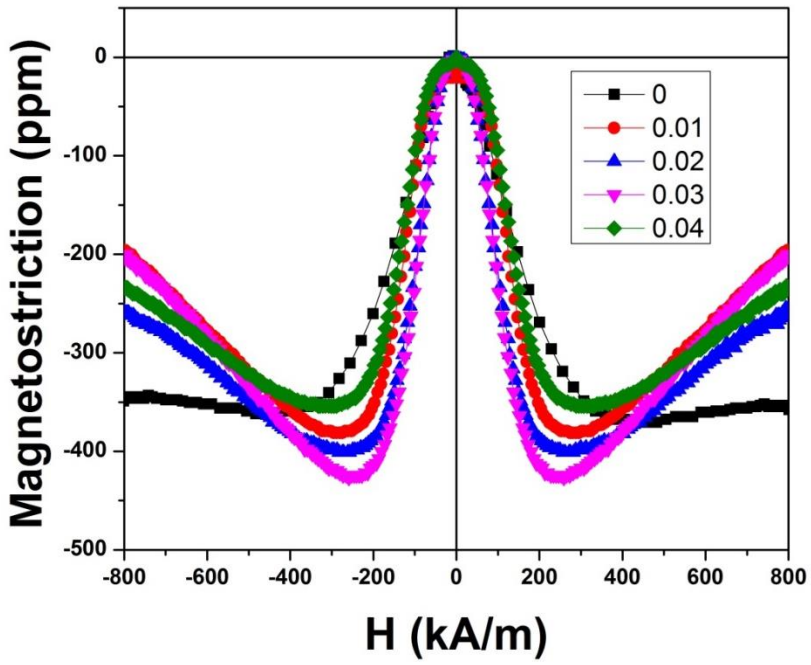

Figure 6.14. Longitudinal magnetostriction curves of $Co_{1+x}Ce_xFe_{2-2x}O_4$, ($0 \leq x \leq 0.04$)-MC samples

As the substitution levels of Ce^{+4} content in the CFO lattice increases, magnetostriction amplitude (λ) is observed to increased up to x = 0.03 composition and is seen to decrease for x = 0.4 composition compared to pure CFO, as shown in Fig 6.15 for both the NC and MC samples. Maximum magnetostrictions (λ_{max}) of ~ -181, -225ppm were observed for normally compacted $CoFe_2O_4$ and $Co_{1.03}Ce_{0.03}Fe_{1.94}O_4$ compositions. For magnetically compacted x = 0, 0.2 samples λ_{max} is observed to be ~ -360, -425ppm. With increasing concentration of tetravalent ions (Ce^{+4}), FWHMs of the magnetostriction curves are observed to decrease, which might be related to the field sensitivity of magnetization (dM/dH). Tachiki proposed that anisotropy constant increase over a particular substitution level of Co^{+2} ions in B-site of CFO lattice. Since spin-orbit coupling is the main origin of anisotropy and magnetostriction [14], the observed increase in λ_{max} for $Co_{1+x}Ce_xFe_{2-2x}O_4$ up to x = 0.03 concentration compared to undoped cobalt ferrite could be due to the presence of optimum level of Co^{+2} ions in B-site of substituted CFO lattice. For x = 0.04 compositions of Ce-substituted cobalt ferrites, due to the presence of extra phases (CeO_2), magnetostriction is observed to decrease.

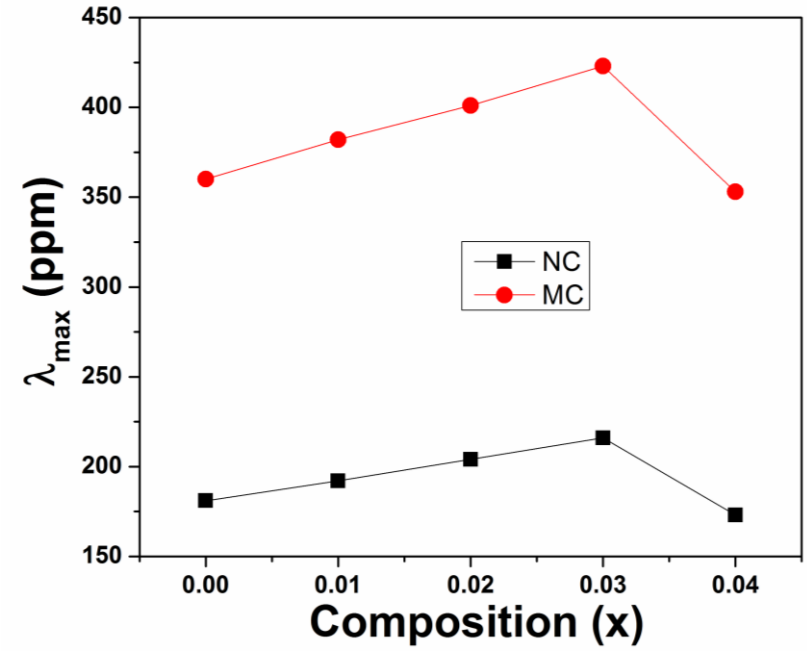

Figure.6.15. Variation of magnitude of maximum magnetostriction as a function of composition, x and their comparison with NC samples

Strain derivative ($d\lambda/dH$) of normally and magnetically compacted $Co_{1+x}Ce_xFe_{2-2x}O_4$ ($0 \leq x \leq 0.04$) samples, estimated from the magnetostriction curves, as a function of applied magnetic field are shown in Fig 6.16 and 6.17. For both the series of samples $(d\lambda/dH)_{max}$ is observed to increase with increasing concentrations of Ce from x = 0 to x =

0.03, as shown in Fig. 6.18, this could be due to the reduced exchange interaction strength between the cations in tetra and octahedral sub lattices with the substitution of non-magnetic ions into the CFO lattice.

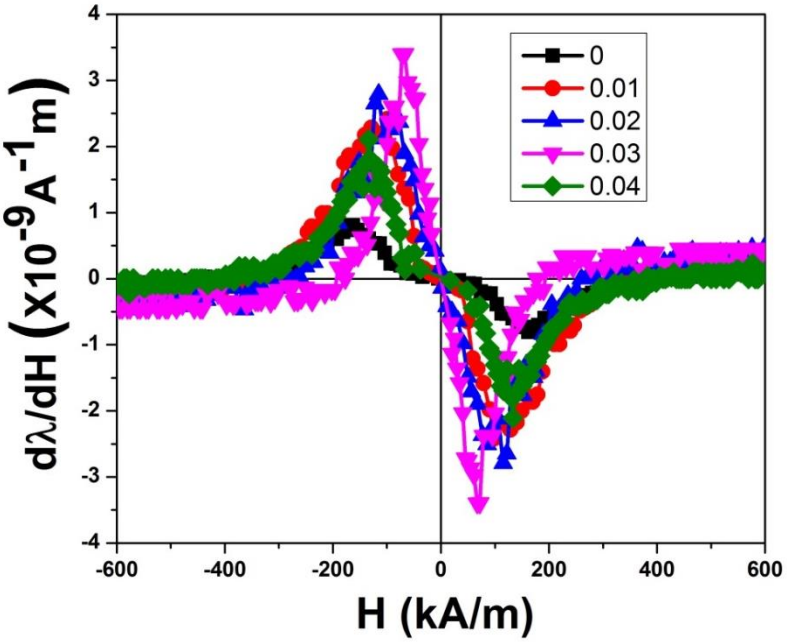

Figure.6.16. Magnetic field (H) dependence of strain derivative (dλ/dH) for $Co_{1+x}Ce_xFe_{2-2x}O_4$, ($0 \leq x \leq 0.04$)-NC samples

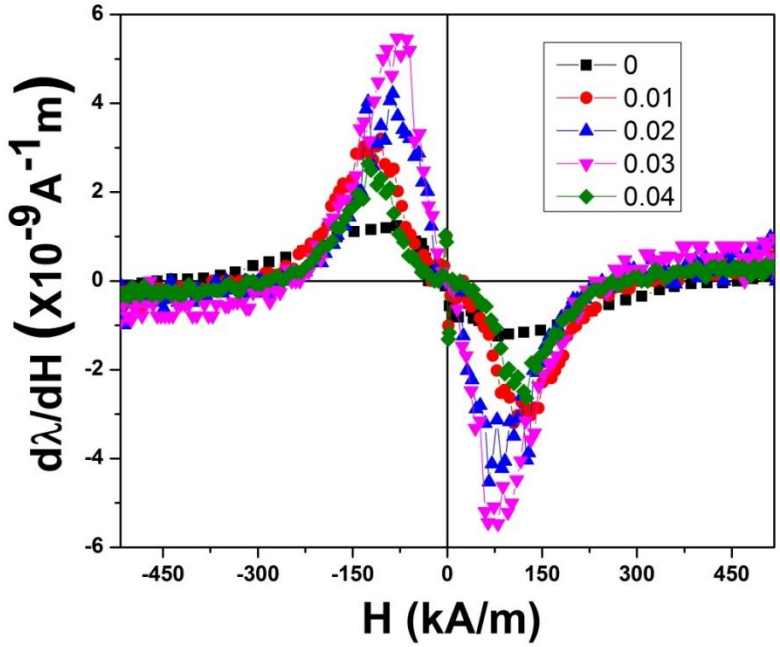

Figure 6.17. Magnetic field (H) dependence of dλ/dH for $Co_{1+x}Ce_xFe_{2-2x}O_4$, ($0 \leq x \leq 0.04$)-MC samples

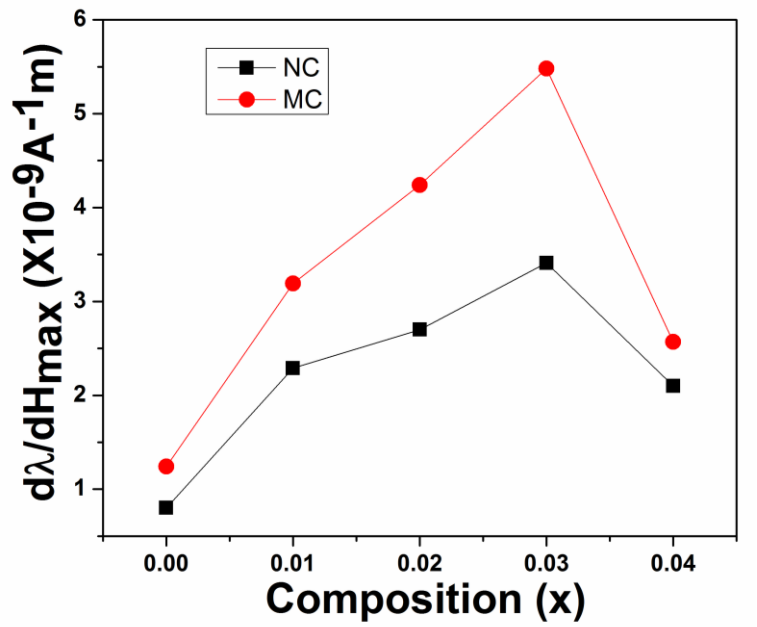

Figure.6.18. Variation of maximum strain derivative, $(d\lambda/dH)_{max}$ as a function of composition and its comparison with normal compaction

Decrease in strain derivative observed for x = 0.04 composition of both the substituents could be due to the presence of extra phase (CeO_2) at grain boundaries, which hindrances the domain wall motion. A remarkable 325 and 588 % enhancement in dλ/dH has been observed for normally and magnetically pressed $Co_{1+x}Ce_xFe_{2-2x}O_4$ (x = 0.03) composition compared to normally compacted pure cobalt ferrite. In the low field region magnetization process depends on exchange interaction strength. Reduction in exchange interaction strength with Ce^{+4} substitution increases the domain wall thickness, which in turn reduces the angle between the spin moments. Thus, the amount of field required to get $(d\lambda/dH)_{max}$ decreases.

6.5. Conclusioons:

- Maximum magnetostriction of ~216 ppm and ~423 ppm is achieved at room temperature for normal and magnetic field assisted compacted $Co_{1+x}Ce_xFe_{2-2x}O_4$, (x = 0.03) samples, respectively.
- A remarkable ~ 265% increase in dλ/dH was observed for field pressed $Co_{1.03}Ce_{0.03}Fe_{1.94}O_4$ composition compared to pure $CoFe_2O_4$ (~5.42 X 10^{-9} $A^{-1}m$ vs. ~1.5 X 10^{-9} $A^{-1}m$).

6.6. References

[1] S. D. Bhame and P. A. Joy, Enhanced magnetostrictive properties of Mn substituted cobalt ferrite $Co_{1.2}Fe_{1.8}O_4$, J. Appl. Phys. 99 (2006) 073901

[2] K. Kriebel, C. C. H. Lo, Y. Melikhov and J. E. Snyder, Investigation of Cr substitution in Co ferrite ($CoCr_xFe_{2-x}O_4$)($CoCr_xFe_{2-x}O_4$) using Mossbauer spectroscopy, J. Appl. Phys. 99 (2006) 08M912

[3] Y. Melikhov, J. E. Snyder, D.C. Jiles, A. P. Ring, J. A. Paulsen, C. C. H. Lo and K. W. Dennis, Temperature dependence of magnetic anisotropy in Mn-substituted cobalt ferrite, J. Appl. Phys. 99 (2006) 08R102

[4] Nalla Somaiah, Tanjore V. Jayaraman, P.A. Joy, Dibakar Das, Magnetic and magnetoelastic properties of Zn-doped cobalt-ferrites—$CoFe_{2-x}Zn_xO4$(x = 0, 0.1, 0.2, and 0.3), J. Magn. Magn. Mater. 324 (2012) 2286–2291

[5] W. Bayoumi, Structural and electrical properties of zinc-substituted cobalt ferrite, J. Mater. Sci. 42 (2007) 8254-8261

[6] M. R. De Guire, R. C. O'Handley and G. Kalonji, The cooling rate dependence of cation distributions in $CoFe_2O_4$, J. Appl. Phys. 65 (1989) 3167

[7] Vinitha Reddy Monaji, Dibakar Das, Influence of Zr doping on the structural, magnetic and magnetoelastic properties of cobalt-ferrites, J. Alloys Compd. 634 (2015) 99–103

[8] J. Slonczewski, Origin of Magnetic Anisotropy in Cobalt-Substituted Magnetite, Physical Review, 110 (1958) 1341–1348

[9] M. Tachiki, Origin of the Magnetic Anisotropy Energy of Cobalt Ferrite, Progress of Theoretical Physics, 23 (1960) 1055–1072

Chapter – 7

Summary and Conclusions

This chapter provides the summary and conclusions of the results of the present work and also the scopes for future research in this area

7.1. Effect of non-magnetic ion (Zr and Ti) substitution on structural and magnetic properties of cobalt ferrite

Magnetic and magnetoelastic properties of $Co_{1+x}M_xFe_{2-2x}O_4$ (M = Zr, Ti; $0 \leq x \leq 0.4$) samples have been studied. X-ray spectral analysis indicated the presence of cubic-spinel phase only and the lattice parameter (a), saturation magnetization (M_S) have been found to increase and decrease with increasing Zr^{+4} and Ti^{+4} substitution in the CFO lattice respectively. The effect of temperature and composition dependence of $Co_{1+x}M_xFe_{2-2x}O_4$ ($0 \leq x \leq 0.4$ and M = Zr, Ti) samples on the magnetic properties have been studied. As the temperature decreases high magnetocrystalline anisotropy prevented complete approach to saturation magnetization and maximum magnetization was observed around 150 K for all the samples. Direct relationship was observed between coercive field and magnetocrystalline anisotropy coefficient for all the samples. Transition temperature was observed to decrease and increase with Zr and Ti substitution, respectively, in CFO lattice. Maximum magnetostriction of ~185 and 196ppm are achieved for x = 0.2 composition of Zr and Ti substituted cobalt ferrites respectively. A remarkable 300 and 345% increase in $d\lambda/dH$ was observed for $Co_{1.2}Zr_{0.2}Fe_{1.6}O_4$ and $Co_{1.2}Ti_{0.2}Fe_{1.6}O_4$ respectively, compared to pure $CoFe_2O_4$ (~3.32 x 10^{-9} $A^{-1}m$ vs. ~0.8 x 10^{-9} $A^{-1}m$).

7.2. Effect of non-magnetic ion (Zr and Ti) substitution and magnetic field assisted compaction on structural, magnetic and magnetostrictive properties of cobalt ferrite

Structural, magnetic and magnetoelastic properties of magnetically compacted $Co_{1+x}M_xFe_{2-2x}O_4$ (M = Zr, Ti; $0 \leq x \leq 0.4$) samples have been studied and the results were compared with the normal pressed samples. Parallel and perpendicular magnetization data of magnetically pressed Zr- and Ti-substituted cobalt ferrite samples indicated an induced easy direction of magnetization and that was developed at nearly 90˚ to the direction of compaction, which introduced some uniaxial anisotropy in the samples along the same direction. Magnetostriction and strain sensitivity are increased by ~111% and 435%, respectively, for magnetically pressed $Co_{1.2}Zr_{0.2}Fe_{1.6}O_4$ compared to CFO-NC. Approximately 128% and 625% increment in magnetostriction and strain sensitivity is

observed for x = 0.2 Ti- substituted CFO sample compared to CFO-NC. Substitution of non-magnetic ions, having preference for octahedral coordination, is more effective in increasing the magnetostriction of CFO. Magnetic field assisted compaction strongly influences the strain sensitivity of substituted CFO samples. The present study indicates that magnetic compaction could be an alternate and effective method to magnetic annealing for improving the magnetoelastic properties of CFO.

7.3. Effect of Ce substitution and magnetic field assisted compaction on structural, magnetic and magnetostrictive properties of cobalt ferrite

XRD of $Co_{1+x}Ce_xFe_{2-2x}O_4$ sintered at 1300^{o}C for 12 hrs confirms single cubic spinel phase except for x = 0.04 composition. Lattice parameter is observed to increase with Ce substitution into the CFO lattice. Lattice parameter of magnetically compacted $Co_{1+x}Ce_xFe_{2-2x}O_4$ samples is decreased compared to normally pressed samples. Maximum magnetostriction ~ 225 ppm is achieved for $Co_{1.03}Ce_{0.03}Fe_{1.94}O_4$. Maximum magnetostriction of ~360 and 425 ppm is observed for magnetically compacted pure CFO and Ce substituted cobalt ferrite samples, respectively. Approximately 135% increment in magnetostriction is observed for magnetically pressed Ce substituted CFO sample compared to normally pressed CFO. A remarkable ~ 325% and 588% increase in $d\lambda/dH$ was observed for NC and MC $Co_{1.03}Ce_{0.03}Fe_{1.94}O_4$ samples, respectively, compared to pure $CoFe_2O_4$ (5.5 X 10^{-9} $A^{-1}m$ vs. ~0.8×10^{-9} $A^{-1}m$)

7.4. Conclusions

- $Co_{1+x}M_xFe_{2-2x}O_4$ (M = Zr, Ti and Ce) samples were synthesized by conventional ceramic method
- XRD of $Co_{1+x}M_xFe_{2-2x}O_4$ (M = Zr, Ti and Ce) samples sintered at 1300^{o}C for 12 hrs confirms single cubic spinel phase except for x = 0.4 composition.
- Lattice parameter is observed to decrease with Ti substitution and increase with Zr and Ce substitution into the CFO lattice
- Lattice parameter of magnetically compacted $Co_{1+x}M_xFe_{2-2x}O_4$ (M = Zr, Ti and Ce) samples is decreased compared to normally pressed samples
- Saturation magnetization (M_S) and coercivity (H_C) have been found to increase with increasing Zr^{+4} substitution and decrease with increasing Ti^{+4} and Ce^{+4} substitution in the CFO lattice

- Coercivity of magnetically compacted $Co_{1+x}M_xFe_{2-2x}O_4$ (M = Zr, Ti and Ce) samples is decreased compared to normally pressed samples because of the presence of induced anisotropy in the system
- Maximum magnetostriction ~186, 195 and 225 ppm is achieved for $Co_{1.2}Zr_{0.2}Fe_{1.6}O_4$, $Co_{1.2}Ti_{0.2}Fe_{1.6}O_4$ and $Co_{1.03}Ce_{0.03}Fe_{1.94}O_4$ samples respectively.
- Maximum magnetostriction of ~360, 380, 412 and 425 ppm is observed for magnetically compacted pure CFO, Zr, Ti and Ce substituted cobalt ferrite samples, respectively. Approximately 135% increment in magnetostriction is observed for magnetically pressed Ce substituted CFO sample compared to normally pressed CFO.
- A remarkable ~ 310, 340, 325% increase in $d\lambda/dH$ was observed for $Co_{1.2}Zr_{0.2}Fe_{1.6}O_4$, $Co_{1.2}Ti_{0.2}Fe_{1.6}O_4$, $Co_{1.03}Ce_{0.03}Fe_{1.94}O_4$ samples, respectively, compared to pure $CoFe_2O_4$ (~3.3, 3.5, 3.4 X 10^{-9} $A^{-1}m$ vs. ~0.8 X 10^{-9} $A^{-1}m$).
- A Dramatic ~435, 625, 588% increase in $d\lambda/dH$ was observed for $Co_{1.2}Zr_{0.2}Fe_{1.6}O_4$, $Co_{1.2}Ti_{0.2}Fe_{1.6}O_4$, $Co_{1.03}Ce_{0.03}Fe_{1.94}O_4$ samples, respectively, compared to pure $CoFe_2O_4$ (~4.3, 5.8, 5.5 X 10^{-9} $A^{-1}m$ vs. ~0.8 X 10^{-9} $A^{-1}m$).
- From the observed results it can be concluded that magnetically compacted Ti-substituted CFO can be used as a potential material for stress sensor applications

7.5 Scope of future work

- The magnetostrictive properties of cobalt ferrite based material can further be enhanced by optimizing the field applied during compaction and inducing texturing in the particles by various methods including molten salt synthesis and field induced gel casting technique.

LIST OF PUBLICATIONS

A. **List of peer-reviewed publications from the thesis work:**

1) **Vinitha Reddy Monaji,** Abdellah Lisfi, Sabin Pokharel and Dibakar Das, "Colossal Piezomagnetic Response in Magnetically Pressed Zr^{+4} Substituted Cobalt Ferrites", Scientific reports,7:7935, DOI: 10.1038/s41598-017-08160-1
2) **Vinitha Reddy Monaji**, Srinivas Indla, Sudhindra Rayaprol, Shara Sowmya, A. Srinivas, Dibakar Das, "Temperature dependent magnetic properties of $Co_{1+x}T_xFe_{2-2x}O_4$ (T = Zr, Ti), *Journal of Alloys and Compounds, 700, 92-97 (2017)*
3) **Vinitha Reddy Monaji** and D. Das, "Development of A Novel Magnetostrictive Material With Large Piezomagnetic Coefficient For Stress Sensor Applications", AIP proceedings, 1832, 140035 (2017)
4) **Vinitha Reddy Monaji**, Dibakar Das, "Influence of Zr doping on the structural, magnetic and magnetoelastic properties of cobalt-ferrites", *Journal of Alloys and Compounds 634, 99–103 (2015)*

B. Manuscripts to be communicated:

1) **Vinitha Reddy Monaji**, Abdellah Lisfi, Sabin Pokharel and Dibakar Das, "Large enhancement in magnetoelastic properties of magnetic field pressed Ti- substituted cobalt ferrites"
2) **Vinitha Reddy Monaji**, Dibakar Das, "Effect of Ce^{+4} substitution and magnetic field pressing on magnetic and magnetoelastic properties of CFO"
3) **Vinitha Reddy Monaji**, Sudhindra Rayaprol, Dibakar Das, "Neutron diffraction study of Zr- substituted cobalt ferrites"

C. List of other publications:

1) **Vinitha Reddy Monaji**, Paul Praveen J, Dibakar Das, "Magneto-electric properties of in-situ prepared $xCoFe_2O_4$-(1-x)$(Ba_{0.85}Ca_{0.15})(Zr_{0.1}Ti_{0.9})O_3$ particulate composites, *Ceramics International* 42, 17827-33 (2016)
2) **Vinitha Reddy M**, Paul Praveen J, Dibakar Das, "Powder metallurgy processing and characterization of a novel ferrite for automobile torque sensor applications", Trans. PMAI, vol.40 (1), 73-77 (2014)

3) **Vinitha Reddy Monaji**, Paul Praveen J, Manivel Raja, Dibakar Das, "Influence of cation distribution on the structural and magnetoelectric properties of $Co_{1-x}Zn_xFe_2O_4$ ($0 \leq x \leq 0.3$) ceramics", AIP proceedings, 1728, 020503, 2016

4) **M Vinitha Reddy**, J Praveen Paul, and Dibakar Das, "Effect of zinc doping on magnetic and magnetoelastic properties of cobalt ferrite synthesized by autocombustion process", AIP Conf. Proc. 1536, 1015 (2013)

5) I. C. Nlebedim, **M. Vinitha**, P. J. Praveen, D. Das, and D. C. Jiles, "Temperature dependence of the structural, magnetic, and magnetostrictive properties of zinc-substituted cobalt ferrite", J. Appl. Phys. 113, 193904 (2013)

6) Sateesh Prathapani, **M. Vinitha**, T. V. Jayaraman, and D. Das, "Effect of Er doping on the structural and magnetic properties of cobalt-ferrite", J. Appl. Phys. 115, 17A502 (2014)

7) Paul Praveen J, **Vinitha Reddy M** and Dibakar Das, "Magnetoelectric Properties Of $(Ba_{0.85}Ca_{0.15})(Zr_{0.1}Ti_{0.9})O_3$ -$CoFe_2O_4$ Particulate Composites", AIP conference proceedings, 1728, 020568, 2016

8) Paul Praveen J , **Vinitha Reddy Monaji** , Dibakar Das, "Synthesis, characterization and dielectric properties of $(1-x)(Ba_{0.85}Ca_{0.15})(Zr_{0.1}Ti_{0.9})O_3–xCoFe_2O_4$ multiferroic composites", Journal of Applied ceramic technology, 1-11 (2016)

Conference Presentations:

1) **Vinitha Reddy Monaji**, Paul Praveen J, Dibakar Das, "Effect of zinc doping on magnetic and magnetomechanical properties of cobalt ferrite", presented in AMPC conference-2013, Chennai

2) **Vinitha Reddy M**, Paul Praveen J and Dibakar Das, "Studies on magnetic and dielectric behavior of magnetoelectric $CoFe_2O_4$ – BCZT composites", presented in MAGMA 2013 in Guwahati.

3) Paul Praveen J ,**Vinitha Reddy M** and Dibakar Das, "Synthesis, characterization and dielectric properties of $(1-x)(Ba_{0.85}Ca_{0.15})(Zr_{0.1}Ti_{0.9})O_3–xCoFe_2O_4$ multiferroic composites", Presented in MAGMA 2013 in Guwahati.

4) **Vinitha Reddy M** ,Paul Praveen J , and Dibakar Das, "A study on ferroelectric and ferromagnetic properties of $(1-x)(Ba_{0.85}Ca_{0.15})(Zr_{0.1}Ti_{0.9})O_3–xCoFe_2O_4$ multiferroics composites", Poster presented at International Conference on Advanced Functional Materials (ICAFM-2014) in Thiruvananthapuram

5) **Vinitha Reddy Monaji**, Paul Praveen J, Manivel Raja, Dibakar Das, "Influence of cation distribution on the magnetic and dielectric properties of Zn doped CFO ceramics", presented in ICC conference-2015, Rajasthan

6) **Vinitha Reddy Monaji**, Dibakar Das, "Novel processing of substituted cobalt ferrites for stress sensing applications", presented in ICCGR-EI conference-2016, Hyderabad

7) **Vinitha Reddy Monaji**, Dibakar Das, "Development of A Magnetostrictive Material With Large Piezomagnetic Coefficient For Stress Sensor Applications", presented in DAE conference-2016, Bhuvaneswar